minerals

MDPI

Review

Geobiological and Biochemical Cycling in the Early Cambrian: Insights from Phosphoritic Materials of South Spain

Ting Huang [1,2] and David C. Fernández-Remolar [1,2,3,4,*]

[1] SKL Lunar and Planetary Sciences, Macau University of Science and Technology, Macau 999078, China; thuang@must.edu.mo
[2] CNSA Macau Center for Space Exploration and Science Macau, Macau 999078, China
[3] Department of Lithospheric Research, Faculty of Earth Sciences, Geography and Astronomy, University of Vienna, 1090 Vienna, Austria
[4] ISA, Iceland Space Agency, 101 Reykjavik, Iceland
* Correspondence: dcfremolar@must.edu.mo

Abstract: In the early Cambrian period, a severe greenhouse effect subjected the Gondwanan continents to accelerated erosion, enriching oceanic waters with essential nutrients, including phosphate, silicon, calcium, magnesium, iron, and trace elements. The nutrient flux, sourced from the volcanic composition of west Gondwana, was recorded as sequences of nodular phosphoritic limestones intercalated with chlorite-rich silts, containing ferrous phyllosilicates such as chamosite and chlorite. The abundant and diverse fossil record within these deposits corroborates that the ion supply facilitated robust biogeochemical and nutrient cycling, promoting elevated biological productivity and biodiversity. This paper investigates the early Cambrian nutrient fluxes from the Gondwanan continental region, focusing on the formation of phosphoritic and ferrous facies and the diversity of the fossil record. We estimate and model the biogeochemical cycling within a unique early Cambrian ecosystem located in South Spain, characterized by calcimicrobial reefs interspersed with archaeocyathids that settled atop a tectonically elevated volcano-sedimentary platform. The configuration enclosed a shallow marine lagoon nourished by riverine contributions including ferric and phosphatic complexes. Geochemical analyses revealed varying concentrations of iron (0.14–3.23 wt%), phosphate (0.1–20.0 wt%), and silica (0.27–69.0 wt%) across different facies, with distinct patterns between reef core and lagoonal deposits. Using the Geochemist's Workbench software and field observations, we estimated that continental andesite weathering rates were approximately 23 times higher than the rates predicted through modeling, delivering, at least, annual fluxes of 0.286 $g \cdot cm^{-2} \cdot yr^{-1}$ for Fe and 0.0146 $g \cdot cm^{-2} \cdot yr^{-1}$ for PO_4^{3-} into the lagoon. The abundant and diverse fossil assemblage, comprising over 20 distinct taxonomic groups dominated by mollusks and small shelly fossils, indicates that this nutrient influx facilitated robust biogeochemical cycling and elevated biological productivity. A carbon budget analysis revealed that while the system produced an estimated $1.49 \cdot 10^{15}$ g of C over its million-year existence, only about 0.01% was preserved in the rock record. Sulfate-reducing and iron-reducing chemoheterotrophic bacteria played essential roles in organic carbon recycling, with sulfate reduction serving as the dominant degradation pathway, processing approximately $1.55 \cdot 10^{11}$ g of C compared to the $5.94 \cdot 10^{8}$ g of C through iron reduction. A stoichiometric analysis based on Redfield ratios suggested significant deviations in the C:P ratios between the different facies and metabolic pathways, ranging from 0.12 to 161.83, reflecting the complex patterns of organic matter preservation and degradation. The formation of phosphorites and ferrous phyllosilicates was primarily controlled by suboxic conditions in the lagoon, where microbial iron reduction destabilized Fe(III)-bearing oxyhydroxide complexes, releasing scavenged phosphate. This analysis of nutrient cycling in the Las Ermitas reef–lagoon system demonstrates

Academic Editor: Edward J. O'Loughlin

Received: 21 December 2024
Revised: 25 January 2025
Accepted: 28 January 2025
Published: 20 February 2025

Citation: Huang, T.; Fernández-Remolar, D.C. Geobiological and Biochemical Cycling in the Early Cambrian: Insights from Phosphoritic Materials of South Spain. *Minerals* **2025**, *15*, 203. https://doi.org/10.3390/min15030203

how intensified continental weathering and enhanced nutrient fluxes during the early Cambrian created favorable conditions for the development of complex marine ecosystems. The quantified nutrient concentrations, weathering rates, and metabolic patterns established here provide a baseline data for future research addressing the biogeochemical conditions that facilitated the Cambrian explosion and offering new insights into the co-evolution of Earth's geochemical cycles and early animal communities.

Keywords: phosphorites; verdine facies; continental weathering; microbial activity; stochiometric analysis; calcimicrobes; cambrian communities

1. Introduction

At the onset of the early Cambrian period, the northern marginal areas of Gondwana, formed by different volcano-sedimentary systems [1,2], were exposed to active weathering promoted by a climatic thermal event [3]. Under such climatic and geological settings, a likely Terreneuvian transgressive pulse [4] triggered the flooding of the former continental areas as an initial stage of the Hercynian cycle for the Iberian terrains [5]. As a result, the ancient volcano-sedimentary materials were covered by a deepening sequence that included fluvial and marine deposits with the development of mixed carbonate platforms [6,7]. This transgressive event brought about the development of various reefal structures built by calcimicrobial consortia [8–11], which favored the emergence of a diverse metazoan community associated with the Cambrian explosion [12–14].

In this context, the early Cambrian marked a pivotal period in Earth's history, characterized by significant changes and complexation in biogeochemical cycles and a remarkable increase in ecological diversity [15]. The onset of the Cambrian explosion witnessed a rapid diversification of metazoan life, with the emergence of complex ecosystems and the development of novel ecological interactions [16]. This evolutionary radiation was closely intertwined with substantial alterations in biogeochemical cycles, particularly those involving nutrients such as phosphorus, nitrogen, and iron [17,18].

The weathering of the Gondwanan volcanosedimentary systems during the Early Cambrian played a crucial role in the supply of nutrients to the oceans [19,20]. The enhanced weathering processes, driven by the prevailing greenhouse conditions, led to an increased flux of phosphorus [21,22], a key limiting nutrient for primary productivity [23]. The delivery of phosphorus to the marine realm likely stimulated primary production, supporting the expansion of micro- and macroalgal communities and the subsequent development of complex food webs [18]. Moreover, the weathering of continental materials containing iron from the continents resulted in an elevated supply of bioavailable iron to the oceans [24]. Iron is an essential micronutrient for many marine organisms, and its increased availability may have further facilitated primary production and the growth of primary producers [25].

The diversification of metazoan life during the Cambrian explosion was closely linked to these changes in biogeochemical cycles. The increased availability of nutrients and the expansion of primary production provided the foundation for the development of complex food webs and the evolution of diverse feeding strategies among metazoans [26]. The rise of bioturbation, facilitated by the evolution of burrowing organisms, further influenced biogeochemical cycling by enhancing the mixing of sediments and the recycling of nutrients [27]. The expansion of reef-building organisms, such as archaeocyathids and calcimicrobes, also contributed to the creation of new habitats and the partitioning of ecological niches, promoting the diversification of benthic communities [28].

The integration of geochemical and paleontological data from the early Cambrian strata provides valuable insights into the intricate relationship between biogeochemical cycles and the evolution of early metazoan ecosystems [18]. The sedimentary record of phosphorites and ferrous phyllosilicates, as well as the associated fossil assemblages, offer a window into the environmental conditions and ecological interactions that shaped the biosphere during this transformative period in Earth's history [29,30].

In this context, the nutrient flux, sourced from the volcanic composition of west Gondwana, was recorded in south Iberia as sequences of nodular phosphoritic limestones intercalated with chlorite-rich silts, containing ferrous phyllosilicates such as chamosite and chlorite [29]. Moreover, the intensified carbon cycle during the early Cambrian likely facilitated the development of the earliest reefal structures in the region. These reefs were primarily constructed by microbial communities, such as calcimicrobes and stromatolites, which thrived under the prevailing environmental conditions and played a crucial role in the formation and growth of these early reef systems [6,31]. The abundant and diverse fossil record within these deposits [32] corroborates that the ion supply facilitated robust biogeochemical and nutrient cycling, promoting elevated biological productivity and biodiversity. Although macroalgae likely played a crucial role within early Cambrian ecosystems, their preservation in carbonatic facies has been limited due to taphonomic constraints [33,34].

This paper explores how the sedimentary and paleontological record reflects the interplay between phosphorus, iron, and silicon biogeochemical cycles and their role in the development of Early Cambrian reef systems. By analyzing phosphorites, ferrous phyllosilicates, and associated fossil assemblages, we examine the interactions between these cycles and early reef ecosystems. Materials from the Cambrian (Series 2) Pedroche Formation in Sierra de Córdoba, south Spain, were studied, including calcimicrobial reefs with archaeocyathids atop a tectonically elevated volcano-sedimentary platform enclosing a nutrient-rich shallow lagoon. Our findings shed light on the paleoenvironmental conditions and the emergence of complex communities during this pivotal period in Earth's history.

2. Biogeochemical Alterations in the Nutrient Cycles

The phosphorus, iron, and silica biogeochemical cycles are fundamentally interconnected and play crucial roles in the evolution and development of marine ecosystems [35,36]. These cycles are driven by a complex interplay of processes, including weathering of minerals on land, nutrient transport via rivers, and biological uptake and assimilation by marine organisms [37,38]. The sedimentary and paleontological records of Las Ermitas, Cordoba, offers a unique opportunity to investigate the main features of these cycles and their influence on the establishment and growth of reef systems during the early Cambrian [11,39–41]. By examining the sedimentary record of phosphorites and ferrous phyllosilicates, as well as the associated fossil assemblages, we aim to unravel the interrelationships between the P, Fe, and Si cycles and their impact on the development of early marine ecosystems in this area.

2.1. Iron Biogeochemical Cycle

Iron is an essential nutrient for marine organisms, particularly for primary producers such as phytoplankton, cyanobacteria, and macroalgae [42]. These organisms require iron for a variety of critical cellular processes, including photosynthesis, respiration, and nitrogen fixation [43,44]. In photosynthesis, iron is a key component of the electron transport chain, facilitating the transfer of electrons during the light reactions [43]. Iron is also necessary for the synthesis of chlorophyll, the pigment responsible for capturing light energy in

photosynthetic organisms [45]. Without sufficient iron, primary producers cannot efficiently convert light energy into chemical energy, leading to reduced growth and productivity [46].

In addition to its role in photosynthesis, iron is crucial for nitrogen fixation, a process carried out by some cyanobacteria and other microorganisms [47]. Nitrogen fixation involves the conversion of atmospheric nitrogen (N_2) into biologically available forms, such as ammonium (NH_4^+), which can be utilized by other marine organisms [48]. In this regard, the enzyme responsible for nitrogen fixation, nitrogenase, requires iron as a cofactor [45]. Thus, iron availability can limit nitrogen fixation rates in marine environments, affecting the overall nitrogen budget and the productivity of the ecosystem [49]. Furthermore, iron plays a significant role in respiration, as it is a component of cytochromes and other enzymes involved in the electron transport chain [50]. These enzymes are essential for the oxidation of organic compounds and the generation of adenosine triphosphate (ATP), the primary energy currency of the cell. Iron limitation can impair respiratory processes, leading to reduced energy production and growth in marine organisms [51].

Despite its importance, iron is often a limiting nutrient in many marine environments, particularly in the open ocean [52]. This is due to the low solubility of iron in oxygenated seawater and the rapid uptake and utilization of bioavailable iron by marine organisms [53]. As a result, primary producers have evolved various strategies to acquire and utilize iron efficiently, as discussed in the previous paragraphs [42,54]. The ability of these organisms to adapt to iron-limited conditions has significant implications for the structure and function of marine ecosystems, as well as the global carbon cycle, as primary producers play a critical role in the sequestration of atmospheric carbon dioxide through photosynthesis [55].

In marine environments, iron is available from various sources [25], including the atmospheric deposition of dust particles, fluvial input from rivers (main iron source in the Cambrian reefal communities described in this work), hydrothermal vents, sediment resuspension, and glacial meltwater. These sources provide iron in different forms, such as dissolved inorganic iron, organically complexed iron, colloidal iron, and particulate iron [53,56,57]. Marine primary producers, including phytoplankton, cyanobacteria, and macroalgae, have evolved diverse strategies to acquire iron from these sources [58]. Phytoplankton and cyanobacteria can efficiently uptake dissolved inorganic iron, particularly ferric iron, directly from ferric complexes using cell surface reductases that reduce Fe^{3+} to the more bioavailable ferrous iron (Fe^{2+}) [59]. Some cyanobacteria, like *Trichodesmium*, produce siderophores, organic compounds that bind to iron and facilitate its uptake [60]. Macroalgae in coastal environments can acquire iron through both dissolved and particulate pathways, depending on the species and environmental conditions [54].

2.2. Phosphorous Biogeochemical Cycle

Phosphorus is an essential nutrient for all life on Earth, playing a crucial role in various biological processes [45]. Phosphate, the bioavailable form of phosphorus, is a key component of nucleic acids (DNA and RNA), phospholipids in cell membranes, and ATP, the primary energy currency in cells [45]. Phosphate is also involved in cellular signaling, the regulation of enzymatic activities, and bone mineralization in some invertebrates, and vertebrates [61]. The phosphorus biogeochemical cycle involves the transfer of phosphorus between different reservoirs, including rocks, soils, water, and living organisms [37]. The primary source of phosphorus in the biosphere is the weathering of phosphate-bearing rocks, such as phosphatic minerals, on land [37]

Once in the soil, phosphate can be taken up by plants, which incorporate it into their biomass and transfer it to other organisms through food webs [62]. Phosphate in the soil can also be adsorbed onto soil particles, particularly clay minerals and metal oxides, forming complex associations that can limit its bioavailability [37,63]. Additionally,

phosphate can precipitate with cations such as calcium, iron, and aluminum, forming insoluble compounds that further reduce its accessibility to living organisms [64].

Phosphate is transported from land to aquatic ecosystems through various pathways, including surface runoff, subsurface flow, and groundwater discharge. In this regard, rivers play a significant role in the delivery of phosphate to coastal and marine environments, where it supports primary productivity [65]. In the marine environment, phosphate is taken up by phytoplankton and other microorganisms, which form the base of the marine food web [65,66]. As these organisms die and sink to the seafloor, phosphate is incorporated into sediments, where it can be buried for long periods or released back into the water column through various processes, such as upwelling and sediment resuspension [37,66].

2.3. Silicon Biogeochemical Cycle

The silicon biogeochemical cycle is a vital component of the Earth's geochemical processes, playing a crucial role in the distribution and availability of silicon in various ecosystems [35]. Silicon is the second most abundant element in the Earth's crust and is essential for the growth and development of certain organisms [67]. In the biosphere, silicon is primarily present in the form of silica (SiO_2), which is a key component of the cell walls of radiolarians and diatoms [68,69]. These organisms use dissolved silicic acid (H_4SiO_4) to construct their intricate cell walls. Radiolarians and diatoms are responsible for a significant portion of the global primary productivity in aquatic ecosystems and have played a vital role in the carbon cycle [35].

Furthermore, sponges play a crucial role in the marine silica cycle, particularly in the cycling of biogenic silica [70]. Sponges, especially those belonging to the class Hexactinellida (glass sponges) and the subclass Heteroscleromorpha of the class Demospongiae, are known for their ability to produce intricate siliceous skeletons [71]. These sponges take up dissolved silicic acid from seawater and precipitate it as amorphous hydrated silica, which forms the basis of their skeletal structures [72]. The silica uptake by sponges can be substantial, with some species capable of removing up to 95% of the available silicic acid from the surrounding water [73]. Upon the death and decay of sponges, the siliceous spicules are released back into the environment, contributing to the sedimentary silica pool [70,74].

The primary source of silicon in the biogeochemical cycle is the weathering of silicate rocks on land [67,75]. Weathering processes, such as physical disintegration and chemical dissolution, break down silicate minerals, releasing dissolved silicic acid into the soil solution and groundwater [76]. This dissolved silicic acid is then transported to aquatic ecosystems through rivers and streams [77]. In the ocean, diatoms, radiolarians and other siliceous organisms take up dissolved silicic acid from the water column and incorporate it into their cell walls. When these organisms die, their frustules sink to the seafloor, where they accumulate in sediments and contribute to the formation of siliceous oozes [78]. Over geological timescales, these sediments can be transformed into siliceous rocks, such as chert and diatomite [79]. Additionally, upwelling events can bring silicon-rich deep waters to the surface, supporting primary productivity in coastal regions [80].

2.4. Inter-Relationships Between the Silicon, Phosphorous, and Iron Cycles

The interrelationships between the Si, P, and Fe biogeochemical cycles are complex and multifaceted. Interestingly, the delivery of phosphorus and silicon to the oceans is sourced in the same weathering pathways on the different continental materials, particularly igneous substrates [81]. Furthermore, the adsorption of phosphorus onto iron oxides and hydroxides can regulate its availability in marine environments [22,37].

The interconnectedness of the Si, P, and Fe biogeochemical cycles has significant implications for the evolution and development of marine ecosystems, including reef systems [12]. During the early Cambrian, the establishment and expansion of reef ecosystems were likely influenced by the availability of these key nutrients in the oceans [82–84]. Changes in the weathering patterns of silicate, phosphate, and iron-bearing minerals on land, driven by tectonic activity or climatic shifts, could have altered the supply of these nutrients to the oceans, thereby affecting the growth and distribution of reef-building organisms [85].

3. Geological Settings of Las Ermitas Area

The Las Ermitas section, located in the Sierra de Córdoba area of southern Spain (Figure 1A), preserves an exceptional record of early Cambrian sedimentary deposits that provide valuable insights into the paleogeography, paleoenvironmental conditions, and biological diversity of this time period. The section is part of the Pedroche Formation, which unconformably overlies the San Jerónimo Formation [29] (Figure 1B) and represents a transition from the terminal Cadomian to the initial Hercynian orogenic cycles [5]. The Pedroche Formation at Las Ermitas exhibits a SE-NW gradient in its thickness and lithological composition, allowing the identification of three distinct sedimentary sectors: southern, central, and northern (Figures 1C and S1–S3) [29]. The southern sector (Figure 2A), with a maximum thickness of 120 m, comprises a diverse array of facies including detrital and bioclastic nodulose carbonates, silicified limestones with stromatolites, phosphatic limestones, dolomites, and calcimicrobial limestones (Figures 2B and S4A,B). The presence of brecciated limestones with angular and flat intraclasts at the bottom of the southern section suggests formation under shallow, unstable sedimentary conditions (Figure S5).

The central sector records a conglomeratic and silty unit (Figures 3, 4A, 5A,B and 6A–C) followed by several shallowing-upward cycles of calcimicrobial limestones alternating with nodulose limestones, green and purple siltstones, and phosphorites with carbonatic nodules (Figures 6B,C, 7, S6A–C and S7A,B). The Cambrian materials rest on a local paleorelief high (Figure 4A,B; Figures S1 and S3), hosting the thickest reefal facies in the form of calcimicrobial limestones [6,86]. The San Jerónimo Formation in this area is composed of highly eroded andesitic materials with an irregular surface featuring cracks, fissures, and cavities (Figure 8A,B), suggesting a complex dynamic driven by tectonic activity [87]. The northern sector is primarily composed of fine-grained detrital deposits, with ochre silts at the bottom followed by purple and greenish silts with an increasing carbonate content in the form of nodules [29,88].

3.1. Mineral and Geochemical Composition

The XRD analysis (Figure S8A–F) from the samples collected from the different Ermitas areas (Figures S1 and S2) show that the main autochthonous minerals correspond with chamosite ($Mg_{2.5}Fe_{1.65}Al_{1.5}Si_{2.2}Al_{1.8}O_{10}(OH)_8$), trioctahedral illite ($K_{0.5}(Al, Fe, Mg)_3(Si, Al)_4O_{10}(OH)_2$), carbonate fluorapatite ($Ca_{10}(PO_4)_5CO_3F_{1.5}(OH)_{0.5}$), calcite ($CaCO_3$), and α-quartz (SiO_2) [29,88]. Furthermore, glauconite ($K_{0.6\text{-}0}(Fe^{3+},Mg,Al)_2(Si,Al)_4O_{10}(OH)_2$) might also be present as observed in similar materials of Cambrian age [89]. Interestingly, the concentration of ferruginous phyllosilicates and the fluorapatite occurrence is higher in the materials emplaced behind the reefal core than in the samples collected from sections in the southern area, which correspond with the reefal forebasin area (Figures S3 and S8A–F). This is exemplified by samples collected in the southern sections (Figure S8A) which show a lower intensity in the diffraction peaks for the non-soluble phases like chlorite/chamosite and illite (Figure S8B), which, in addition, show a higher increment in the XRD peaks for the carbonate fluorapatite (Figure S8C,D). The higher phosphate concentration was

also identified, through a much more diverse fossil record, in the materials infilling the internal area behind the reefal ridge, resulting from an extensive phosphatization in the Cambrian [22]. The XRD analyses of the carbonates that have not been attacked by acidic solutions (Figure S8E) show a different mineral content which results from the shallowing sequences [29] starting in the greenish facies with a higher content in detrital material and syngenetic minerals (e.g., phosphate and chlorite/chamosite) and ending in reefal mounds, which are primarily composed of calcite. Furthermore, the higher intensity of the feldspars and quartz in the purple siltstones (Figure S8F) suggests that their formation is associated with a higher erosion in the continent. Consequently, the sedimentary sequence in Las Ermitas should start with erosive episodes recorded as purple siltstones, which would end in the formation of calcimicrobial mounds. In between, the sedimentary sequence would be completed by a decreasing phosphate but increasing calcite content from the greenish facies to the archaeocyathid limestones [29,88].

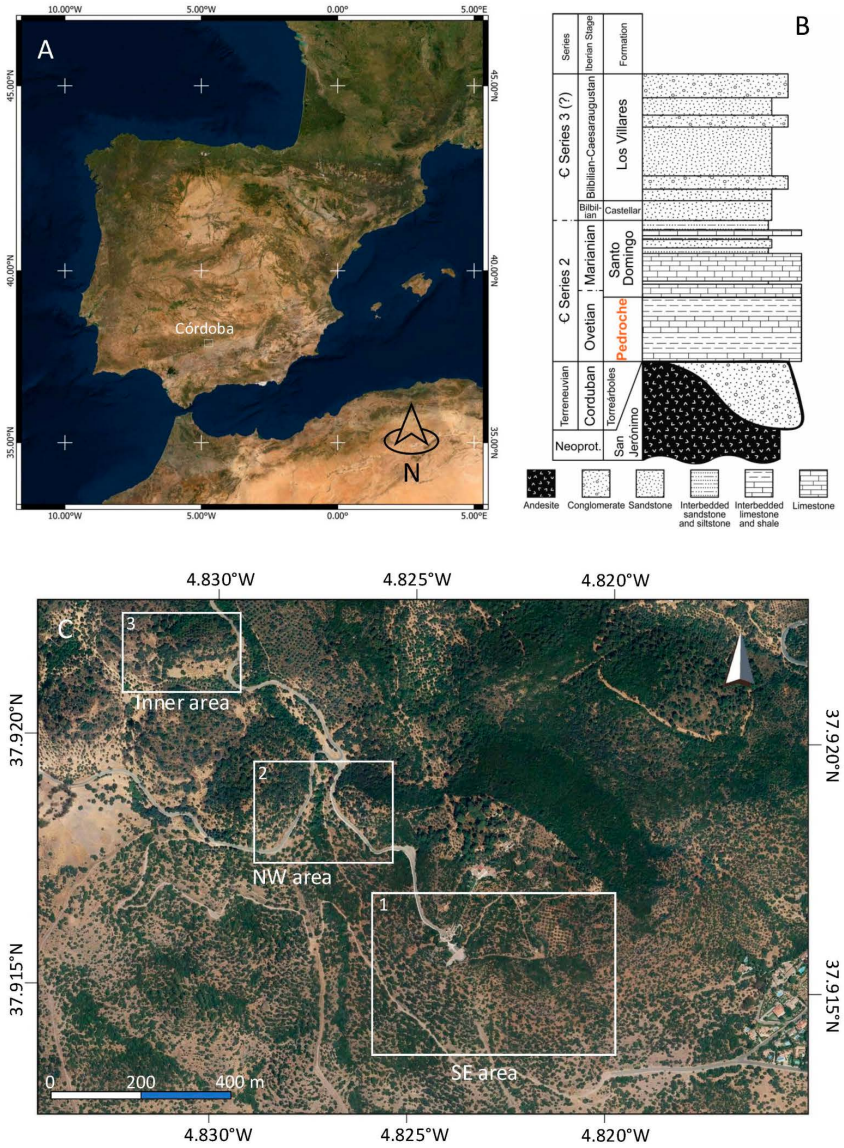

Figure 1. General location and settings of the lower Cambrian Pedroche Formation outcrops. (**A**) The Iberian Peninsula, with emphasis on the study area. (**B**) The chronostratigraphic section of the Sierra de Cordoba region, illustrating the major stratigraphical units, including the Lower Cambrian Pedroche Formation examined in this study (adapted from Creveling et al. [6]). (**C**) Geographical distribution of the three sedimentary areas within Las Ermitas, corresponding to the southeastern (SE), northwestern (NW), and inner regions of the Pedroche Formation at Las Ermitas.

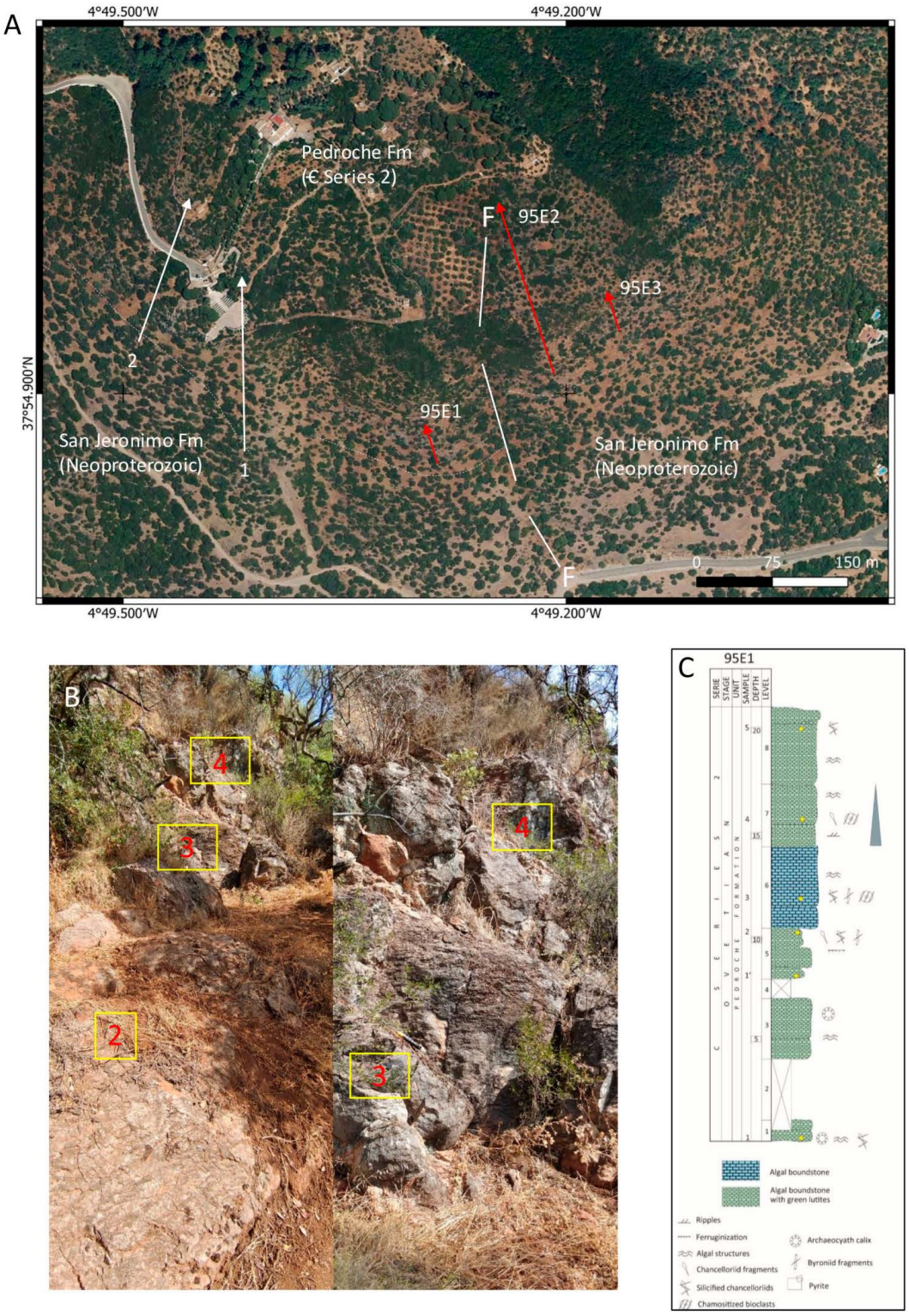

Figure 2. Facies in the SE area of the Pedroche Formation, tracing (**A**) the different stratigraphic columns (95E1, 95E2, and 95E3) as red arrows, and sections 1 and 2 (white arrows) shown in Figure S1), occurring as a resistant scarp in the Las Ermitas hillside. (**B**) Calcimicrobial boundstones, alter-nating with boundstones that contain greenish lutites, corresponding with levels 2 to 5 in (**C**) the 95E1 section.

Figure 3. Image of the NW facies area of Pedroche Formation in Las Ermitas contacting the San Jeronimo Formation (terminal Precambrian to early Cambrian) through a major discordance. Different sections including LE/VIII (Creveling et al. [6]; Moreno-Eiris [86]), 95E5, and 95E7 (Fernandez-Remolar [29]) are traced as white arrows. Numbers 1 to 3 are targeting outcrops, shown in Figure 4A,B; Figure 5A,B and Figure 5C–D; and Figure 7, respectively.

3.2. Paleoenvironmental and Paleogeographical Conditions

The facies distribution, the mineral composition and the paleorelief topology at Las Ermitas indicate the emplacement and development of a reefal complex in the early Cambrian during a transgressive episode [6,29,86]. The reef structure grew on an elevated area with favorable paleoecological conditions for photosynthetic bioconstructions in the form of mounds and bioherms associated with archaeocyathids [11,39,86]. The reefal complex acted as a semipermeable barrier, partially isolating a lagoonal area with distinct paleoenvironmental conditions, which led to the formation of phosphorites and various greenish facies (Figures 6B,C, 7, S6A–C and S7A,B) [29].

The distribution of facies and minerals in the sedimentary record of Las Ermitas is consistent with the formation of a reefal complex that partially enclosed a marginal lagoon. The occurrence of conglomeratic levels with different sedimentary features (e.g., highly imbricated vs heterometric) evidence that the lagoonal area was supplied by a changing alluvial activity (Figure S3) that was likely affected by tectonic activity. The partial isolation of the lagoon by the reefal structure growing on the paleorelief ridge surely limited the oxygen availability, which greatly affected the geochemical conditions in the environment. Furthermore, the sedimentary record in Las Ermitas (e.g., weathering rims in conglomerate boulders and pebbles in Figure 6A) shows that the continental area was exposed to a

high alteration rate supplying the raw chemicals for the mineral formation in the lagoon. The mineral composition of the green siltstones and the phosphorites in the Pedroche Fm of Las Ermitas suggest that the chlorite-like phyllosilicates and the carbonate phosphate resulted from the reduction of the Fe(III)-bearing oxyhydroxide complexes scavenging and transporting phosphate and other ions into the basin [22,90]. Under suboxic conditions, the microbial reduction of Fe^{3+} to Fe^{+2} destabilizes the oxyhydroxide structure and releases the different ionic content into the seawater and the lagoon sediment. In these circumstances, the PO_4^{3-} and Fe^{2+} can reach oversaturation and promote the precipitation of phosphates and ferrous phyllosilicates. While the driving redox conditions leading the mineral precipitation are unknown, the occurrence of small crystals of pyrite (<300 microns) occurring inside phosphatic steinkerns suggests that anoxia happened very locally and at the microscale (Figure 9B). Furthermore, some fossils like hyoliths and mollusk steinkerns display drastic changes in the mineral composition going from phosphate to silica, which is ultimately recrystallized to quartz [91]. The boundary that limits the phosphate and silica areas in the steinkerns shows enrichment in greenish phyllosilicates, which is also evidenced by the abundant silicified archaeocyathid calyxes [29]. Such a mineral occurrence strongly suggests that the solutions promoting the mineral precipitation in the sediment were saturated in silica, which first precipitated as chlorite after the phosphate became undersaturated.

The formation of carbonate phosphate and syngenetic silica-bearing minerals is the result of the silica and phosphate oversaturation in porewaters. As it has been discussed above, the high weathering rates in the volcano-sedimentary materials under a CO_2 atmospheric concentration of >6000 ppm estimated for the early Cambrian [3], would have been the main source of such compounds. While phosphate could also have been sourced from the decomposition of biomolecules, simple mass balance estimations suggest that the release of phosphate from the biological compounds only accounts for a minor amount of the needed phosphorous to precipitate primary francolite [22,37]. Such a calculation can be easily done by considering the total P in las Ermitas phosphatic steinkerns of archaeocyathids, which are marine sponges. The total phosphorous dry weight in modern marine sponges [92] is only <0.35%, while the steinkern fluorapatite contains up to a 20% total weight of phosphorous [93]. In this context, the chloritic compounds would have also formed through a supply of clays from the continent like kaolinite which would have combined with the ferric oxyhydroxides to produce Fe^{3+}/Fe^{2+}-bearing phyllosilicates [94,95].

The phosphatic deposits formed in different energy conditions that were eventually exposed to high energy recurrent episodes concentrating phosphatic elements in condensed levels (Figure S6A,B). The levels are separated by sharp boundaries limited by chlorite-like rims and contain centimeter-sized elements coated by the same ferruginous phyllosilicates, which likely correspond with multiepisodic phosphorites formed by current-induced erosion and sedimentation fluctuations [37]. Their occurrence suggests that the lagoon and, therefore, the whole reefal system were affected by seasonal currents that were likely of a marine origin, as they would not influence detrital materials of continental sources [29].

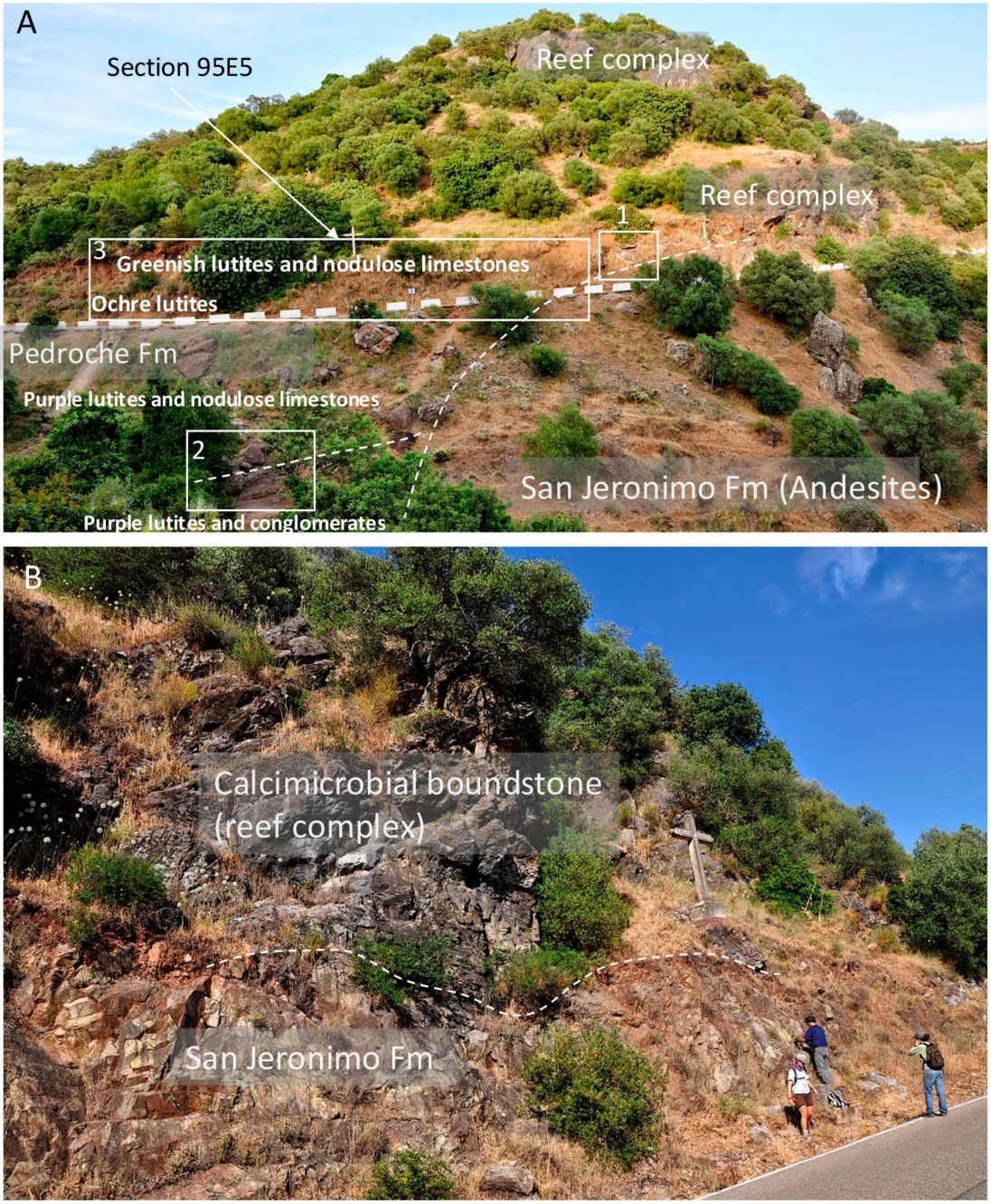

Figure 4. An exploration of the NW outcrops of the Pedroche Formation in Las Ermitas, revealing the facies' variability and disconformity. (**A**) An illustrative depiction showcasing the three distinct sites (1 to 3), as depicted in Figure 3. These locations encompass the following: (1) The boundary between the San Jeronimo and Pedroche Formations, indicating a transition between the different rock units. (2) Conglomeratic and sandy deposits infilling a deep trough, representing sedimentary accumulation in a subsided area. (3) Lagoonal carbonates containing phosphorites, which will be thoroughly examined in Figures 4B, 5 and 7. This configuration demonstrates rapid facies changes within the reefal system. (**B**) A detailed view of the geological sequence, exhibiting andesitic materials from the San Jeronimo Formation, which are unconformably overlain by a calcimicrobial boundstone. This disconformity indicates a significant time gap or erosional event separating the two rock units. The figures provide valuable insights into the facies' variability and disconformity, observed in the NW outcrops of the Pedroche Formation in Las Ermitas. These observations contribute to our understanding of the geological processes shaping the region and highlight the dynamic nature of the Cambrian reefal system.

Figure 5. Detail of sedimentary features at sites 1 and 2. (**A**) Site 1 showcases the complex contact between the Pedroche and San Jeronimo Formations, where microbial carbonates fill cavities and cracks. (**B**) A close-up view of a cavity filled with carbonate, displaying thrombolytic and stromatolitic structures that encrust the walls and ceilings of the volcanic host rock from the San Jeronimo Formation. At site 2 (**C**,**D**), the Pedroche Formation outcrops consist of upward-fining sequences comprising conglomerates, sandstones, and purple lutites that transition into purple nodulose limestones. This sequence indicates the evolution of alluvial fans towards littoral conditions, leading to the formation of the nodulose limestones.

The occurrence of conglomeratic levels with different sedimentary features suggests that the lagoonal area received varying alluvial inputs, likely influenced by tectonic activity and a high continental weathering rate [19]. The XRD analyses of the samples acquired from multiple sites within the Ermitas area (see Section 3.1) reveal that the predominant autochthonous mineral phases are chamosite, trioctahedral illite, carbonate fluorapatite, calcite, and α-quartz. The relative abundances of ferruginous phyllosilicates and fluorapatite are substantially higher in the sediments deposited in the back-reef environment compared to those in the southern reefal fore basin region. This mineral assemblage is congruent with their genesis under conditions typified by a significant influx of various compounds originating from continental sources and transported via fluvial processes, which resulted from intense weathering facilitated by elevated pCO_2 [3].

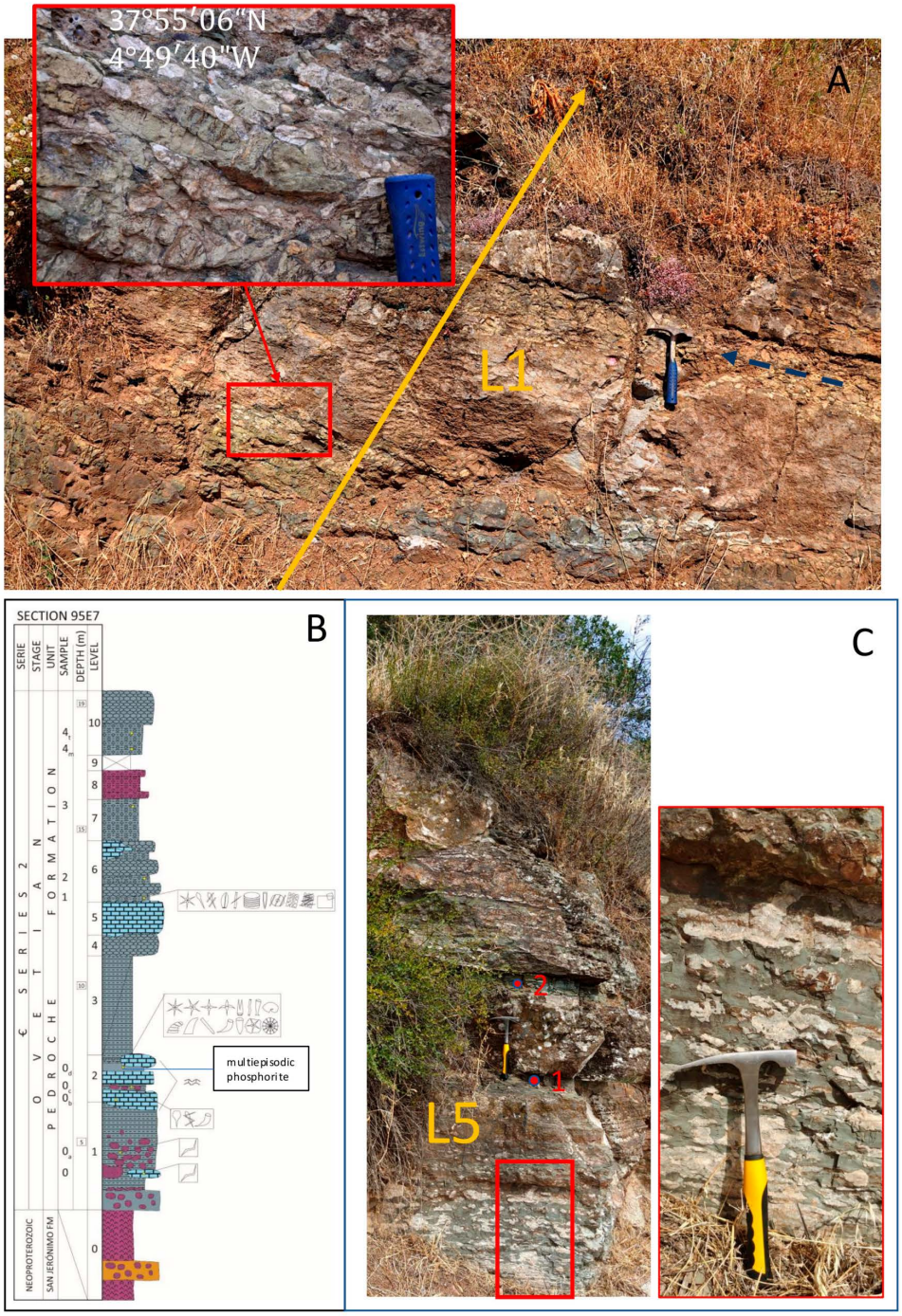

Figure 6. The lithological and sedimentary characteristics of the Pedroche Formation at site 4 provide valuable insights into the paleoenvironmental conditions within the lagoonal area. (**A**) Conspicuous conglomeratic deposits at level 1 (L1) of Section 95E7 (**B**) exhibit the imbrication of elongated pebbles with a discernible weathering aureole. (**C**) Section 95E7 also reveals the presence of alternating calcimicrobial boundstones and greenish nodulose lutites and limestones in level 5 (L5). These variations in lithology suggest dynamic fluctuations in the paleoenvironmental conditions experienced within the marginal lagoon. For a comprehensive understanding of the lithology and paleontological content in column 95E7 (**B**), please refer to the legend provided in Figure 7.

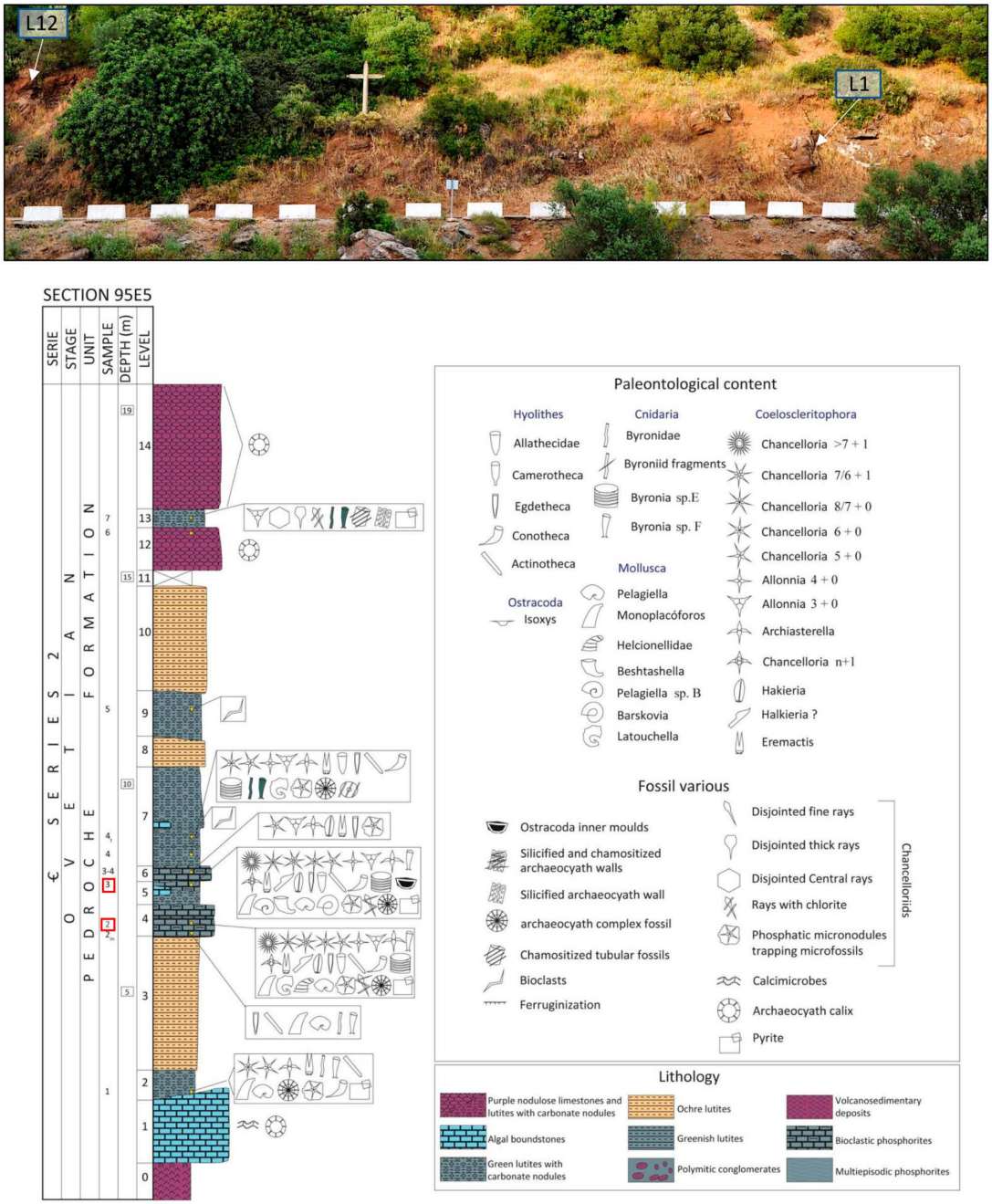

Figure 7. Showcases Section 95E5 at site 3, which served as the sampling location for the organic compound analysis of samples 95E5/2 and 95E5/3. This section exhibits a distinctive assemblage of fine-grained facies, including purple, ochre, and green lutites, interspersed with calcimicrobial boundstones and syngenetic and episodic phosphorites. The observed succession of these facies indicates fluctuations in water energy and oxygenation levels within the lagoon. The greenish materials, such as nodulose lutites and carbonates, harbor a diverse paleontological record. These findings are suggestive of a rich and productive community that thrived within the lagoon. Levels 1 and 12 (L1 and L12) are provided as reference points within the section. Samples 95E5/2 and 95E5/3, subjected to organic analysis using GC/MS and ToF-SIMS techniques, respectively, are indicated by small red squares in the corresponding stratigraphic section below.

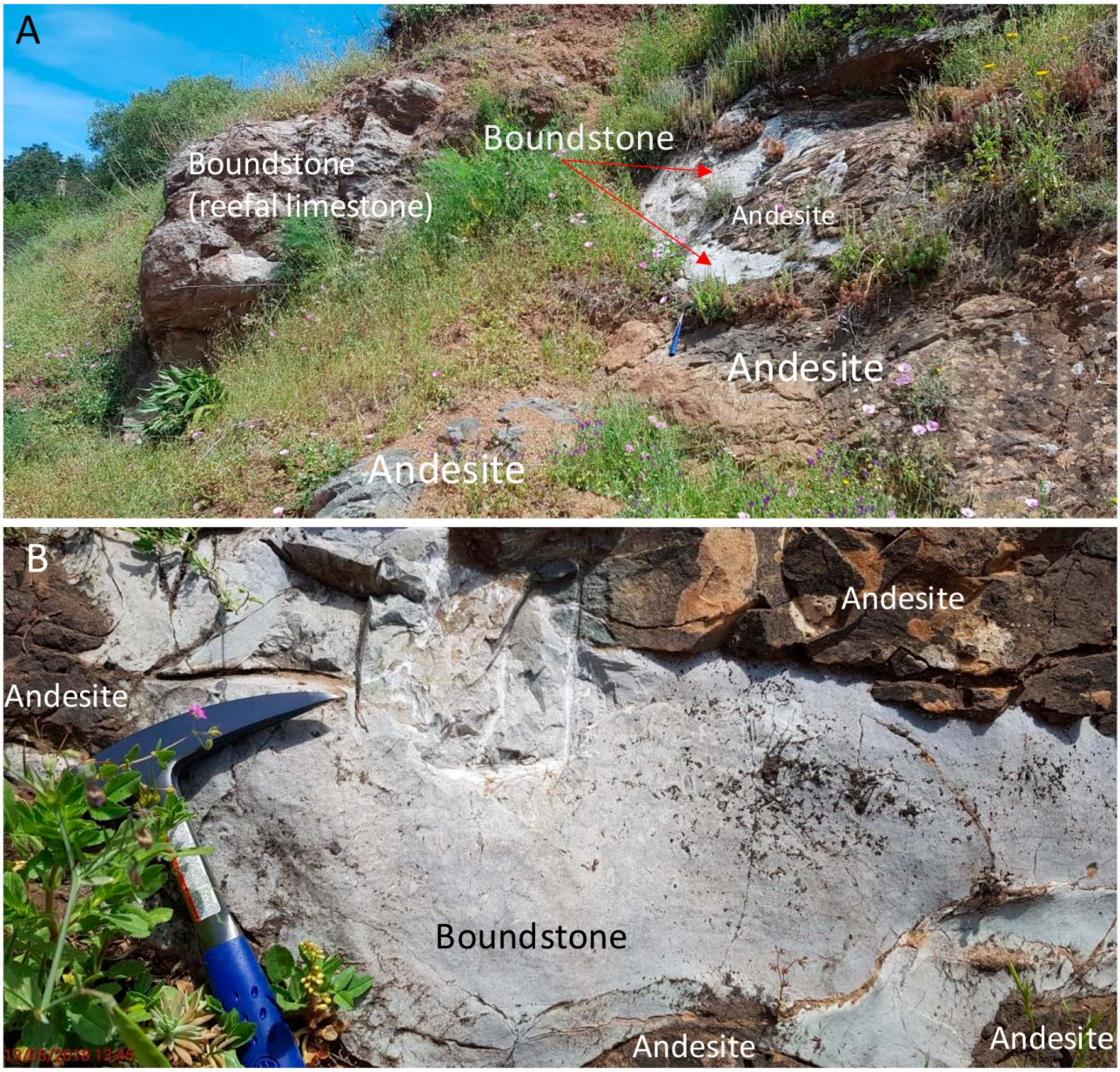

Figure 8. The Pedroche Formation exhibits a complex sedimentary distribution, as illustrated by (**A**) the infilling of cracks and cavities within the San Jeronimo Unit by boundstones. (**B**) A closer view reveals boundstones composed of diverse stromatolitic and thrombolytic microbial structures, which intrude into the volcanic materials of the San Jeronimo Unit.

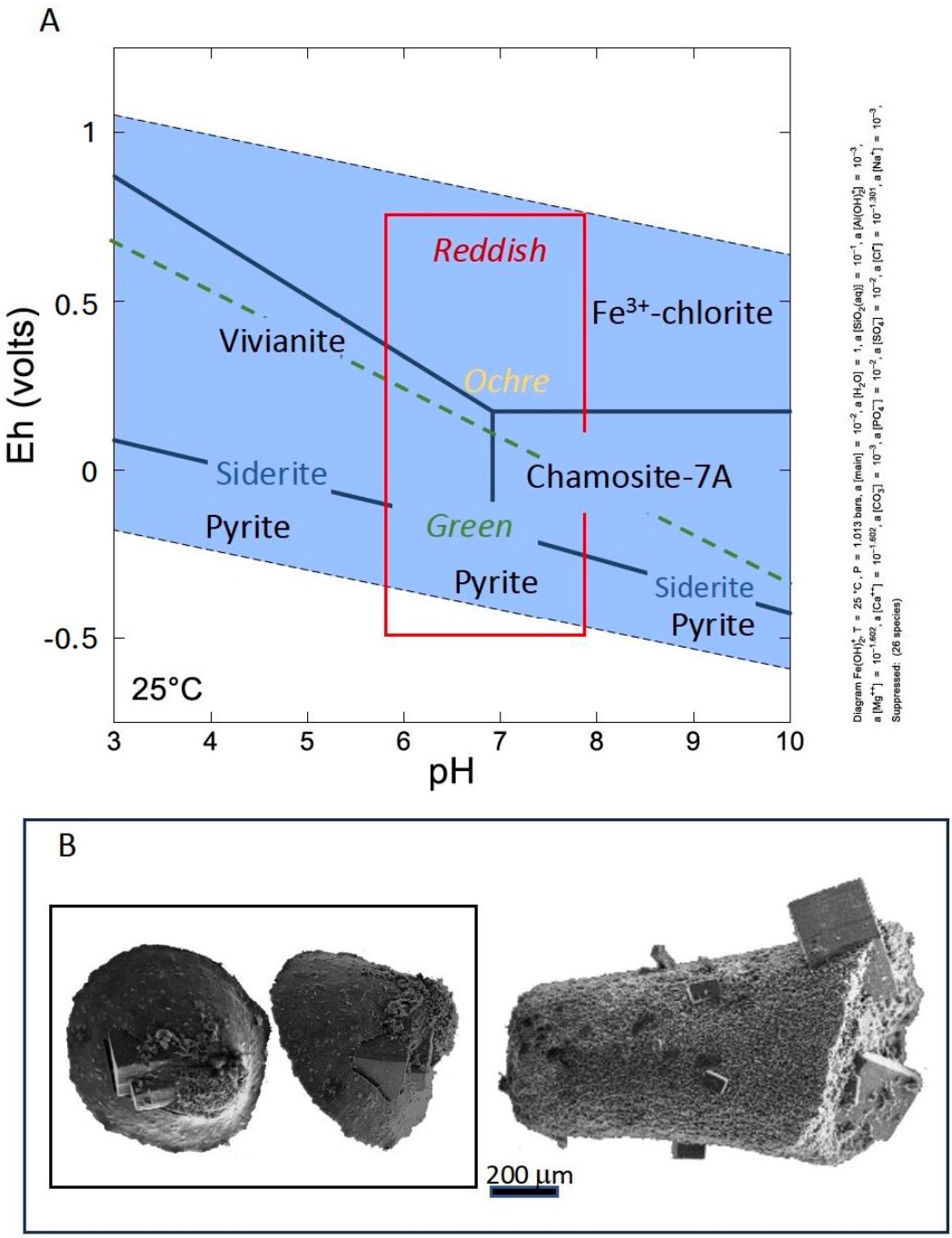

Figure 9. The influence of redox conditions on the mineral composition of the lagoon deposits within the Pedroche Formation depicted in Figure 8. (**A**) The diagram illustrates the pH and Eh stability fields for various minerals found in the sedimentary deposits of the Pedroche Formation, highlighting the varying oxidation states of iron minerals such as hematite (Fe_2O_3), chamosite ($Fe^{2+}{}_2Al_2SO_5(OH)_4$), and pyrite ($FeS_2$), in relation to the distribution of phosphatic minerals represented by vivianite ($Fe^{2+}{}_3(PO_4)_2{\cdot}8H_2O$). Additionally, the diagram indicates the Eh and pH stability ranges for other phosphatic minerals like francolite ($Ca_5(PO_4)_3F$), which serves as a precursor to apatite ($Ca_5(PO_4)_3$). The mineral distribution in this diagram provides insights into the paleoenvironmental changes governed by the availability of oxygen. According to the mineral distribution scheme, the occurrence of different fine-grained deposits, initially composed of clays, follows a sedimentary sequence influenced by an Eh gradient. Under oxidizing conditions, purple deposits form, which subsequently transition to more reducing conditions characterized by the presence of siderite ($FeCO_3$) and pyrite (FeS_2). (**B**) This pattern is evident in the micritic matrix that fills certain skeletal structures and in phosphatic fossil steinkerns that associate with sulfides in form of pyrite cubes.

4. Paleobiological Record

4.1. Fossil Content

To accurately estimate the biogeochemical fluxes of P, Fe, and Si within the reefal system, it is essential to comprehensively evaluate the various components of the paleoecosystem, as these ultimately influence the biomass produced and, consequently, the quantity of organic and inorganic carbon preserved in the record. The Cambrian deposits of Las Ermitas contain a diverse paleobiological record that documents the establishment and development of the reefal ecosystem (Figure S9A). This record is substantiated by the presence of three distinct groups of fossil bodies, including a varied assemblage of phosphatized and/or silicified shelly fossils from the lagoon environment, a diverse association of reef-flanking archaeocyathids, and the reef-forming calcimicrobial structures [32,39–41,91,96]. Interestingly, the observation of thin sections under the microscope from the Las Ermitas paleoecological record also provides evidence that brachiopods and trilobites were likely organisms that, if not abundant, were common components of the lagoon habitat. Furthermore, the inclusion of numerous phosphatized filamentous microstructures and other complex phosphatic elements corresponding to preserved fungi (Figure S9B–E) is noteworthy [32,91,96]. Intriguingly, a significant portion of the reefal and lagoon paleoecosystem, specifically the chemolithotrophic and chemoautotrophic bacteria, was indirectly recorded in the form of ferrous deposits. These deposits will be considered in the estimation of nutrient fluxes within the reefal area. By thoroughly examining each of these ecosystem components, we can construct a comprehensive understanding of the biogeochemical processes that governed the cycling of P, Fe, and Si within the ancient reefal system. Phosphatized external molds in the lagoon deposits might correspond to microbial envelopes of phosphatized fungal mats covering various biogenic elements, such as archaeocyathid calyxes [29,88]. These heterotrophic structures, likely representing fungal colonies subjected to phosphatization, are extensively documented as mineralized hyphal networks intertwined with other biological remains (Figure S9C–E). Additionally, their association with other fossils suggests a highly active decomposing trophic level, further evidenced by the abundant production of ferrous iron in the form of Fe^{2+}-bearing phyllosilicates within the greenish siltstones.

The sedimentary and geochemical conditions favored the preservation of skeletal remains, biasing the record of the paleocommunity diversity (Figure S9A). This process involved the phosphatization and silicification of chitinous exoskeletons of *Byronia*, and ostracods shells [32], and the formation of simple phosphatic to very complex steinkerns composed of phosphate, chlorite, and silica in coeloscleritophorans and hyoliths [32,91,96]. Whether autochthonous or allochthonous, tommotiid fossils were recovered from the forereef area [29,32,96] and, consequently, should not be considered as part of the indigenous biota inhabiting the lagoonal paleoenvironment.

From an autoecological perspective, the preponderance of the taxon *Byronia* [97,98], intimates that the environmental conditions were particularly propitious for sessile, benthic organisms anchored to the substrate. These organisms likely flourished due to the confluence of factors present within the reef's protective confines, which simultaneously offered shelter from turbulent waters and an abundance of nutrients, thereby fostering a highly productive ecosystem. Furthermore, the phosphatized organic walls of *Byronia* indicate that, while they had a soft body covered by a chitinous exoskeleton prone to decay, they were preserved through phosphatization [6,32,99] as a result of a large supply of phosphate into the lagoon. This is also supported by the high abundance of small shelly fossils like *Conotheca*, *Actinotheca*, *Turcutheca*, as well as indeterminate hyoliths and numerous mollusks pointing to a rich diversity of mobile and sessile epifaunal suspension feeders and grazers [100–102], which would include arthropods like trilobites and sessile benthos such as

brachiopoda. These animals would have exploited the nutrients and organic matter in the water column and on surfaces within the lagoon. Furthermore Chancelloridae, represented by phosphatic inner molds in sclerites, were produced by sessile, epifaunal suspension feeders that were an important group inhabiting the lagoonal area [103].

The paleocommunity appears to have had a complex trophic structure with primary producers, suspension feeders, grazers, and likely some higher-level consumers [102,104]. The reef itself, built by calcimicrobes and archaeocyaths, would have provided a physical substrate for sessile organisms to attach to and shelter for mobile fauna [105]. The high abundance and diversity of suspension feeders suggests the lagoonal waters were productive, with abundant nutrients and organic matter delivered by currents or runoff [106]. The dominance of epifaunal and suspension-feeding modes of life, rather than infaunal or deposit-feeding, points to a well-oxygenated benthic environment. Taphonomically, the phosphatization of organic tissues and inner molds allowed the preservation of soft-bodied and lightly mineralized organisms that are not always captured in the fossil record [107]. The lagoonal environment, with calm waters and rapid burial, likely enabled this exceptional preservation.

The paleobiological record of the Las Ermitas Cambrian reefal system reveals a diverse and complex ecosystem, reminiscent of the celebrated Burgess Shale fauna [108]. The paleoecological analysis, based on both abundance and biomass data (Figure S9A), provides a multifaceted view of the community structure, allowing us to draw important parallels and distinctions with other Cambrian ecosystems. The faunal assemblage at Las Ermitas exhibits a remarkable diversity, with over 20 distinct taxonomic groups identified. This diversity is comparable to that observed in the Burgess Shale, although the taxonomic composition differs significantly. As shown in Figure S9A, the community is dominated by mollusks (Helcionellidae, Pelagiellidae) and various small shelly fossils (e.g., Byroniidae, Chancelloriidae), whereas the Burgess Shale fauna was primarily dominated by arthropods.

Following the approach in [108] of considering both numerical abundance and biomass (analogous to the use of biovolume), our data reveal intriguing patterns in the ecological significance of different groups. For instance, while Helcionellidae comprises 15.37% of the total individuals, it accounts for a striking 27.70% of the total biomass, suggesting a disproportionate ecological impact. Conversely, the numerous but small Byroniidae represents 7.76% of individuals but only 5.94% of the biomass. This disparity between abundance and biomass highlights the importance of considering both metrics when assessing the ecological roles of different taxa, a key insight from [108]. The diversity and abundance patterns observed in our data allow us to identify a "trophic nucleus" of dominant species, a concept emphasized in [108]. In the Las Ermitas system, this nucleus appears to consist primarily of Helcionellidae, Pelagiellidae, and Byroniidae, which collectively account for over 30% of both individuals and biomass. This concentration of ecological importance in a few groups mirrors the patterns observed in the Burgess Shale, although the taxonomic composition of the dominant groups differs.

However, it is crucial to note that our understanding of the Las Ermitas ecosystem may be biased by preservation factors. One study [108] emphasized the importance of soft-bodied organisms in the Burgess Shale, which are largely absent from our data. The low representation of groups like Bradoriida in our samples may reflect taphonomic biases rather than true ecological scarcity. This preservation bias underscores the need for caution when reconstructing ancient ecosystems based solely on mineralized remains. Despite these limitations, our data suggests a complex community structure with multiple trophic levels. The presence of various mollusks, chancelloriids, and other small shelly fossils indicates a range of feeding strategies, from suspension feeding to grazing and possibly predation. This ecological diversity, while not as explicitly clear as in the Burgess Shale due to the

absence of soft-bodied fossils, nonetheless points to a well-developed and functionally diverse ecosystem.

Furthermore, the dominance-diversity curve for the Las Ermitas lagoon community (Figure S9F) provides valuable insights into the structure and diversity patterns of this lower Cambrian ecosystem. The curve follows a log-normal distribution, a pattern commonly observed in many natural communities [109]. This distribution suggests a complex community structure where multiple factors influence species abundance, rather than a single dominant factor controlling the ecosystem.

The steep initial decline of the curve indicates that a small number of taxa dominate the biomass in this community. This pattern is consistent with the concept of the "trophic nucleus" discussed earlier, in which a few key species play disproportionately large roles in the ecosystem. In the Las Ermitas community, these dominant taxa are primarily mollusks and small shelly fossils, contrasting with the arthropod-dominated Burgess Shale fauna [108]. The long tail of the curve, representing numerous taxa with a relatively low biomass, suggests the high diversity of rarer species in the community. This feature is often indicative of a stable and mature ecosystem [3]. It is important to note that this curve only represents the preserved biomass, and the absence of soft-bodied organisms due to a taphonomic bias may affect our interpretation of the community structure. Interestingly, the curve lacks clear breaks or discontinuities, which might suggest a lack of distinct ecological guilds or niches within the community. This contrasts with some modern marine ecosystems, in which such breaks are more apparent [4]. However, more detailed analysis would be needed to confirm whether this reflects a true ecological pattern or is an artifact of preservation and sampling. The shape of this dominance-diversity curve for Las Ermitas bears similarities to those described for other Cambrian communities [1,5], suggesting some commonalities in the community structure across different Cambrian ecosystems. However, the taxonomic composition contributing to this structure differs significantly between Las Ermitas and other well-known Cambrian lagerstätten.

The microbial and archaeocyathid reef builders biomineralized to carbonate were also subjected to eventual silicification and phosphatization as external molds and steinkerns (Figures 8 and S9A,B). As a result, the fossil assemblage of Las Ermitas recorded the diversity of the mineralized and/or skeletal-bearing organisms, including the calcimicrobial cyanobacteria consortia-building reefal microbialites, in the form of mounds and bioherms. Although they were mainly composed of microbial algae like *Girvanella*, *Epiphyton*, and *Renalcis* [105,110,111], the whole microbial community in the reefal core would be completed by different chemosynthetic and chemoheterotrophic microorganisms like sulfur-reducing bacteria and methanogens [112,113]. In addition, the specimen abundance and the high number of archaeocyathid genera, identified as up to 30 [40,114], in a small area suggests that sponges, together with the calcimicrobial algae accounted for a substantial part of the productivity of the reefal core, which likely had a significant impact in the total biomass in the whole reefal system.

In this context, the early Cambrian archaeocyath-bearing reefs of the Pedroche Formation in Spain [6] appear to align closely with the Type 2 reefs outlined by Gandin and Debrenne [115]. Type 2 reefs are calcimicrobial thrombolitic framestones, dominated by *Renalcis* with associated low-diversity clusters of archaeocyaths [115]. Creveling et al. [6] report that preliminary research on early Cambrian carbonates suggests skeletons contributed up to ~20% of the total carbonate production, with archaeocyathan material dominating this skeletal input. This aligns with the fact that archaeocyaths in Type 2 reefs typically comprise 10–20% of the reef volume [115]. To estimate the total amount of organic carbon contained in archaeocyaths, we need to consider several factors: the volume of the archaeocyaths in the reef, the proportion of the archaeocyath skeleton that was organic material versus

mineral, and the total volume of archaeocyath-bearing reefs during the early Cambrian. While precise data for all these factors are not available, based on the range provided by these studies, we will use an average of 15% for the volume of archaeocyaths in reefs.

To estimate the primary productivity and biomass of the Las Ermitas lagoon, we can draw comparisons with modern and past reefal systems. In modern reefs, the primary production is mainly driven by benthic algae, with productivity values ranging from 0.5 to ~120 g $C \cdot m^{-2} \cdot d^{-1}$ [116,117]. In particular, the likely presence of Chlorophyta and Rhodophyta in the backreef lagoon would have significantly contributed to the primary production and the overall biomass of the system. In the reef core and certain lagoonal calcimicrobial patches, the primary production was likely driven by microbial mats, which were composed of cyanobacteria and other photosynthetic microbes. Studies of analogous modern microbial communities have revealed that their primary productivity ranges from approximately 1 to 360 g $C \cdot m^{-2} \cdot d^{-1}$ [118,119]. As mentioned above, archaeocyathids are a secondary component accompanying the calcimicrobial community in the reef core and reefal patches, whose productivity should be considered. However, given that those remains correspond with porifera, which were heterotrophic filterers, they were not considered as part of the reef structure primary productivity. Although the question might arise as to whether such organisms, such as some other porifera [120,121], had symbiosis with photosynthetic microorganisms, there is no evidence with which to answer such a question, and they will be not accounted for in the primary productivity estimations and, therefore, in relation to the biogeochemical cycling of carbon and the nutrients like phosphate, iron, and silicon that are considered in this work.

In the Las Ermitas Cambrian reefal system, the energy transfer efficiency from primary producers to higher trophic levels likely followed a similar pattern to that observed in modern shallow marine environments. Lindeman's law estimates that approximately 10% of the energy fixed by the microbial mats, early macroalgae, and potentially green and red algae in the Las Ermitas lagoon would have been transferred to the primary consumers in the ecosystem [122]. This energy would have then propagated through the food web, supporting a diverse assemblage of herbivores, detritivores, and higher trophic levels. However, as mentioned earlier, the actual energy transfer efficiency in the Las Ermitas system may have varied slightly from the 10% average, depending on the specific organisms present and the environmental conditions [123]. Nonetheless, this 10% energy transfer efficiency provides a reasonable estimate for understanding the flow of energy and the trophic structure within this ancient reefal ecosystem, highlighting the crucial role of primary producers in supporting the diverse Cambrian marine community.

4.2. Taphonomic Processes and Fossilization

The fossilization of biological elements, from the living community (biocoenosis) to the death assemblage (taphocoenosis) and the final fossil association [124], plays a crucial role in capturing the nutrient fluxes within the lagoonal system serving as a dynamic sink for them. By characterizing the composition and structure of the various fossilized elements found in the Las Ermitas material, three distinct fossilization processes can be identified: phosphatization, chloritization, and silicification (Figure 9A,B) [29,91,96]. These processes interplayed and maintained a dynamic equilibrium with the sediment and seawater solutions. Variation in the mineralization composition can be attributed to local changes in the sediment solution chemistry (Figure 9A), which are recorded in the composition of the inner molds that fossilize the skeletal structures of organisms such as hyoliths and chancelloriids (Figure 9A). The presence of pyrite as a secondary mineral within the phosphatic molds is particularly intriguing, as it results from the local microbial reduction of sulfate and ferric ions supporting anoxic conditions [125] at the microscale.

In general, the fossil assemblage within the lagoonal materials (Figures 4–8 and S1–S3) is characterized by three distinct components: (1) phosphatic steinkerns or molds filling carbonate shells, such as those of coeloscleritophorans and hyoliths; (2) phosphatized chitinous exoskeletons, exemplified by byroniids; and (3) silicified or chloritized walls, as observed in archaeocyathid. The selective phosphatization of chitinous exoskeletal structures in Cambrian invertebrates, while carbonate structures remain unphosphatized, is a result of several interrelated factors stemming from the inherent properties of the materials and the prevailing geochemical conditions in the depositional environment. Chitin, the primary component of many invertebrate exoskeletons, exhibits higher chemical reactivity compared to calcium carbonate, making it more susceptible to phosphatization during early diagenesis [126,127]. Furthermore, the presence of an organic matrix within chitinous exoskeletons provides a template for phosphate mineralization, offering nucleation sites for the precipitation of calcium phosphate minerals like apatite, which can replace the original chitinous material [128].

The decay processes associated with the degradation of organic matter within chitinous exoskeletons create localized microenvironments characterized by elevated phosphate concentrations and a reduced pH. These conditions favor the precipitation of calcium phosphate minerals, leading to the phosphatization of the chitinous structures [128,129]. In contrast, many Cambrian depositional environments likely had seawater that was saturated or near-saturated with respect to calcium carbonate, promoting the preservation of carbonate structures in their original mineralogy without significant phosphatization [130,131].

The kinetics of phosphatization also plays a crucial role in the differential preservation of chitinous and carbonate structures. The phosphatization process is generally more rapid than the replacement of carbonate by phosphate minerals, allowing chitinous structures to be preferentially phosphatized before carbonate structures are significantly affected [127]. Moreover, the higher permeability of chitinous exoskeletons compared to carbonate structures facilitates the more efficient infiltration of phosphate-rich fluids during early diagenesis, enhancing the phosphatization process in chitinous structures [126].

The formation of phosphatic molds or steinkerns in the early Cambrian is an important mode of preservation that provides valuable insights into the morphology and ecology of early animal life. In the Las Ermitas fossil assemblage, phosphatic molds were formed through the precipitation of phosphate minerals within the void spaces left by the decay of soft tissues, rather than the replacement of carbonatic shells [99]. This process is thought to occur under suboxic conditions, where low oxygen levels favor the release of phosphate ions from organic matter by microbial activity [132,133] and the ferric reduction of iron-bound phosphates in the sediment [37]. In suboxic environments, oxygen levels are very low (<0.5 mg/L) but not completely absent. Interestingly, under these conditions, microorganisms can use alternative electron acceptors for respiration, such as NO_3^-, manganese oxides, and Fe^{3+}, in a sequence determined by their redox potential and oxygen concentration [134]. The formation of phosphatic molds in the Las Ermitas assemblage is likely related to the development of oxygen-deficient conditions within the sediment, which may have been influenced by factors such as high organic matter input and reduced circulation, or increased productivity resulting in the higher demand for oxygen in the lagoonal area.

5. Organic Carbon and $\delta^{13}C_{carb}$ Chemostratigraphy

The analysis of total organic carbon (C_{org}) in Cambrian rocks from Las Ermitas reveals varying concentrations, with the highest being 9.45 wt% and the lowest being 0.03 wt% [88]. The average C_{org} content in the Las Ermitas materials (0.24 wt%) is generally lower than those found in the mixed platform deposits of the Arroyo Pedroche location

(0.51 wt%) [29,86], which lack phosphates but exhibit a higher pyrite content [29,88]. The complementary distribution pattern between phosphate and pyrite (Figure 10A) suggests that the Arroyo Pedroche materials were exposed to open sea conditions, hindering phosphate formation but allowing for lower oxygen availability during early diagenesis, favoring organic matter preservation and pyrite formation.

The carbon isotope composition of the carbonates ($\delta^{13}C_{carb}$) in the Las Ermitas section exhibits a consistent average value of –1.5‰, aligning with the isotopic pattern observed at the upper levels of other Cambrian locations in Cordoba [6]. The correlation of the Pedroche Formation's $\delta^{13}C_{carb}$ record with the radiometrically calibrated Cambrian Terreneuvian-Series 2 $\delta^{13}C_{carb}$ curve establishes an absolute depositional age ranging from 520.93 ± 0.14 Ma to 517.0 ± 1.5 Ma [6]. The age constraints derived from the chemostratigraphic and biostratigraphic analyses of the Pedroche Formation in the Las Ermitas area are consistent with the archaeocyathid biostratigraphy, which shows a strong correlation with the Atdabanian stage of the Siberian Platform [39–41].

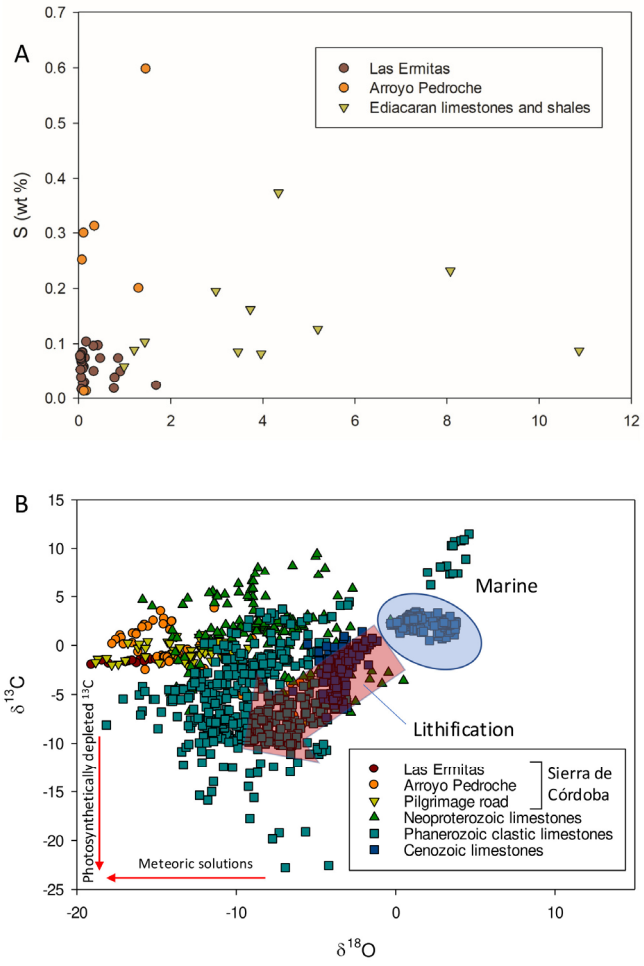

Figure 10. Geochemical scatterplots regarding the organic and inorganic content in the Pedroche Fm. (**A**) The total organic carbon (Corg) against the total sulfur (wt%) from the Cambrian rocks in Las Ermitas, compared with the same unit in the Arroyo Pedroche location [29] and the Edicaran limestones and shales from Central Spain. The scatterplot shows that the Corg average in the Las Ermitas materials is lower than the average content of the organic carbon from the mixed platform deposits of the Arroyo Pedroche location. (**B**) Diagram plotting ^{13}C fractionation ($\delta^{13}C$carb) against ^{18}O fractionation ($\delta^{18}O$carb) from carbonate samples collected in Las Ermitas and other Pedroche Fm outcrops [6]. The oxygen and carbon isotope records in Las Ermitas and the other Cordoba locations align with the Neoproterozoic and Phanerozoic isotopic record, indicating similar diagenetic processes involving meteoric solutions [135].

The chemostratigraphic analysis supports the biostratigraphic assignment of the Pedroche Formation to the lower part of Cambrian Series 2, Stage 3. Furthermore, correlating the $\delta^{13}C_{carb}$ values of the Pedroche Formation to the radiometrically calibrated Cambrian Terreneuvian-Series 2 $\delta^{13}C_{carb}$ curve suggests an absolute depositional age of between 520.93 ± 0.14 Ma and 517.0 ± 1.5 Ma [6], indicating a sedimentation period of approximately 4 million years. Given that the Las Ermitas deposits, which include lagoonal and reefal facies, are correlated with the upper third of the complete Pedroche Formation in the Sierra de Cordoba [6], it can be inferred that the formation of these deposits lasted around 1 million years, assuming a constant sedimentary rate. The temporal framework established through the chemostratigraphic and biostratigraphic analyses provides a basis for estimating the biogeochemical cycling in the reef–lagoon system represented by the Las Ermitas materials. By constraining the depositional age and duration of the Las Ermitas deposits, it becomes possible to assess the rates and dynamics of biogeochemical processes within this ancient marine environment.

The covariation between the $\delta^{13}C_{carb}$ and the oxygen isotope ($\delta^{18}O_{carb}$) composition in the lower section of the Las Ermitas sequence suggests an increased influx of meteoric water associated with a higher supply of photosynthetically depleted ^{13}C, originating from the subaerial recharge area [135]. The oxygen and carbon isotope records in Las Ermitas and other locations in Cordoba align with the Neoproterozoic and Phanerozoic isotopic record (Figure 10B), indicating the influence of similar diagenetic processes involving meteoric solutions.

6. Estimation of Nutrient Fluxes and Paleoproductivity in Las Ermitas Reef–Lagoon System

The procedures employed in this study involve quantifying nutrient reservoirs and sinks within the specific temporal framework of the early Cambrian period, approximately 520 million years ago. Although this approach does not provide precise measurements of energy and matter fluxes, as these parameters are not preserved in the geological record, it offers a valuable estimation of the potential fluxes that supported the emergence and development of the reefal community in a region of the southwestern Gondwana supercontinent.

By carefully examining the available sedimentological, geochemical, and paleontological data, we aimed to reconstruct the nutrient dynamics and their role in the establishment of these ancient reef ecosystems. Despite the limitations imposed by the incomplete nature of the fossil record, this methodology represents an approach to understanding the complex interplay between biogeochemical cycles and the evolution of early marine communities during this pivotal period in Earth's history.

To estimate the chemical composition and flux rates of the solutions that transported nutrients into the lagoonal area, resulting from continental weathering, we employed the Geochemist's Workbench © version 12 [136]. This geochemical modeling software package enables users to simulate a wide range of geochemical processes and reactions, including aqueous speciation, saturation indices calculation, reaction path modeling, and reactive transport modeling.

6.1. Time Framework

As discussed in Section 5, the temporal framework for the early Cambrian reef–lagoonal system of Las Ermitas can be reasonably estimated as 1 million years based on the chemostratigraphic and biostratigraphic analyses of the Pedroche Formation. The $\delta^{13}C_{carb}$ values of the Pedroche Formation, when correlated with a radiometrically calibrated Cambrian Terreneuvian–Series 2 $\delta^{13}C_{carb}$ curve, suggest an absolute depositional age of between 520.93 ± 0.14 Ma and 517.0 ± 1.5 Ma [6], indicating a total sedimentation period of ap-

proximately 4 million years. Given that the Las Ermitas deposits, which include lagoonal and reefal facies, are correlated with the upper third of the complete Pedroche Formation in the Sierra de Cordoba [6], it is reasonable to infer that the formation of these deposits lasted around 1 million years, assuming a constant sedimentary rate. This 1-million-year interval provides a suitable framework for estimating the biogeochemical fluxes within the Las Ermitas reef–lagoon system, as it allows for the assessment of the rates and dynamics of biogeochemical processes within this ancient marine environment over a geologically significant time scale.

6.2. Continental Reservoir for Nutrients

The continental composition and the climatic conditions strongly suggest that western Gondwana was the main reservoir and the source of a great part of the different nutrients that fed the emerging Phanerozoic communities [3,18,22]. The petrological composition of the Neoproterozoic materials preceding the lower Cambrian transgressive deposits [137], which outcrop in South Spain and, particularly, in the Las Ermitas location show that were composed of volcanic rock with varying textures [29,138]. Furthermore, the are some intercalations of sedimentary deposits mainly detrital alternating with some carbonatic levels [139].

The Cambrian volcanic rocks from the Cordoba area in the Ossa-Morena Zone (OMZ) can be classified into two main groups: felsic and mafic lithotypes [140,141]. The felsic rocks are classified as rhyolites, dacites, trachytes, and quartz trachytes, while the mafic lava consists of mainly basalts, often strongly affected by hydrothermal metamorphism [141]. Furthermore, both felsic and mafic volcanic rocks have undergone a late Variscan metamorphic/hydrothermal overprint, which promoted the development of secondary mineral assemblages. This secondary mineralogy hinders the petrographic and mineralogical characterization of the primary rocks [141]. Considering the high petrological diversity observed in the volcanic materials of the Cordoba area, and the predominance of felsic compositions in the deposits of the Las Ermitas outcrops, an andesitic composition is regarded as the most representative for the primary continental reservoir that supplied nutrients to the reefal-lagoonal system. This choice is based on the understanding that andesitic rocks, which are intermediate in composition between felsic and mafic endmembers, can effectively capture the average geochemical characteristics of the heterogeneous volcanic suite.

6.3. Release of Nutrients from the Continental Crust Through Weathering

The weathering of volcanic basements plays a crucial role in the release and subsequent transport of essential nutrients, such as silica, phosphate, and ferric iron, from terrestrial to aquatic environments. When exposed to atmospheric conditions, volcanic rocks undergo chemical weathering, which is primarily driven by the interaction between rock-forming minerals, water, and atmospheric gases, such as CO_2 [142]. For our model, as the volcanic basement is weathered, silicate minerals, such as plagioclases, feldspars and pyroxenes, dissolve, releasing dissolved silica and other elements, including iron and phosphate, into the aqueous phase as dissolved or particulate complexes [143]. In the early Cambrian, with atmospheric pCO_2 levels of around 0.00896 atm and an average temperature of 25 °C, the meteoric solutions could have had a pH of around 5.4 assumming equilibrium conditions [3]. Under the slightly acidic pH conditions prevalent, the released ferrous iron would have been partially oxidized to ferric iron [144,145], with some fraction remaining as dissolved Fe^{2+} in the aqueous phase [146]. The oxidation of ferrous iron to ferric iron would have been facilitated by the presence of dissolved oxygen in the meteoric water, albeit at lower concentrations compared to modern levels. According to most recent studies,

the atmospheric O_2 level during the early Cambrian was likely between 10% and 40% of the present atmospheric level (PAL) [147–149]. This means that the atmospheric O_2 concentration was approximately 2% to 8% by volume, compared to the modern level of about 21%, which ranged between 0.027 to 0.11 mmol·L^{-1} or 0.87 to 3.5 mg·L^{-1}. This is significantly lower than the modern value of 0.27 mmol·L^{-1} or 8.7 mg·L^{-1} calculated for meteoric water in equilibrium with the present-day atmosphere.

The iron oxidation leads to the formation of insoluble ferric iron oxides and hydroxides, which play a significant role in the adsorption and transport of phosphate in fluvial systems [22,37]. As the weathering of the volcanic basement progresses, the released nutrients, including silica, phosphate, and ferric iron, are transported downstream by fluvial streams, ultimately reaching the oceans where they contribute to primary productivity and the biogeochemical cycling of these elements [150].

We employed the react module of the Geochemist's Workbench (GWB) software to simulate the weathering of 1 kg of andesite over one year, using parameters that reflect the early Cambrian environment. The model assumed a slightly acidic pH of 5.4, consistent with higher atmospheric CO_2 levels of the time, and a dissolved oxygen concentration of 0.05 mmol/L, lower than present-day levels. To represent subtropical conditions, we set a meteoric flow rate of 1500 mm/year and a temperature of 25 °C. These parameters created a water-to-rock ratio of 15:1, simulating the interaction between rainfall and the rock surface.

The andesite composition in our model reflected a typical mineralogy, comprising 40% anorthite, 20% albite, 10% annite, 4% phlogopite, 15% hedenbergite, 2% enstatite, 5% magnetite, 3% quartz, and 1% fluorapatite (Table 1). This diverse mineral assemblage allowed us to track the release of various elements, with a focus on iron, aluminum, silicon, and phosphorus, all of which play crucial roles in biological processes.

Table 1. The primary mineral phases in andesite contributing to the continental reservoir of Fe, Al, Si, and P during early Cambrian weathering. The calculations are based on 1 kg of andesite with a density of 2.65 g/cm^3 [151], occupying a volume of approximately 377.358 cm^3.

Mineral	Chemical Formula	Mass (gr)
Anorthite	$CaAl_2(SiO_4)_2$	400
Albite	$NaAlSi_3O_8$	200
Annite (Fe-biotite)	$KFe_3AlSi_3O_{10}(OH)_2$	100
Phogopite (Mg-biotite)	$KAlMg_3Si_3O_{10}(OH)_2$	40
Henderbegite	$CaFe(SiO_3)_2$	150
Enstatite	$MgSiO_3$	20
Magnetite	Fe_3O_4	50
Ilmenite	$FeTiO_3$	20
Quartz	SiO_2	30
Fluorpapatite	$Ca_5(PO_4)_3F$	10

The simulations revealed that under early Cambrian conditions, approximately 167.3 g of the original 1 kg of andesite would dissolve over one year. This significant dissolution rate reflects the enhanced weathering conditions of the time, driven by slightly acidic pH and a subtropical climate. Based on this dissolution, we calculated the release of key elements and compounds.

In the absence of terrestrial plants during the early Cambrian, microbial activity likely played a crucial role in the weathering of the andesitic substrate. Microorganisms can enhance the dissolution of silicate minerals by producing organic acids and forming biofilms, which create localized acidic microenvironments on rock surfaces, thereby accelerating mineral breakdown. Studies have shown that various microorganisms can stimulate silicate

mineral dissolution at near-neutral pH levels [152,153]. Additionally, microbial biofilms can facilitate the chelation and mobilization of cations such as Fe^{2+}, Mg^{2+}, and Ca^{2+}, further promoting mineral dissolution [154,155]. This microbial-mediated weathering would have contributed significantly to nutrient fluxes into marine environments, supporting biogeochemical cycles and the development of early Cambrian ecosystems. While direct evidence from the early Cambrian is limited, modern analogs suggest that such microbial processes were likely instrumental in shaping the geochemical landscape of that era. Furthermore, localized deposits enriched in sulfides, formed through igneous activity, could have provided an additional source of acidic solutions [156]. These sulfide-rich environments, combined with the activity of acidophilic and chemolithotrophic microbes, likely produced sulfuric acid, further enhancing weathering rates by promoting rapid mineral dissolution under highly acidic conditions.

The results showed that in one year, the weathering process would release 18.05 g of iron, 17.42 g of aluminum, 73.31 g of SiO_2, and 0.92 g of PO_4 from 1 kg of andesite (Table 2). Extrapolating these figures to a time scale of 1 Ma provides insight into the long-term nutrient flux from continental weathering. Over this extended period, our model suggests the potential release of 18,050 kg of Fe, 17,420 kg of Al, 78,310 kg of SiO_2, and 920 kg of PO_4 from the same initial mass of andesite. The model, based on a 1 kg sample with a surface area of 100 cm^2, estimates the following annual release rates per square centimeter: 0.0908 $gr{\cdot}yr^{-1}{\cdot}cm^{-2}$ for Fe, 0.5548 $gr{\cdot}yr^{-1}{\cdot}cm^{-2}$ for SiO_2, 0.1227 $g/year/cm^2$ for Al, and 0.0049 $gr{\cdot}yr^{-1}{\cdot}cm^{-2}$ for PO_4^{3-}. These rates reflect the weathering conditions of the early Cambrian, characterized by a slightly acidic pH of 5.4, low dissolved oxygen levels (0.05 mmol/L), and subtropical climate with annual rainfall of 1500 mm. The high release rate of SiO_2 underscores the significant breakdown of silicate minerals, while the substantial Fe and Al release rates indicate the potential for these elements to play crucial roles in early ocean chemistry and biological processes. The lower, yet notable, release rate of PO_4^{3-} suggests a consistent supply of this essential nutrient to early Cambrian marine ecosystems.

Table 2. The annual production of SiO_2, PO_4^{3-}, Fe^{3+}, and Al^{3+} from the weathering of 1 kg of early Cambrian western Gondwana andesite, with estimated total production over 1 Ma used to calculate nutrient fluxes in the early Cambrian Las Ermitas reef–lagoon system. Ca^{2+} is included to demonstrate its high availability, which significantly impacts carbonate oversaturation and high rates of phosphate mineral production.

Ion	$g{\cdot}yr^{-1}$	$g{\cdot}yr^{-1}{\cdot}cm^{-2}$	Total Mass in 1 Ma (kg)
SiO_2	78.31	1.24	78,310
PO_4^{3-}	0.92	0.0146	920
Fe^{3+}	18.05	0.286	18,050
Al^{3+}	17.42	0.276	17,420
Ca^{2+}	14.09	0.223	14,090

Furhtermore, the model predicts a significant release of calcium through the weathering of andesite over geological timescales, with approximately 9947 kg or 248,000 moles of Ca^{2+} released per 1 kg of andesite over 1 million years. This translates to a Ca flux of about 0.0318 $gr{\cdot}yr^{-1}{\cdot}cm^{-2}$ in the lagoonal area. This substantial influx of calcium into aqueous systems could significantly impact carbonate and phosphate supersaturation. The elevated Ca^{2+} concentrations would likely promote higher degrees of supersaturation with respect to calcium carbonate minerals like calcite and aragonite, potentially leading to the increased precipitation of these minerals in the lagoon and similar marine environments. Similarly, the increased Ca^{2+} levels could enhance phosphate mineral supersaturation,

possibly resulting in increased formation of calcium phosphate minerals such as apatite. These processes could have far-reaching effects on biogeochemical cycles in the lagoon, affecting carbon sequestration, phosphorus availability for biological processes, and the overall chemical composition of the lagoonal waters.

7. Discussion

7.1. Nutrient Transport into the Marine Area

The transport of particulate and dissolved ferric iron and phosphate in fluvial streams to the oceans during the early Cambrian would have been significantly influenced by the unique environmental conditions of that time. As discussed above, under a pCO2 of approximately 0.00896 bar and an average temperature of 25 °C [3], the pH of rainwater would have been around 5.4. These slightly acidic conditions would have favored the dissolution of the Gondwanan volcanic basement, producing two different fractions: dissolved and particulate matter, both equilibrated to the environmental conditions [143]. Furthermore, in the early Cambrian, the dissolved and particulate organic iron and phosphorous fractions were likely minor due to the absence of complex terrestrial communities, which means organic production would have been dominated by microbial life [157]. This suggests that the organic iron and phosphorous input from terrestrial areas would have been significantly lower compared to later periods.

The most probable dissolved ferric iron complexes under these conditions would have been Fe^{3+}, $FeOH^{2+}$, $Fe(OH)_2{}^{+}$, $FeH_2PO_4{}^{2+}$, and $FeSO_4{}^{+}$, with the relative abundance of each complex depending on the specific pH and the presence of other ions like phosphate and sulfate [143]. However, the solubility of ferric iron would have been limited by the formation of insoluble iron oxides and hydroxides, such as ferrihydrite ($Fe(OH)_3$), which would have tended to precipitate out of solutions and become a part of the particulate fraction [158]. Furthermore, particulate ferric iron transport would have likely dominated in the early Cambrian, primarily as iron oxides and hydroxides formed during weathering and precipitation processes. These particulate ferric iron phases would have been transported downstream as suspended sediment in fluvial streams and eventually deposited in floodplains, estuaries, or marine environments like the lagoonal area recorded in Las Ermitas [145]. The absence of extensive terrestrial vegetation and limited soil development in the early Cambrian would have reduced the stability of land surfaces and increased the potential for erosion and transport of particulate ferric iron [159]. The lack of rooted land plants during this time would have resulted in higher physical erosion rates and increased sediment transport compared to later periods with widespread terrestrial vegetation. This enhanced erosion and transport would have facilitated the delivery of iron-rich particles to aquatic environments, where they could have played a significant role in the adsorption and cycling of nutrients, such as phosphate.

Phosphate dissolution and transport would have been influenced by the slightly acidic pH conditions, which would have favored the dissolution of phosphate-bearing minerals like apatite. The most probable dissolved phosphate complexes under these conditions would have been $H_2PO_4{}^{-}$ and $HPO_4{}^{2-}$, with the relative abundance of each species depending on the specific pH and the presence of other ions like calcium and magnesium [143]. As mentioned, the dissolved organic phosphate (DOP) input would have been relatively low due to the limited presence of terrestrial organic matter and the absence of extensive terrestrial vegetation. However, some DOP could have been derived from the decomposition of the microbial biomass in continental aquatic environments [160].

Particulate phosphate transport would have occurred primarily through the adsorption of phosphate ions onto the surfaces of iron oxides and hydroxides, clay minerals, and calcium carbonate minerals. The adsorption of phosphate to iron oxides and hydroxides

would have been favored under the slightly acidic to neutral pH conditions, forming stable particulate phosphate phases [6,161]. The adsorption of phosphate onto ferric iron oxides and hydroxides can be represented by the following equation [143]:

$$\equiv\text{Fe-OH} + \text{H}_2\text{PO}_4^- \rightarrow \equiv\text{Fe-H}_2\text{PO}_4 + \text{OH}^-$$

where ≡Fe represents iron at the compound surface.

In addition to ferric iron, aluminum oxides and hydroxides, such as gibbsite ($Al(OH)_3$), could have also played a role in the adsorption and transport of phosphate in the early Cambrian [161]. Aluminum oxides and hydroxides have a high affinity for phosphate and can form stable particulate aluminum-phosphate complexes under slightly acidic to neutral pH conditions. The adsorption of phosphate onto aluminum oxides and hydroxides can be represented by the following equation [143]:

$$\equiv\text{Al-OH} + \text{H}_2\text{PO}_4^- \rightarrow \equiv\text{Al-H}_2\text{PO}_4 + \text{OH}^-$$

where ≡Al represents aluminum at the compound surface.

The formation of stable particulate ferric iron-phosphate and aluminum-phosphate complexes could have limited the availability of both nutrients for biological uptake, acting as a sink for these elements during transport [65]. However, changes in environmental conditions, such as a shift to more reducing conditions or a decrease in the pH, could have led to the release of adsorbed phosphate and ferric iron back into the water, potentially affecting the nutrient dynamics and the primary productivity in downstream environments [145].

Furthermore, during the weathering of andesitic rocks, dissolved silicon and aluminum can form various complexes and colloids that play a crucial role in element transport. These Si-Al complexes often serve as precursors to the formation of clay minerals in the lagoonal area [95,162]. These complexes can remain stable in solution for extended periods, facilitating the transport of both Si and Al from weathering sites, which, after transportation, would become in the backbone of the chamositic minerals in the depositional environments like lagoons. The solubility and transport of these aluminosilicate species in the early Cambrian would have been primarily governed by inorganic factors. Unlike in modern environments, where organic ligands play a significant role, the early Cambrian lacked terrestrial vegetation and complex organic matter. Consequently, the dissolution and mobility of Si-Al complexes would have been more directly influenced by factors such as the pH, temperature, and the ionic composition of the weathering fluids [163].

This inorganic-driven weathering regime would have resulted in a distinct pattern of element release and transport, potentially affecting the composition and distribution of nutrients in early Cambrian lagoonal environments. In the context of early Cambrian shallow marine areas, these Si-Al complexes could have served as an important source of dissolved and colloidal material, potentially influencing the formation of authigenic clay minerals and the bioavailability of silicon and aluminum to early organisms. The gradual transformation of these complexes into clay minerals like kaolinite would have occurred as they encountered changing physicochemical conditions in the lagoonal environment [37,95].

Therefore, the transport of key elements from weathered andesitic sources to lagoonal areas in the early Cambrian should have occurred through a combination of particulate and dissolved forms. Based on our understanding of element behavior under the slightly acidic (pH 5.4) and low-oxygen conditions (0.05 mmol·l dissolved O_2) of the early Cambrian, we can estimate the relative proportions and main chemical species for each element. Iron, being highly sensitive to redox conditions, was predominantly transported as particulate matter (70%–80%), primarily in the form of ferric oxides and hydroxides such as ferrihydrite and goethite, with the remaining 20%–30% likely existing in dissolved

forms [38,144]. Under the slightly acidic conditions (pH 5.4) of the early Cambrian, the most probable dissolved ferric iron complexes would have been Fe^{3+}, $FeOH^{2+}$, $Fe(OH)_2{}^{+}$, and $FeH_2PO_4{}^{2+}$ [143,146,158]. Additionally, $FeCl^{+}$ and $FeSO_4{}^{+}$ would be locally abundant depending on specific conditions in the source area, such as the presence of evaporitic deposits or volcanic inputs that could increase the local chloride or sulfate concentrations [145,164]. This higher proportion of dissolved iron, compared to modern oxidizing environments, can be attributed to the lower oxygen levels of the early Cambrian atmosphere [148]. Phosphorus transport was more evenly distributed between particulate and dissolved forms, with each accounting for approximately 40%–60% of the total phosphorus flux [165]. Particulate phosphorus would have been primarily adsorbed to iron oxides or present in organic compounds, while dissolved phosphorus existed as inorganic phosphate ions ($H_2PO_4{}^{-}$, $HPO_4{}^{2-}$) and dissolved organic phosphorus compounds. This distribution reflects the complex interplay between phosphorus and iron cycling in early Earth conditions [166].

Silicon, being more soluble, was likely transported predominantly in dissolved form (60%–70%) as silicic acid (H_4SiO_4) [167]. The remaining 30%–40% would have been in particulate form, including colloidal silica and silicon incorporated into clay minerals. This high proportion of dissolved silicon would have played a crucial role in the formation of early siliceous organisms and sediments [168].

Aluminum, despite its generally low solubility at a neutral pH, may have had a higher dissolved fraction (10%–20%) in the slightly acidic early Cambrian waters. This dissolved aluminum would have existed as Al^{3+}, $Al(OH)^{2+}$, and $Al(OH)_2{}^{+}$. However, the majority (80%–90%) would still have been transported as particulate matter, primarily as $Al(OH)_3$ and aluminosilicate clays [143,169].

It's important to note that these percentages are estimates based on our estimations of the early Cambrian conditions discussed herein. The actual proportions may have varied depending on local factors such as weathering intensity, runoff rates, and the specific mineral composition of source rocks. Furthermore, the presence of Si-Al complexes, as discussed earlier, would have influenced the transport dynamics of both silicon and aluminum, potentially increasing their mobility in the early Cambrian weathering environment [95,170].

Interestingly, the absence of extensive terrestrial vegetation and limited soil development in the early Cambrian would have resulted in higher physical erosion rates and increased sediment transport compared to later periods [171,172]. This enhanced erosion and transport would have facilitated the delivery of particulate forms to aquatic environments, where they could have played a significant role in the adsorption and cycling of nutrients. These transport mechanisms would have played a crucial role in delivering nutrients and minerals to early Cambrian lagoonal ecosystems, influencing the chemical composition of these environments and potentially impacting the evolution of early life forms. The interplay between particulate and dissolved forms would have affected the bioavailability of these elements, with dissolved forms generally being more readily accessible to organisms [173].

7.2. The Geochemical Distribution of Iron, Phosphate, and Silica in the Biosedimentary Reservoirs of the Las Ermitas Reefal Complex

The diverse sedimentary units and fossilized biotic components within the reef–lagoon system serve as repositories for a significant portion of the total iron, phosphate, and silica budget. This budget represents the cumulative release of these elements over the estimated one-million-year duration of the reef–lagoon complex. Quantifying the total content of these ions and compounds is a crucial prerequisite for elucidating the flux patterns of these nutrients across various reservoirs within the reef–lagoon system. These

reservoirs include, notably, the biosphere compartment, represented in this context by the reef–lagoon paleocommunity.

To achieve a comprehensive understanding of nutrient cycling within this ancient ecosystem, it is imperative to first determine the total nutrient concentrations within the geological and paleontological materials. This foundational data will subsequently facilitate the estimation of nutrient allocation to the biosphere reservoir, thereby providing insights into the biogeochemical dynamics of the paleoenvironment. This approach enables a holistic reconstruction of nutrient pathways and their partitioning among different ecosystem components, offering valuable insights into the functioning of this Cambrian reef–lagoon system. Such an analysis not only enhances our understanding of ancient marine ecosystems but also provides a framework for comparing nutrient dynamics across geological time scales.

In quantifying the nutrient budget preserved within the biosedimentary reservoir, the initial step involves estimating the total volume of the diverse materials recorded in the study area. This estimation can be derived from two key parameters: the total areal extent, which spans 2.24 km^2, and the thickness of various materials corresponding to distinct sedimentary deposits identified within the Las Ermitas sedimentary record (Figure 10A) [29]. Of the total 1.80 km^2 area, approximately 0.26 km^2 comprises the reefal core, composed predominantly of massive calcimicrobial limestone (Figure 10A). This structure constitutes a distinct biosedimentary unit, characterized by its $CaCO_3$ content. Table 3 presents an initial estimation of the various lithofacies identified in the study area, delineated by their respective thicknesses. Notably, the sedimentary sections observed in the Las Ermitas outcrops do not exceed 20 m in thickness. This observation indicates that the exposed outcrops have undergone considerable erosional processes and possible tectonic activity, leading to a substantial decrease in the original thickness of the sedimentary deposits. To address this limitation and obtain a more comprehensive stratigraphic record, an additional sedimentary succession, designated as Los Lagares-1, has been incorporated into the study. This stratigraphic sequence, acquired through subsurface drilling of Cambrian strata by the Instituto Geológico y Minero de España (Spanish Geological Survey), has been largely shielded from the erosional processes and tectonic disturbances that have affected surface exposures. Consequently, it offers a more complete and undisturbed representation of the original depositional environment. The Los Lagares-1 section, in particular, preserves over 100 m of Cambrian sedimentary material, providing a comprehensive record that is analogous to other stratigraphic sections in the region [6].

Los Lagares-1 section is situated in direct proximity to another reef structure, which exhibits a more extensive lateral development compared to the calcimicrobial limestones observed at Las Ermitas. This spatial relationship provides compelling evidence for a more expansive reef–lagoon system in this area. The reef belt associated with this larger structure extends for at least 2 km along the paleotopographic basement ridge, suggesting a significant influence of antecedent topography on reef development and distribution. The most substantial accumulation of calcimicrobial massive limestones is observed at Las Ermitas hill, where the section attains a thickness of approximately 50 m. While this considerable thickness potentially represents the complete temporal development of the reef core, it is crucial to consider the geological evidence of landscape modification in the area. Recent erosional processes have significantly impacted the upper portions of the Lower Cambrian strata in this region [174]. Chemostratigraphic data suggest that the massive reef limestones of Las Ermitas correspond to the uppermost part of the Lower Cambrian sequence in the area [6]. This stratigraphic position supports the inference that the observed thickness of approximately 50 m likely represents the majority of the main reef core, primarily composed of calcimicrobial massive limestones. The significant thickness

disparity between the Los Lagares-1 section (>100 m) and the calcimicrobial limestones at Las Ermitas is consistent with the presence of a paleotopographic relief. This ancient topography appears to have featured a steep gradient descending into a local depocenter, facilitating the accumulation of thicker sedimentary deposits in the lower-lying areas.

Table 3. Comparative analysis of lithofacies thickness and mineral composition across three stratigraphic sections in the Las Ermitas area. Data presented include measurements from the Lagares-1 drilled section and two surface exposures (95E5/5 and 95E5/7). Thickness is reported in meters (m) and as a percentage (%) of total section thickness for each lithofacies. Dashes (-) indicate the absence of a particular lithofacies in the corresponding section.

Lithofacies	Lagares-1		95E5/5		95E5/7	
	m	%	m	%	m	%
Ochre siltstones	-	-	6.80	40.60	-	-
Green siltstones	29.70	28.03	3.10	18.51	3.00	17.96
Green siltstones with conglomerates	-	-	-	-	2.70	16.17
Green siltstones with nodulose limestones	-	-	2.60	15.52	5.10	30.54
Reddish nodulose limestone w siltstones	-	-	4.00	23.88	0.80	4.79
Phosphoritic limestone	-	-	0.40	2.39	-	-
Nodulose limestone	36.85	34.78	4.75	28.36	1.40	8.38
Massive limestone	39.40	37.19	1.90	11.34	3.70	22.16
Total (m)	105.95		16.75		16.70	

Based on these sedimentological observations and interpretations, the quantification of nutrients sequestered within the biosedimentary materials will consider two distinct depositional settings. An average thickness of approximately 100 m is assumed for the lagoon area, while a thickness of 50 m is attributed to the reef core. These estimates provide a framework for assessing the spatial distribution and volume of nutrient-rich sediments across the ancient reef–lagoon system. Utilizing these thickness approximations in conjunction with the areal extent of the deposits, volumetric calculations have been performed for the Lower Cambrian sedimentary units. The results indicate a total volume of $1.8 \cdot 10^6$ m^3 for the lagoon deposits, encompassing the Los Lagares-1 location, while the core reef deposits yield a volume of $1.3 \cdot 10^5$ m^3 (Figure 11A).

The geochemical composition of the Las Ermitas materials was analyzed using Laser Ablation-Inductively Coupled Plasma/Mass Spectrometry (LA-ICP/MS) (Table 4). This analysis focused on Fe, P, Si and Al concentrations in various components of the sedimentary record, including steinkern fossils, the carbonatic matrix, and siltstones. In addition, we analyzed siltstones with nodular limestones, and phosphoritic limestones. The results shown on different plots (Figures 11B,C and 12), reveal a clear correlation between Fe and Al concentrations across all the sample types. This correlation suggests a consistent relationship between these elements in the Las Ermitas depositional environment. To refine our analysis, extreme values of Al and Fe were identified and removed from the dataset. This step was taken to eliminate potential outliers that could skew the results and to focus on the most representative samples.

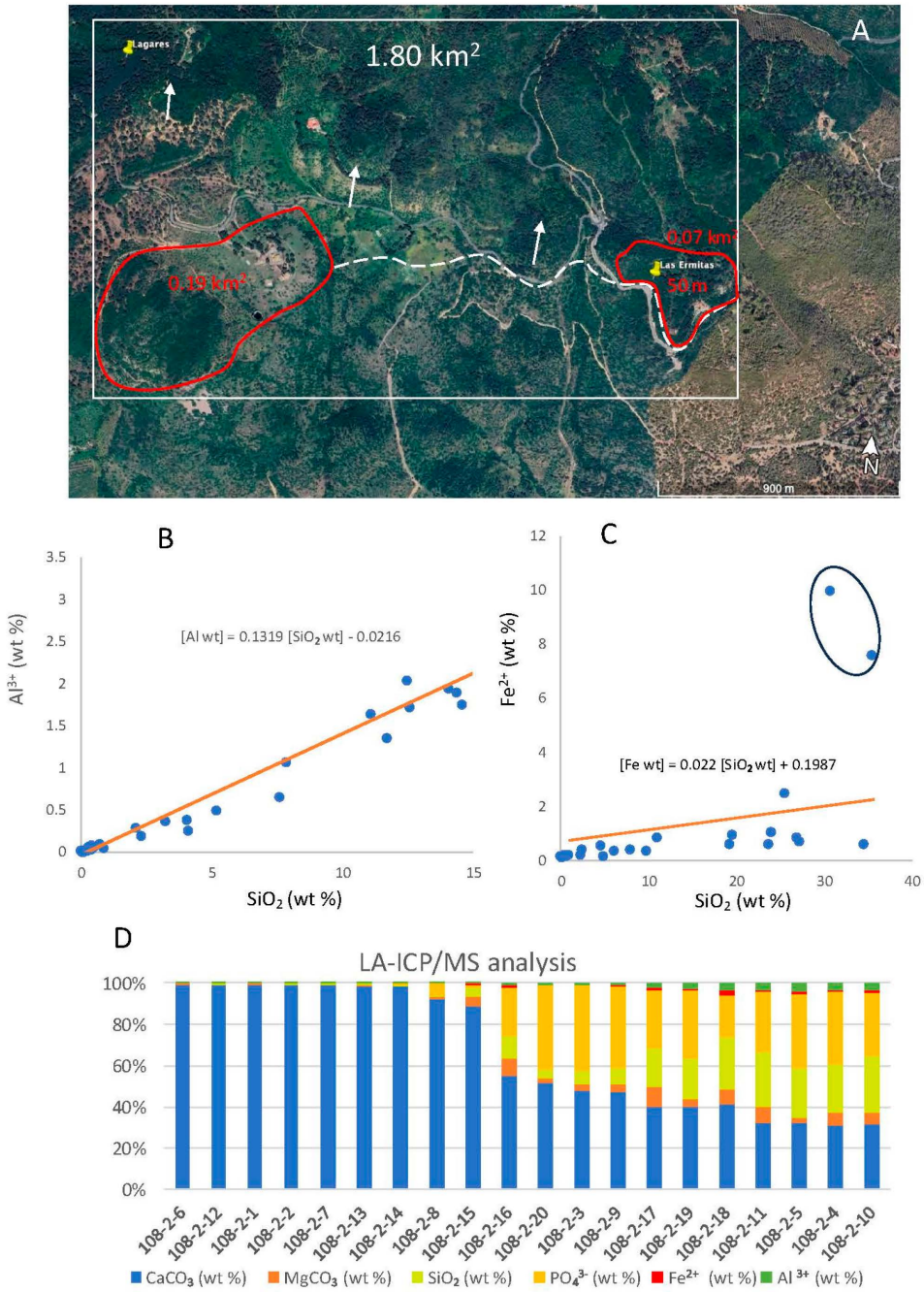

Figure 11. The overview and analysis of the sedimentary materials and the geochemical data from the Las Ermitas area and the Lagares system, integrating the spatial distribution and elemental composition. (**A**) An aerial view showing the spatial extent and volumetric estimation of sedimentary materials within the Las Ermitas and the Lagares areas, covering a total surface area of approximately 1.80 km^2. The outlined regions highlight key sedimentary deposits, with 0.31 km^2 corresponding to the Las Ermitas deposits and 0.07 km^2 to the Lagares area. (**B**) A scatter plot showing the correlation between Al (wt%) and SiO_2 (wt%) in core samples from the Los Lagares drilling, indicating a strong linear relationship ($Al = 0.1353 \times SiO_2 - 0.0216$, $R^2 = 0.97$). (**C**) A scatter plot displaying the relationship between PO_4 (wt%) and $CaCO_3$ (wt%) in the Los Lagares core samples, with notable clustering indicating the carbonate matrix's association with phosphates. (**D**) A bar chart summarizing the LA-ICP-MS results for core samples from the Los Lagares drilling. The compositional distribution is presented as weight percentages (wt%) for key components, including $CaCO_3$, $MgCO_3$, SiO_2, PO_4, Fe, and Al.

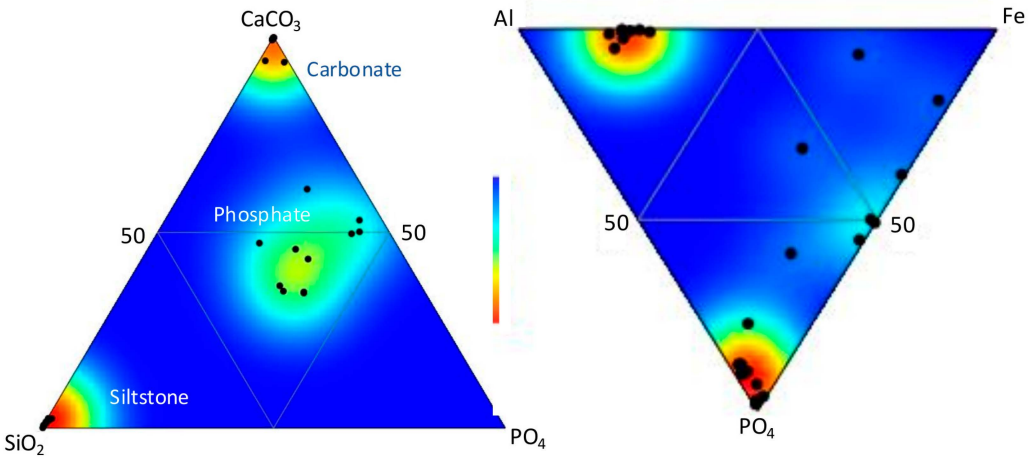

Figure 12. A ternary diagram illustrating the compositional analysis of carbonate and siltstone matrices from lower Cambrian materials in Los Lagares-1, based on the LA-ICP/MS analysis of 30 sampling points. The plot shows the relative proportions of $CaCO_3$, SiO_2, and PO_4, reflecting the composition of these matrices. Most of the data points cluster in the phosphate-dominant region from a fossil steinkern, suggesting a significant phosphatic component in the analyzed materials. This distribution provides insights into the varying compositions of carbonate and siltstone matrices in the sampled lower Cambrian strata.

Table 4. Geochemical composition (wt%) of three distinct lithofacies from Los Lagares-1 materials as determined by LA-ICP/MS analysis. The table presents average concentrations of major ions and compounds including Si, P, Fe, Al, and Ca, based on 30 sampling points across the mineral matrices. Data for calcimicrobial limestone, green siltstone, and phosphatic steinkern illustrate the compositional variability across different depositional environments within the Los Lagares-1 sequence, providing insights into the diverse geochemical conditions during formation. $CaCO_3$ content is included to highlight the carbonate-rich nature of the calcimicrobial limestone facies.

Element/Ion	Calcimicrobial Lmst	Green Siltstone	Phosphatic Steinkern
$CaCO_3$	96.93	1.01	24.80
SiO_2	0.27	69.00	10.10
PO_4^{3-}	0.10	0.21	20.00
Fe^{3+}	0.14	3.23	0.46
Al^{3+}	0.02	11.40	1.30
Ca^{2+}	38.81	0.40	16.27

Following this data refinement, a linear regression analysis was performed allowing us to determine the average concentrations of Al and Fe in the Las Ermitas materials. In the siltstone matrix, the analysis yielded average concentrations of 11.40 wt% and 3.23 wt% for Al and Fe, respectively. On the contrary, both element concentration was lower than 0.15 wt%. These average concentrations are particularly significant as they provide a basis for estimating the total inventory for those elements sequestered in the sedimentary record of the lagoonal environment. By considering an average for Al and Fe concentrations across all sample types—including siltstones, siltstones with nodular limestones, nodular limestones, massive limestones and phosphoritic limestones—we can simplify calculations and obtain a comprehensive view of element sequestration in this paleoenvironment.

To quantify the total nutrient and elemental content sequestered within the sedimentary record of the reef–lagoon system, a comprehensive volumetric and compositional analysis is essential. The system comprises two distinct components: the lagoon deposits, with a calculated volume of $1.8 \cdot 10^6$ m^3, and the core reef deposits, encompassing $1.3 \cdot 10^5$ m^3. To accurately assess the elemental sequestration, it is imperative to determine the density of

each lithofacies present, which necessitates the calculation of average mineral proportions across the total rock volume.

The estimation for the total concentration of elements and nutrients sequestered in the reef–lagoon materials of Las Ermitas, a composite lithofacies distribution model was developed. This model integrates data from three stratigraphic successions: Los Lagares-1 (105.95 m), 95E5/5 (16.75 m), and 95E5/7 (16.70 m). Given the significant discrepancy in thickness, Los Lagares-1 was utilized as the primary reference due to its more comprehensive stratigraphic record. However, to account for the lithological variability observed across the system, data from the shorter successions were incorporated to create a more representative model. This integration resulted in a composite distribution comprising eight distinct lithofacies: nodulose limestone (30%), massive limestone (30%), green siltstones (25%), green siltstones with nodulose limestones (5%), reddish nodulose limestone with siltstones (4%), phosphoritic limestone (1%), ochre siltstones (3%), and conglomerates with green siltstone matrix (2%). The three dominant lithofacies—nodulose limestone, massive limestone, and green siltstones—collectively account for approximately 85% of the total estimated volume. For the purpose of nutrient and element estimation, we focused on the non-detrital components of the system. Consequently, the ochre siltstones and conglomeratic deposits with siltstone matrix, comprising 5% of the total volume, were excluded from the initial calculations due to their presumed detrital origin.

The composite model was then applied to the total estimated volume of the reef–lagoon system to calculate the volume of each lithofacies. Subsequently, geochemical data obtained through LA-ICP/MS analysis (Table 4) were used to estimate the total concentration of elements and nutrients within each lithofacies. This approach allows for a more nuanced understanding of element and nutrient sequestration across the entire reef–lagoon system, accounting for lithological variations observed in different stratigraphic successions. However, it is important to note that this method relies on several assumptions and extrapolations from limited data points. As such, the resulting estimates should be considered as indicative rather than definitive, providing a foundation for further investigation into the geochemical dynamics of the Las Ermitas reef–lagoon system during the Lower Cambrian period.

Furthermore, based on the XRD diffractograms (Figure S8) and lithofacies analysis (Table 3), four primary minerals have been identified as the main sequestering agents for elements in the sedimentary record of the Las Ermitas reef–lagoon system: chamosite ($(Fe^{2+},Mg,Fe^{3+})_5Al(AlSi_3O_{10})(OH)_8$), calcite ($CaCO_3$), francolite ($Ca_{10}(PO_4,CO_3)_6F_{2–3}$), and quartz ($SiO_2$). To quantify the total amount of nutrients and elements sequestered within the sedimentary rock volume, it is essential to consider both the relative abundances and densities of these minerals. The relevant mineral densities are as follows [175,176]: chamosite (3.15 gr·cm^{-3}), calcite (2.71 gr·cm^{-3}), francolite (3.15 gr·cm^{-3}), and quartz (2.65 gr·cm^{-3}).

Based on the geochemical analysis of the carbonatic matrix (Table 4) and corroborating X-ray diffraction data (Figure S8), calcite constitutes approximately 97 wt% of the composition, with trace amounts of other elements present. Given this high calcite content and the minor presence of phosphate and pyrite, we propose a slightly adjusted density of 2.75 gr·cm^{-3} for these carbonate-dominated lithofacies. This value reflects a modest increase from pure calcite (2.71 gr·cm^{-3}) due to the incorporation of denser accessory minerals [29].

Further analysis of the siltstone lithofacies reveals a composition dominated by chamosite and quartz in approximately equal proportions, with a slight predominance of quartz (Figure S8B). X-ray diffraction patterns demonstrate a pronounced quartz peak at 3.35 Å, which surpasses in intensity the primary chamosite peak at 7.10 Å. However,

the diffractogram exhibits multiple significant chamosite peaks distributed throughout the pattern, indicative of its substantial presence in the mineral assemblage. Considering these observations, we might estimate a ratio of approximately 55%–60% quartz to 40%–45% chamosite in this sample. Such a mineral composition would be characteristic of a quartz-rich chloritic siltstone. This type of siltstone would represent a fine-grained clastic sedimentary rock with a significant clay mineral component alongside abundant quartz grains. The presence of both minerals in such proportions suggests a depositional environment that supplied both terrigenous quartz and iron-rich clay minerals, consistent with a lagoonal setting where both terrestrial input and marine chemical precipitation could occur. Given these mineral proportions and their respective densities (quartz at 2.65 g·cm^{-3} and chamosite averaging 3.15 gr·cm^{-3}), we can estimate the density of this siltstone to be approximately 2.87 gr·cm^{-3}.

Using the inferred density for each lithofacies, Table 5 presents the total estimated sequestration of key nutrients and elements within the Las Ermitas Reef–lagoon system over a 1-million-year period. The calculations consider the volumetric proportions of distinct lithofacies in both the lagoon and reef core, as well as the distribution of siltstone versus limestone components. The table provides elemental quantities (SiO_2, PO_4, Fe, Al, and $CaCO_3$) in grams, illustrating the varying contributions of each lithofacies to the overall nutrient budget. Notably, the massive limestone reef core is treated separately due to its distinct depositional environment, while detrital materials in specific lithofacies are excluded from nutrient estimations.

Table 5. Estimated total amounts of nutrients and elements sequestered in the Las Ermitas Reef–lagoon system over a period of 1 million years, based on a lagoon volume of $1.8{\cdot}10^{12}$ cm^3 and a reef core volume of $1.3{\cdot}10^{11}$ cm^3. Values are presented for each lithofacies, showing their volumetric percentage and the proportion of siltstone versus limestone components. Quantities of SiO_2, PO_4, Fe, Al, and $CaCO_3$ are given in grams. The '-d-' notation indicates detrital materials not considered in the nutrient estimation. The massive limestone (reef core) is presented separately due to its distinct depositional environment.

Lithofacies	Volume %	Siltstone vs. Limestone Component		SiO_2	PO_4	Fe	Al	$CaCO_3$
		Siltstone	Limestone					
Ochre siltstones	3.00	-d-	-d-	-d-	-d-	-d-	-d-	-d-
Green siltstones	25.00	1.00	0.00	$1.07{\cdot}\times 10^{11}$	$3.26{\cdot}\times 10^{8}$	$5.01{\cdot}\times 10^{9}$	$1.77{\cdot}\times 10^{10}$	$1.55{\cdot}\times 10^{9}$
Green siltstones with conglomerates	2.00	-d-	-d-	-d-	-d-	-d-	-d-	-d-
Green siltstones with nodulose limestones	5.00	0.80	0.20	$1.43{\cdot}\times 10^{11}$	$4.84{\cdot}\times 10^{8}$	$6.76{\cdot}\times 10^{9}$	$2.36{\cdot}\times 10^{10}$	$4.82{\cdot}\times 10^{10}$
Reddish nodulose limestone with siltstones	4.00	0.90	0.10	$1.29{\cdot}\times 10^{11}$	$4.11{\cdot}\times 10^{8}$	$6.05{\cdot}\times 10^{9}$	$2.12{\cdot}\times 10^{10}$	$2.11{\cdot}\times 10^{10}$
Phosphoritic limestone	1.00	0.00	1.00	$1.61{\cdot}\times 10^{7}$	$1.63{\cdot}\times 10^{7}$	$7.19{\cdot}\times 10^{6}$	$1.73{\cdot}\times 10^{6}$	$3.75{\cdot}\times 10^{7}$
Nodulose limestone	30.00	0.10	0.90	$1.40{\cdot}\times 10^{12}$	$1.66{\cdot}\times 10^{9}$	$6.89{\cdot}\times 10^{9}$	$1.80{\cdot}\times 10^{10}$	$1.30{\cdot}\times 10^{12}$
Massive limestone	30.00	0.00	1.00	$4.01{\cdot}\times 10^{9}$	$1.49{\cdot}\times 10^{9}$	$2.08{\cdot}\times 10^{9}$	$2.97{\cdot}\times 10^{8}$	$1.44{\cdot}\times 10^{1}$
Massive limestone (reef core)	100.00	0.00	1.00	$9.65{\cdot}\times 10^{8}$	$3.58{\cdot}\times 10^{8}$	$2.73{\cdot}\times 10^{10}$	$8.09{\cdot}\times 10^{10}$	$3.47{\cdot}\times 10^{11}$

The decision to use a single average for all these diverse sedimentary components was made to streamline the estimation process. While this approach may not capture the nuanced variations between different lithologies, it provides a practical and representative estimate of the overall Al and Fe content in the Las Ermitas formation. These findings offer important insights into the geochemical composition of the Las Ermitas formation and its capacity to sequester elements. The consistent relationship between Fe and Al across different sample types suggests uniform depositional conditions or similar source materials throughout the lagoonal environment, which is consistent with a weathering source (Figure 13A).

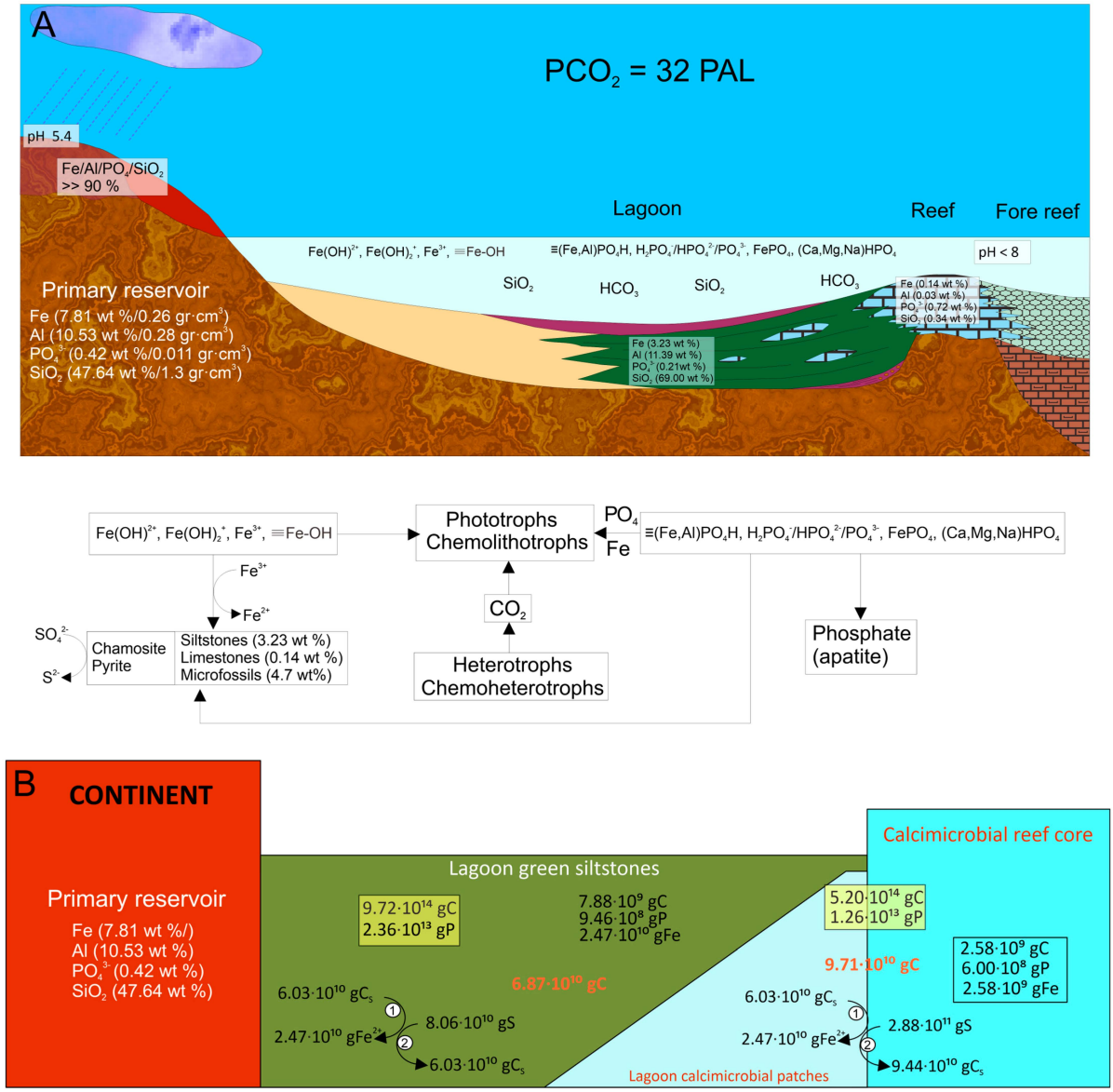

Figure 13. Overview of nutrient reservoirs, geochemical pathways, and organic distribution within the Las Ermitas system. (**A**) Schematic representation of the main reservoir composition of key elements and nutrients, including Fe, Al, PO_4, and SiO_2, across the Las Ermitas paleoenvironment. The system is divided into the primary reservoir, lagoon, reef, and fore reef, with associated pH and compositional gradients. Biogeochemical processes are highlighted, illustrating the interplay between phototrophs, chemolithotrophs, and heterotrophs in cycling carbon, phosphorus, and iron. Phosphate deposition (as apatite) and its interactions with microbial communities are detailed. (**B**) Distribution of organic carbon in the Las Ermitas system, categorized by lithology shown in Table 5. The total carbon estimation aligns with values derived from modern reefal systems, as described in the text, providing a comparative baseline for understanding the productivity and carbon dynamics of the Las Ermitas paleoenvironment.

The elemental analysis of Las Ermitas materials reveals an enrichment of Fe and Al within microfossils compared to the limestone matrix (Table 4). This phenomenon aligns with the role of microfossils as elemental traps in sedimentary environments [99]. The data indicate that microfossils contain the average concentrations of both Al (1.30 wt%) and Fe (0.46 wt%), exceeding the levels observed in the carbonatic matrix. This preferential accumulation can be attributed to several mechanisms. Microfossils, with their intricate structures and high surface areas, serve as excellent substrates for elemental adsorption and

incorporation. The process may involve surface adsorption, elemental substitution within the crystal structure during diagenesis, and the precipitation of secondary minerals within pore spaces. Furthermore, the association of Fe and Al with phosphates, as suggested by Crevelling et al. [22], may play a crucial role in this enrichment, given the propensity of phosphates to co-precipitate or form complexes with these elements. Interestingly, microscopic examination of the microfossil molds reveals that the phosphatic components are either intergrown with or succeeded by highly crystalline chamosite and silica-rich phases. This observation suggests an enrichment of SiO_2, Al, and Fe in the mineralizing fluids that permeated the skeletal structures during fossilization [88,91].

Furthermore, early mineralization of biological remains can enhance their capacity to incorporate Fe and Al, particularly through the creation of microenvironments conducive to the precipitation of Fe and Al-bearing minerals during organic matter decomposition powered by microbial chemoheterotrophic activity [177]. Additionally, the potential for biological concentration during the lifetime of the organisms that formed these microfossils cannot be discounted, suggesting that elevated levels of Fe and Al may have been present prior to fossilization.

The enrichment of Fe and Al in microfossils has significant implications for paleoenvironmental reconstruction and geochemical cycling. It may serve as an indicator of terrigenous input or changes in water chemistry that favored the precipitation of Fe and Al-bearing phases. Moreover, this phenomenon underscores the role of microfossils as important sinks for these elements, potentially affecting their availability and distribution in ancient water columns.

7.3. Weathering Flux and Reef–Lagoon Sequestration Balance

The analysis of element accumulation in lagoon deposits, when compared to the weathering rates of andesitic rocks, provides intriguing insights into the intensity of weathering processes during the late Neoproterozoic to the early Cambrian period. Our calculations, based on the assumption of an andesitic continental composition, suggest a remarkably high rate of weathering during this crucial time in Earth's history. The data indicate that to account for the observed elemental accumulations in lagoon deposits over a period of 1 million years, the weathering rates of the andesitic continent would need to be significantly higher than initially assumed (Table 6). On average, the required weathering rate is 23.22 times greater than the baseline rate for andesitic weathering estimated by GWB software modeling. This suggests an environment of intense chemical and physical weathering during the Neoproterozoic-Cambrian transition. Particularly noteworthy is the extremely high weathering rate required for calcium, at 87.70 $kg \cdot yr^{-1}$ per kilogram of andesite, which is nearly four times the average rate for all the elements studied. This could indicate either an enrichment of calcium in the continental crust of the time, or more likely, additional sources of calcium from different marine sources, including recycling from skeletal organisms [140].

Table 6. Comparison of andesite weathering rates and accumulated element amounts in the early Cambrian lagoon deposits over 1 Ma. The table shows the weathering rates ($g \cdot kg^{-1} \cdot yr^{-1}$) for key elements from andesite, their accumulated amounts (g) in the lagoon deposits, and the required andesite weathering ($kg \cdot yr^{-1}$) to balance the observed accumulation.

Element/Nutrient	Weathering Rate ($g \cdot kg^{-1} \cdot yr^{-1}$)	Accumulated Amount (g)	Required Weathering ($kg \cdot yr^{-1}$)
SiO_2	79.90	$4.94 \cdot 10^{11}$	6.18
PO_4	0.95	$4.74 \cdot 10^{9}$	5.01
Al	17.74	$8.09 \cdot 10^{10}$	4.56
Fe	18.42	$2.33 \cdot 10^{11}$	12.65
Ca	14.37	$1.26 \cdot 10^{12}$	87.7

The analysis suggests that continental weathering was intense, likely due to significant sink mechanisms such as saprolite and laterite formation. However, this interpretation is based on several assumptions that require further validation. The weathering rate estimation methodology employed a simplified approach, utilizing an average andesitic composition derived from Neoproterozoic and early Cambrian volcanic rocks underlying carbonate deposits in Spain [141]. This generalized composition may not accurately represent the specific weathered material under investigation. Furthermore, the weathering calculations were performed using basic geochemical modeling through GWB, which may introduce computational inaccuracies. Despite these methodological limitations, the geological evidence strongly indicates that a substantial proportion of the weathered material underwent minimal or negligible transportation. This observation supports the hypothesis of intense in situ weathering, although the precise extent and nature of this weathering require additional investigation.

This interpretation is corroborated by the presence of extensive and, to a considerable degree, substantial lateritic and saprolitic units observed in various regions of Gondwana, affecting the Neoproterozoic to early Cambrian basement rocks [178]. The presence of these weathering products has been documented in regions that occupied high paleolatitudes during the Neoproterozoic-Cambrian transition, providing compelling evidence for elevated thermal conditions during this crucial period of Earth's history [179]. Furthermore, saprolitic materials have been identified in association with a paleokarst system that affects the lower Cambrian carbonate strata correlative with the Pedroche Formation of Las Ermitas [180]. This geological relationship provides compelling evidence for the regional fractionation of nutrients and other essential elements mobilized through continental weathering processes.

The spatial and temporal coexistence of saprolite formation and karstification provides compelling evidence for intense weathering processes occurring contemporaneously with the development of reefal carbonates [180]. This synchronicity suggests that while the release of nutrients and other elements was ongoing, their flux in marine environments was modulated by fractionation mechanisms associated with continental alteration processes. The juxtaposition of these geological phenomena indicates a complex interplay between terrestrial weathering and marine sedimentation during this period. The formation of saprolites, characterized by extensive chemical weathering, likely served as both a source and a sink for various elements. Concurrently, the development of karstic features in the carbonate substrates suggests a dynamic hydrological regime, potentially influencing element transport and deposition. This geological scenario implies that the geochemical signatures preserved in the reefal carbonates may not directly reflect the intensity of continental weathering. Instead, they likely represent a signal that has been filtered through terrestrial alteration processes, with certain elements preferentially retained in continental settings.

The prevalence of these weathering products indicates that a specific confluence of climatic and geochemical conditions prevailed during this period. The geochemical environment was likely characterized by a mildly acidic pH, estimated to be approximately 6, resulting from the partial buffering of meteoric waters, if had an initial pH of ~5.4 in equilibrium with the atmospheric CO_2. Concurrently, atmospheric oxygen levels are hypothesized to have exceeded 20% PAL [3]. This unique combination of factors appears to have created the optimal conditions for the precipitation and accumulation of various mineral phases enriched in iron, aluminum, and silica. Moreover, it is plausible that substantial quantities of phosphorus were also sequestered within these formations. The preferential concentration of these elements in such weathering profiles can be attributed to their differential mobility under the prevailing physicochemical conditions, limited by

the redox and pH [146]. Of particular note is the capacity of these iron- and aluminum-rich weathering products to effectively sequester phosphate through adsorption processes [181].

While direct evidence is limited, it is plausible that the development of extensive lateritic profiles during the Neoproterozoic–Cambrian transition significantly influenced global phosphorus cycling. The high adsorption capacity of iron and aluminum oxides in these weathering products may have sequestered substantial amounts of phosphate in continental settings, potentially reducing the flux of this essential nutrient in marine environments. The observed concentrations of essential nutrients, specifically iron, aluminum, and phosphate, within the Las Ermitas reef–lagoon complex can be attributed to two primary processes: the formation of saprolite and the subsequent fractionation of phosphate. These interrelated geochemical mechanisms likely played a crucial role in determining the ultimate distribution and abundance of these elements within the sedimentary system.

Moreover, additional sedimentary sinks likely played a significant role in the sequestration of silica, aluminum, iron, and, by extension, phosphate (Figure 13A). These sinks potentially included lacustrine systems and shallow transitional marine environments. Compelling evidence for this sequestration process is found in the siltstone deposits at the upper part of the San Jeronimo and Torrearboles formations [139], which are heterochronous with the Pedroche Formation and, consequently, with the Las Ermitas materials. These siltstone units exhibit notable enrichment in iron oxides, occasionally manifesting as thin laminar deposits. Such features strongly indicate elevated rates of ferric oxyhydroxide production during this period [138]. The presence of these iron-rich deposits is particularly significant due to the high phosphate adsorption capacity of ferric oxyhydroxides. The presence of saprolite formation is further corroborated by the alteration rims observed on boulders and pebbles within the basal conglomeratic units of Las Ermitas (Figure 6A). These weathering features provide indirect evidence of extensive chemical weathering processes active during the depositional period.

This temporal ubiquity of iron-rich deposits implies that the geochemical conditions favorable for ferric oxyhydroxide formation and subsequent phosphate adsorption were not restricted to a single, brief interval. Rather, they appear to have been a recurring or continuous feature of the regional paleoenvironment. Consequently, it is reasonable to postulate that similar iron-rich sedimentary sinks were actively forming in continental and transitional settings synchronously with the reef development in the Las Ermitas area. Given a paleoenvironment characterized by laterite and saprolite formation, lacustrine systems, and continental-to-marine transitions, the significant sequestration of Fe, Al, SiO_2, and PO_4 would occur in the form of iron oxides and phyllosilicates (Figure 13A). Despite the limited transport of weathering products to the lagoonal area represented by the Las Ermitas sediments, the influx was sufficient to generate deposits significantly enriched in Fe and PO_4. These nutrient-rich sediments subsequently facilitated the development of the early Cambrian metazoan community in western Gondwana.

Based on the preceding analysis, although a portion of the Fe, Al, SiO_2, and PO_4 fluxes to the shallow marine environments remains unaccounted for, it is reasonable to hypothesize that these elemental fluxes were equilibrated through retention in various reservoirs within the lagoonal system. This retention process ultimately manifested in the formation of the greenish and carbonate-rich sedimentary deposits observed at Las Ermitas. However, it is important to note that these deposits likely do not represent the total influx of material to the reef–lagoon area. A significant fraction may have bypassed the area or been lost due to partial recycling within the biological community, as well as through diagenetic processes and differential preservation.

The fluxes of iron, PO_4, SiO_2, and Al reported for the Las Ermitas Cambrian reef and lagoon system were derived using a standardized approach to estimate input rates

over geological time (Table 7). These calculations are based on the total amount of each element or nutrient measured in the Cambrian materials of both the reef and lagoon environments. To convert these total amounts into annual fluxes, we assumed a deposition time of 1 million years (Ma) for the entire sequence, which is a conservative estimate based on regional stratigraphic correlations and available geochronological data. The total amount of each element was divided by this 1 Ma timeframe to obtain a flux in grams per year ($gr{\cdot}yr^{-1}$). To standardize these fluxes for comparison with other geological settings and modern environments, we further divided the annual rates by the estimated average surface area of the reef and lagoon deposits, respectively. This step converted the fluxes into units of grams per square centimeter per year ($gr{\cdot}cm^{-2}{\cdot}yr^{-1}$). It is important to note that this approach assumes a relatively constant deposition rate over the 1 Ma period and uniform distribution across the depositional area. While this method provides a useful approximation of elemental fluxes, it may smooth out short-term variations in input rates and local heterogeneities in deposition. Therefore, these flux values should be interpreted as long-term averages that offer insights into the overall nutrient and elemental dynamics of the Early Cambrian Las Ermitas reef–lagoon system, rather than precise measurements of short-term or localized input rates.

Table 7. Comparison of phosphate (PO_4) and iron (Fe) data from Las Ermitas lower Cambrian deposits with other geological deposits, ranging from Eoarchean to modern times. The table presents both the flux data (in $gr{\cdot}cm^{-2}{\cdot}yr^{-1}$) and the concentration data (in weight percent, wt%). The flux data are presented in the upper portion of the table, while the concentration data are shown in the lower portion. The Las Ermitas data (this study) include both the flux measurements for the reef core and lagoon environments and the concentration measurements for specific lithologies. Comparative flux data are provided for various modern environments and ancient deposits. The concentration data span the geological record from Archean to modern times. This comprehensive presentation allows for the direct comparison of the PO_4 and the Fe distribution across diverse depositional environments and geological times, highlighting the unique characteristics of lower Cambrian phosphatic deposits in the context of Earth's long-term phosphorus cycle evolution. Dashes (-) indicate that the data are not available or not reported in the referenced study.

Environment	Age	PO_4 ($gr{\cdot}cm^{-2}{\cdot}yr^{-1}$)	Fe ($gr{\cdot}cm^{-2}{\cdot}yr^{-1}$)	PO_4 (wt%)	Fe (wt%)	Reference
Las Ermitas reef core	Lower Cambrian	$1.38{\cdot}10^{-7}$	$1.93{\cdot}10^{-7}$	-	-	This study
Las Ermitas lagoon	Lower Cambrian	$3.08{\cdot}10^{-7}$	$1.51{\cdot}10^{-5}$	-	-	This study
Atoll reef flat	Modern	$9.2{\cdot}10^{-6}$	-	-	-	Charpy [182]
Atoll lagoon	Modern	$2.45{\cdot}10^{-4}$	-	-	-	Charpy [182]
Global ocean average fluxes	Prehuman	$5.54{\cdot}10^{-7}$–$8.31{\cdot}10^{-7}$	-	-	-	Filippelli [81]
Erosion/weathering–soils	Modern	$3.79{\cdot}10^{-7}$	-	-	-	Ruttenberg [183]
Soil–surface ocean (river dissolved)	Modern	$1.88{\cdot}10^{-8}$–$3.41{\cdot}10^{-8}$	-	-	-	Ruttenberg [183]
Soil–surface ocean (particulate)	Modern	$3.47{\cdot}10^{-7}$–$3.82{\cdot}10^{-7}$	-	-	-	Ruttenberg [183]
Surface ocean–oceanic biota	Modern	$1.14{\cdot}10^{-5}$–$2.06{\cdot}10^{-5}$	-	-	-	Ruttenberg [183]
Deep sea–surface ocean (upwelling)	Modern	$1.0{\cdot}10^{-5}$–$1.0{\cdot}10^{-6}$				Filippelli [81,183]
Continental margin	Modern	-	$1.68{\cdot}10^{-6}$	-	-	Dale et al. [184]
Continental shelf	Modern	-	$1.49{\cdot}10^{-5}$	-	-	Dale et al. [184]
Deep sea	Modern	-	$9.30{\cdot}10^{-8}$	-	-	Dale et al. [184]
Global average	Modern	-	$1.69{\cdot}10^{-6}$	-	-	Dale et al. [184]
Las Ermitas calcimicrobial limestone	Lower Cambrian	-	-	0.1	0.14	This study
Las Ermitas green siltstone	Lower Cambrian	-	-	0.21	3.23	This study
Las Ermitas phosphatic steinkern	Lower Cambrian	-	-	20.00	0.46	This study
Thorntonia limestone	Lower Cambrian	-	-	~0–11.96	0.06–1.49	Creveling et al. [22]
Arthur Creek Formation	Lower–Middle Cambrian	-	-	0.06–1.23	0.32–2.71	Creveling et al. [22]
Meishucun Formation	Lower Cambrian			13.38–47.75	-	Xin et al. [185]
La Paz Formation	Neoproterozoic	-	-	0.013–0.18	3.09–7.54	Naipauer et al. [186]
El Desecho Formation	Early Cambrian	-	-	0.08–0.13	1.14–5.63	Naipauer et al. [186]
Florida phosphorites	Miocene	-	-	10–30	0.2–2.0	Föllmi [37]

When interpreting phosphorus and iron concentrations and fluxes in the Las Ermitas Lower Cambrian materials, it is important to acknowledge potential biases that may affect our understanding of the paleoenvironmental conditions. Diagenetic processes, selective preservation, and analytical limitations can all influence the measured values. Additionally, the heterogeneous nature of reef–lagoon systems may result in spatial variability that is not

fully captured in our sampling. These factors could lead to the over- or underestimation of nutrient availability and redox conditions in the ancient environment. Therefore, while the following discussion provides valuable insights into the Las Ermitas reef–lagoon system, the interpretations should be considered with these potential biases in mind. Despite these limitations, the comparison of these preserved signals with data from other geological and modern environments can still provide valuable insights into the relative nutrient status and depositional conditions of the Las Ermitas system.

The PO_4 and Fe fluxes and concentrations in the Las Ermitas Lower Cambrian reef–lagoon system reveal interesting patterns that provide insights into nutrient dynamics and environmental conditions during this early stage of metazoan reef development (Table 7). In the reef core, the PO_4 flux ($1.38 \cdot 10^{-7}$ gr·cm^{-2}·yr^{-1}) is lower than in the lagoon ($3.08 \cdot 10^{-7}$ gr·cm^{-2}·yr^{-1}), suggesting a gradient in phosphorus availability across the reef–lagoon system. This pattern is consistent with modern atoll systems, where lagoons typically show higher nutrient concentrations compared to reef flats. However, the magnitude of this difference is much smaller in the Las Ermitas system compared to modern analogues, where lagoon fluxes can be orders of magnitude higher than reef flats (e.g., $2.45 \cdot 10^{-4}$ vs. $9.2 \cdot 10^{-6}$ gr·cm^{-2}·yr^{-1} in modern atolls [182]). Furthermore, the PO_4 fluxes in the Las Ermitas system are comparable to the global ocean average fluxes in pre-human conditions ($5.54 \cdot 10^{-7}$ to $8.31 \cdot 10^{-7}$ gr·cm^{-2}·yr^{-1}) [81] and modern erosion/weathering of soil fluxes ($3.79 \cdot 10^{-7}$ gr·cm^{-2}·yr^{-1}) [187]. This suggests that the Las Ermitas reef–lagoon system operated under nutrient conditions similar to the average global oceanic values, rather than experiencing extreme nutrient enrichment or depletion. The relatively modest PO_4 fluxes may indicate a balance between the nutrient input from terrestrial sources and the biological uptake within the reef ecosystem. Interestingly, the Las Ermitas lagoon flux is remarkably similar to Ruttenberg's estimate [183] for particulate phosphorus flux from soil to surface ocean ($3.47 \cdot 10^{-7}$ to $3.82 \cdot 10^{-7}$ gr·cm^{-2}·yr^{-1}). This similarity suggests that the primary mode of phosphorus input to the Las Ermitas lagoon may have been through particulate transport, possibly indicating significant terrigenous input during the Early Cambrian. The reef core flux, while lower, is still within an order of magnitude of this particulate flux, suggesting a gradient of terrestrial influence across the reef–lagoon system.

Both the Las Ermitas reef and lagoon fluxes are significantly higher than the dissolved phosphorus input from soil to surface ocean via rivers ($1.88 \cdot 10^{-8}$ to $3.41 \cdot 10^{-8}$ gr·cm^{-2}·yr^{-1}) [183]. This difference could indicate that particulate phosphorus transport was more important than dissolved transport in the Las Ermitas system, or that additional sources of phosphorus, such as upwelling or in situ recycling, were contributing to the overall phosphorus budget. The Las Ermitas fluxes are also comparable to the estimate for erosion/weathering to soils ($3.79 \cdot 10^{-7}$ gr·cm^{-2}·yr^{-1}), particularly in the lagoon environment [183]. This similarity could suggest that the rate of phosphorus delivery to the Las Ermitas system was broadly consistent with the rate of phosphorus release from continental weathering, implying a relatively efficient transfer of phosphorus from land to the marine environment during the early Cambrian. However, both the reef and lagoon fluxes in Las Ermitas are considerably lower than estimations for phosphorus flux from the surface ocean to oceanic biota ($1.14 \cdot 10^{-5}$ to $2.06 \cdot 10^{-5}$ gr·cm^{-2}·yr^{-1}) [183]. This difference could indicate lower overall biological productivity in the Las Ermitas system compared to modern oceans, or it might suggest that phosphorus was more efficiently recycled within the water column in this early Cambrian environment, requiring lower overall input fluxes to sustain productivity.

The Fe fluxes show a more pronounced difference between the reef core ($1.93 \cdot 10^{-7}$ gr·cm^{-2}·yr^{-1}) and the lagoon ($1.51 \cdot 10^{-5}$ gr·cm^{-2}·yr^{-1}), with the lagoon experiencing a significantly higher iron input (Table 7). This pattern could reflect a greater terrigenous input into the lagoon or differences in redox conditions between

the two environments, leading to the formation of the green phyllosilicates found in Las Ermitas. The lagoon Fe flux is comparable to modern continental margin values ($1.68{\cdot}10^{-6}$ gr·cm^{-2}·yr^{-1}) [184], suggesting active iron cycling in this part of the system.

The iron fluxes observed in the Las Ermitas lower Cambrian reef–lagoon system provide an interesting contrast to the global estimates derived by Dale et al. [184] (Table 7). Las Ermitas reef core shows an Fe flux of $1.93{\cdot}10^{-7}$ gr·cm^{-2}·yr^{-1}, while the lagoon exhibits a much higher flux of $1.51{\cdot}10^{-5}$ gr·cm^{-2}·yr^{-1}. This pattern could reflect greater terrigenous input into the lagoon or differences in the redox conditions between the two environments, leading to the formation of the green phyllosilicates found in Las Ermitas. The lower Fe flux in the reef core might indicate more stable, oxic conditions favoring carbonate precipitation and reef growth. Comparing these to Dale's estimates [184], we find that the Las Ermitas lagoon flux is remarkably similar to the average continental shelf flux ($1.49{\cdot}10^{-5}$ gr·cm^{-2}·yr^{-1}) [184]. This suggests that the Las Ermitas lagoon may have experienced iron input processes similar to modern continental shelves. In contrast, the Las Ermitas reef core flux is an order of magnitude lower than Dale's deep sea estimate ($9.30{\cdot}10^{-8}$ gr·cm^{-2}·yr^{-1}) and two orders of magnitude lower than the global average ($1.69{\cdot}10^{-6}$ gr·cm^{-2}·yr^{-1}) [184].

The observed difference in the phosphate concentrations between Las Ermitas Cambrian lagoon and the reef core areas is consistent with the patterns observed in modern reef systems, albeit at much lower absolute values. In contemporary reef environments, lagoonal areas typically exhibit higher phosphate concentrations compared to core reef areas. For instance, phosphate levels of 0.1–0.5 μM have been reported in the lagoonal waters of the Great Barrier Reef, compared to 0.05–0.2 μM in reef flat waters [188]. Similarly, phosphate concentrations of 0.2–0.5 μM have been found in French Polynesian atoll lagoons, higher than the surrounding ocean waters (0.1–0.2 μM) [189]. A comparable trend has been observed in the Red Sea, with reef lagoons showing phosphate concentrations of 0.1–0.3 μM, versus 0.05–0.1 μM in fore-reef areas [190]. These findings corroborate the data reported by Charpy [182], as shown in Table 7, where modern atoll lagoons exhibit significantly higher phosphate concentrations ($2.45{\cdot}10^{-4}$ gr·cm^{-2}·yr^{-1}) compared to atoll reef flats ($9.2{\cdot}10^{-6}$ gr·cm^{-2}·yr^{-1}).These differences are attributed to factors such as restricted water circulation in lagoons, higher biomass supporting increased nutrient cycling, sediment-water interactions, and potentially greater terrestrial inputs in lagoonal environments [189,191]. The preservation of this pattern in the Las Ermitas system, despite the much lower absolute concentrations due to diagenetic losses, suggests that similar ecological and environmental dynamics may have been at play in Cambrian reef systems. This underscores the potential for significant biological phosphate cycling in early Cambrian reefs and highlights the importance of considering both modern analogs and taphonomic factors when interpreting nutrient dynamics in ancient marine ecosystems.

Examining the weight percentages of PO_4 and Fe in different facies of the Las Ermitas system (Table 7) provides further insights into nutrient distribution and sedimentary processes. The calcimicrobial limestone shows low concentrations of both PO_4 (0.1 wt%) and Fe (0.14 wt%), consistent with its origin as a primary carbonate deposit in a relatively nutrient-poor, oxic environment. In contrast, the green siltstone facies exhibits a higher Fe content (3.23 wt%) but still has low PO_4 (0.21 wt%), suggesting an increased continental input without significant phosphorus enrichment.

The phosphatic steinkern facies stands out with its extremely high PO_4 concentration (20 wt%), comparable to the Meishucunian phosphorites (13.38–47.75 wt%) and some Permian and Miocene phosphorite deposits (15 to 35 wt%) [37,185] (Table 7). This localized phosphorus enrichment likely represents episodes of enhanced phosphogenesis, possibly driven by changes in the redox conditions that promoted phosphorus concen-

tration and preservation. However, the relatively low Fe content (0.46 wt%) in this facies suggests that iron cycling was not closely coupled to phosphorus enrichment in these specific environments. In contrast, the Neoproterozoic La Paz Formation [186] shows much lower PO_4 concentrations ranging from 0.013% to 0.18%, but higher Fe contents of 3.09%–7.54% (Table 7). Similarly, the early Cambrian El Desecho Formation has PO_4 levels of 0.08%–0.13% and Fe concentrations of 1.14%–5.63% [186]. These comparisons highlight the exceptional phosphate enrichment in the Las Ermitas phosphatic steinkern, which contains PO_4 concentrations of two orders of magnitude higher than those observed in the Caucete Group formations. The Fe concentrations, however, are generally higher in the Caucete Group formations compared to Las Ermitas, except for the Las Ermitas green siltstone, which shows comparable Fe levels (Table 7). Such differences support the hypothesis of a higher supply of Fe and PO_4, along with Al and SiO_2, into the Las Ermitas lagoonal area. This enhanced input, coupled with local and periodical changes in the redox conditions, likely favored Fe enrichment in the form of greenish phyllosilicates and a PO_4 concentration within biological structures of various sizes [22,37].

In conclusion, the PO_4 and Fe flux and concentration data from the Las Ermitas lower Cambrian reef–lagoon system reveal a complex nutrient landscape. The system appears to have operated under generally moderate nutrient conditions, with spatial variability between the reef core and lagoon environments. Episodic events of intense phosphogenesis, recorded as distinct phosphoritic levels (Figures 6 and 7), produced localized phosphate-rich deposits in the Las Ermitas sequence. These phosphogenic episodes reflect the enhanced weathering occurring at the end of the Neoproterozoic and early Cambrian, driven by a strong greenhouse episode. This intensified weathering led to an increased phosphate and iron supply to marine environments. The biological community in the Las Ermitas lagoonal area likely exploited this nutrient influx, enhancing and accelerating nutrient cycling. This biologically-mediated process probably significantly amplified the PO_4 accumulation in the lagoon, mirroring observations in modern lagoonal systems. The interplay between the increased nutrient availability and the biological activity thus created a positive feedback loop, further concentrating phosphate in the local environment. However, much of the PO_4 that was uptaken, accumulated, and recycled by the biological community was subsequently lost through various post-sedimentary and diagenetic processes, leaving behind only a fraction of the originally concentrated phosphate in the preserved sedimentary record. This dynamic interaction between the enhanced weathering, increased nutrient availability, and biological activity highlights the complex nature of nutrient cycling in this early metazoan reef ecosystem, showcasing how global climate changes can influence local depositional environments and early marine ecosystems. Potential episodic upwelling events might have contributed to its productivity and biodiversity. While upwelling could have enhanced phosphogenesis, the reefal barrier likely moderated its impact on the lagoon. Consequently, the phosphate production in Las Ermitas appears to have resulted from a combination of processes: periodic terrestrial sediment influx; intervals of reduced sedimentation, promoting phosphate formation within sediments through iron reduction; and occasional erosive events mobilizing and redepositing phosphatic particles, primarily as steinkerns. This dynamic system suggests a delicate balance between external inputs and internal biogeochemical processes. The alternating phases of sediment influx, quiescence, and erosion created conditions conducive to phosphate accumulation and preservation.

The correlation of silicon, aluminum, and iron in the Las Ermitas geochemical data reveals a complex interplay of terrigenous input, weathering pulses, and diagenetic processes in the reef–lagoon system. This tri-elemental relationship suggests varying intensities and sources of continental weathering, with Fe often indicating the input of iron-bearing clay minerals or oxides/hydroxides [192]. The synchronous increases in these elements likely

represent the episodic intensification of weathering on the adjacent landmass, driven by climatic fluctuations, tectonic activity, or sea-level changes. However, a more nuanced interpretation emerges when considering the mineralogical composition, particularly the presence of chamosite in the lagoon deposits (Figure 13A). While some Si, Al, and Fe undoubtedly represent a direct terrigenous input, a significant portion likely reflects in situ mineral formation. Chamosite typically forms in shallow marine settings through the interaction of iron-rich pore waters with clay minerals under reducing conditions [193]. The lagoon's restricted circulation could have created localized reducing environments conducive to iron reduction and chamosite formation, while maintaining overall oxic conditions in the water column. This scenario is supported by the estimated composition of 55% quartz and 45% chamosite in the greenish deposits, indicating both a detrital input and diagenetic mineral formation. The varying intensities of Si-Al-Fe correlations may thus reflect fluctuations in both the terrigenous input and the diagenetic processes, influenced by changes in lagoon circulation, organic matter flux, and climate-driven variations in weathering patterns [194,195]. These processes would have significantly impacted the reef–lagoon ecosystem, affecting the primary productivity, carbonate precipitation, and benthic community dynamics. The observed variability in PO_4 and Fe fluxes between the reef core and the lagoon further supports this dynamic interplay of terrestrial inputs, marine processes, and localized diagenetic conditions in shaping the Early Cambrian Las Ermitas ecosystem. This interpretation underscores the importance of considering both primary depositional and secondary diagenetic processes in reconstructing the paleoenvironmental conditions of ancient reef–lagoon systems, while acknowledging the potential for complex redox gradients within these environments.

To complete the assessment of the main biogeochemical fluxes of PO_4 and Fe, it is essential to determine the total organic carbon (C_{org}) content in both the calcimicrobial limestones and the greenish deposits (Figure 13B; Table 8). The analysis of the C_{org} in the carbonates and the siltstones yielded averages of 0.14 and 0.40 wt%, respectively. In the Las Emitas sedimentary record, Fe and S appear as major and secondary elements, suggesting that microbial chemoheterotrophs likely promoted the formation of two Fe(II)-bearing mineral phases like chamosite and pyrite (Table 8). Given this context, it may be possible to estimate the loss of organic material through microbial degradation using Fe(III) as an electron acceptor [177]. In addition to iron reduction, another process involving the degradation of organic matter uses SO_4^{2-} as an electron acceptor [196], leading to the formation of pyrite when the resulting sulfide combines with Fe^{2+}. The pyrite content (wt%) in the calcimicrobial limestones and the greenish siltstones are 0.070 and 0.041, respectively. The main reactions describing these degradation processes, which represent metabolic pathways for organic matter oxidation, are as follows (Figure 13B) [177,196]:

$$CH_2O + 4{\cdot}Fe(OH)_3 + 8{\cdot}H^+ \rightarrow CO_2 + 4{\cdot}Fe^{2+} + 11{\cdot}H_2O \quad (1)$$

(Fe^{3+} as electron acceptor)

$$2{\cdot}CH_2O + SO_4^{2-} \rightarrow 2{\cdot}HCO_3^- + H_2S \quad (2)$$

(SO_4^{2-} as electron acceptor)

where CH_2O represents a simplified form of organic matter.

Furthermore, the sulfide produced in the second reaction can then react with Fe^{2+} to form pyrite [197]:

$$Fe^{2+} + 2{\cdot}H_2S \rightarrow FeS_2 \text{ (pyrite)} + 2{\cdot}H^+ \quad (3)$$

It is important to note that reaction (3) is a simplified representation of a more complex process. In reality, pyrite formation involves a series of intermediate steps and various sulfide compounds produced through microbial activity. Pyrite represents the end-member in this sulfide mineralization process, which encompasses multiple biogeochemical reactions and transformations [198].

To determine the amount of organic carbon oxidized to CO_2, we utilized the balanced reaction Equation (1) showing that for every mole of organic carbon (CH_2O) oxidized, four moles of ferric iron [$Fe(OH)_3$] are reduced. Given the total mass of ferric iron as $2.12 \cdot 10^{10}$ g, we first calculated the number of moles of $Fe(OH)_3$ by dividing this mass by its molar mass (106.85 g/mol), yielding $1.98 \cdot 10^8$ moles. Since the stoichiometric ratio of $Fe(OH)_3$ to CH_2O is 4:1, we divided the moles of $Fe(OH)_3$ by four to obtain the moles of CH_2O oxidized ($4.95 \cdot 10^7$ moles). Finally, multiplying this by the molar mass of carbon (12 g/mol) gave us the total mass of carbon oxidized: $5.94 \cdot 10^8$ g or approximately 594 metric tons. This calculation provides an estimate of the organic carbon oxidized to CO_2 through iron reduction in the system, based on the given amount of ferric iron.

Alternatively, an estimation of the total C_{org} consumed through reaction (2) can be made by assuming that the total sulfide content originates from the oxidation of seawater SO_4^{2-}, with organic compounds serving as the energy source. The total weight of the main calcimicrobial limestones is $4.11 \cdot 10^{12}$ g, while the siltstones weigh approximately $1.97 \cdot 10^{12}$ g. Based on these weights, the total sulfur content was estimated to be $2.88 \cdot 10^{11}$ g in the limestones and $8.06 \cdot 10^{10}$ g in the siltstones (Figure 13B; Table 8).

For the sulfate reduction, reaction (2) was utilized, along with the sulfur content in the sedimentary rocks. The calcimicrobial limestones and siltstones contain $1.26 \cdot 10^{11}$ g and $8.06 \cdot 10^{10}$ g of sulfur, respectively. Based on the stoichiometry of the sulfate reduction reaction, it was estimated that $9.44 \cdot 10^{10}$ g of carbon were oxidized in the limestones and $6.03 \cdot 10^{10}$ g in the siltstones, totaling approximately 155,000 metric tons of C_{org} consumed through sulfate reduction.

To estimate the remaining organic carbon in the materials, we used the measured C_{org} contents of 0.14 wt% in the calcimicrobial limestones and 0.40 wt% in the siltstones. Given the total mass of limestones ($1.84 \cdot 10^{12}$ g) and siltstones ($1.97 \cdot 10^{12}$ g), the total C_{org} is approximately $2.58 \cdot 10^9$ g (0.14% of $4.11 \cdot 10^{12}$ g), while for the siltstones, it is around $7.88 \cdot 10^9$ g (0.40% of $1.97 \cdot 10^{12}$ g).

Table 8. The inventory of organic carbon (C_{org}) in the lower Cambrian reef–lagoon system. Values are presented in grams for different lithologies and metabolic pathways. $C_{org}(Fe^{3+})$ represents organic carbon oxidized through iron reduction, $C_{org}(SO_4^{2-})$ through sulfate reduction, as described in reactions (1) and (2). C_{org} is the remaining organic carbon analyzed from samples, and Total C_{org} is the sum of these carbon sources, which represented the estimated organic carbon from the geochemical composition of the Las Ermitas materials. The estimated C lost column shows the calculated amount of organic carbon lost due to biological and geological processes, based on comparisons with modern microbial and lagoon productivity rates [188,199]. Furthermore, the C total accounts for the estimated total amount of organic carbon supplied to the Las Ermitas reef–lagoon system. Calcimicrobial limestones represent the reef environment and calcimicrobial patches in the lagoon, while greenish siltstones represent the lagoonal environment. The table includes a total budget row summarizing the carbon distribution and loss across the entire system. The table shows the distribution of organic carbon across calcimicrobial limestones and greenish siltstones, as well as the total budget for the system. Las Ermitas system organic C distribution is also shown in Figure 13B.

Main Lithology	$C_{org}(Fe^{3+})$	$C_{org}(SO_4^{2-})$	C_{org}	Total C_{org}	C_{bio} Lost	Total C
Calcimicrobial limestones	$7.21 \cdot 10^7$	$9.44 \cdot 10^{10}$	$2.58 \cdot 10^9$	$9.71 \cdot 10^{10}$	$5.18 \cdot 10^{11}$	$5.20 \cdot 10^{14}$
Greenish siltstones	$5.22 \cdot 10^8$	$6.03 \cdot 10^{10}$	$7.88 \cdot 10^9$	$6.87 \cdot 10^{10}$	$9.72 \cdot 10^{11}$	$9.72 \cdot 10^{14}$
Total budget	$5.94 \cdot 10^8$	$1.55 \cdot 10^{11}$	$1.36 \cdot 10^{11}$	$1.66 \cdot 10^{11}$	$1.49 \cdot 10^{12}$	$1.50 \cdot 10^{15}$

The total organic carbon loss in the lower Cambrian reef–lagoon system was estimated by comparing preserved organic carbon with expected productivity based on modern analogues. In Las Ermitas area, the calcimicrobial reef core ($2.60 \cdot 10^5$ m^2) was assigned a productivity rate of $2.00 \cdot 10^3$ C $g \cdot m^{-2} \cdot year^{-1}$, typical of highly productive cyanobacterial mats [200], while the lagoon ($1.80 \cdot 10^6$ m^2) was assigned $5.40 \cdot 10^2$ C $g \cdot m^{-2} \cdot year^{-1}$, based on measurements from modern reef lagoons [201]. The total expected productivity was calculated as $1.49 \cdot 10^9$ C $g \cdot yr^{-1}$. Comparing this to the preserved organic carbon of $6.60 \cdot 10^5$ C $g \cdot year^{-1}$, it was estimated that approximately $1.49 \cdot 10^9$ C $g \cdot yr^{-1}$ or $1.49 \cdot 10^3$ metric tons of carbon per year were lost to biological and geological processes. This suggests that about 99.96% of the expected organic carbon production has been lost over geological time, with only about 0.012% being preserved or detectable in the ancient system.

The organic carbon budget analysis reveals significant degradation and loss patterns across the lower Cambrian reef–lagoon system. In the calcimicrobial reef core, the total carbon produced over 1 Ma was $5.20 \cdot 10^{14}$ g of C, of which only $9.71 \cdot 10^{10}$ g C (0.02%) was accounted for through preserved organic carbon and known degradation pathways. The dominant degradation pathway in the reef environment was sulfate reduction, accounting for $9.44 \cdot 10^{10}$ g of C, while iron reduction played a minimal role with $7.21 \cdot 10^7$ g of C. Only $2.58 \cdot 10^9$ g of C was preserved as organic carbon in the limestone facies.

The lagoon environment, represented by greenish siltstones, exhibited even higher productivity, with $9.72 \cdot 10^{14}$ g C produced over the same period. Of this total, $6.87 \cdot 10^{10}$ g of C (0.01%) was accounted for through preservation and measured degradation pathways. Similar to the reef environment, sulfate reduction was the primary degradation pathway in the lagoon, processing $6.03 \cdot 10^{10}$ g of C, while iron reduction accounted for $5.22 \cdot 10^8$ g C. The preserved organic carbon in the siltstones amounted to $7.88 \cdot 10^9$ g of C.

The total system budget demonstrates that from the $1.49 \cdot 10^{15}$ g of C produced over 1 Ma, only $1.66 \cdot 10^{11}$ g of C (0.01%) can be accounted for through the preserved organic carbon ($1.05 \cdot 10^{10}$ g C) and the measured degradation pathways (SO_4^{2-}: $1.55 \cdot 10^{11}$ g C; Fe^{3+}: $5.94 \cdot 10^8$ g C). This indicates that approximately 99.99% of the originally produced organic carbon was lost through other degradation pathways or processes not captured in the preserved rock record. The dominance of sulfate reduction over iron reduction in both environments suggests that the anaerobic degradation of organic matter was primarily driven by sulfate-reducing bacteria, although this represents only a small fraction of the total organic carbon loss.

The estimated loss of 99.98% of the organic carbon in the lower Cambrian reef–lagoon system, while strikingly high, aligns with the broader understanding of long-term organic carbon preservation in ancient marine sediments. Typically, less than 1% of the primary production in marine environments is preserved in sediments, with preservation rates often being as low as 0.1% [202]. For early Phanerozoic sediments, even lower preservation rates are suggested due to extended periods of diagenesis and other loss processes [203]. Studies on Cambrian-aged sediments have often reported organic carbon burial efficiencies often below 1% [204]. The extremely low preservation rate calculated in this study (about 0.014%) falls within the expected range for sediments of this age, considering multiple cycles of potential remineralization and diagenesis. While the specific figure of 99.98% loss is not directly documented in other references, it is consistent with the general paradigm of organic carbon preservation in ancient marine sediments [202,203,205]. It is important to note that this calculation, based on comparing preserved carbon to modern productivity rates, introduces some uncertainty. Nevertheless, the overall conclusion of very low preservation is well-supported by the literature on long-term carbon cycling and preservation in ancient sediments, underscoring the significance of these findings in contributing to our understanding of early Phanerozoic carbon dynamics.

7.4. Nutrient Flux and Paleoproductivity in the Early Cambrian Reef–Lagoon System of Las Ermitas

Once the total carbon production in the lower Cambrian Las Ermitas reef–lagoon system is estimated, the relationship between nutrient fluxes and paleoecosystem productivity can be assessed using specific biogeochemical correlations. These correlations are derived from the carbon-to-phosphorus Redfield ratio (Table 9) observed in modern primary producers, and they can also be extended to include iron [206–208]. As a vital nutrient, iron plays a key role in photosynthesis, nitrogen fixation, and other essential biochemical processes, as discussed in detail in previous sections.

In the lower Cambrian Ermitas reef–lagoon system, phosphate uptake likely occurred through various mechanisms, driven by a diverse community of primary producers. The dominant photosynthetic organisms, including eukaryotic microalgae (such as prasinophytes), cyanobacteria, Chlorophyta, and Rhodophyta, would have been the principal consumers of dissolved inorganic phosphate (DIP), utilizing active transport systems across their cell membranes [66,209]. These producers, particularly Chlorophyta and Rhodophyta, may have also possessed mechanisms to utilize DOP compounds, especially in phosphate-limited conditions [210]. Rhodophyta, notably, have been shown to have high-affinity phosphate uptake systems allowing them to thrive in low-phosphate environments [211]. Some species of both Chlorophyta and Rhodophyta can produce alkaline phosphatases, enabling them to hydrolyze organic phosphorus compounds and access the resulting inorganic phosphate [212]. Microbial mats, significant components of Cambrian reef ecosystems, likely played a crucial role in phosphate cycling, potentially accessing both dissolved and particulate forms of phosphorus through enzymatic processes [213]. The archaeocyathids, being phylogenetically related to sponges, may have had some capacity for direct phosphate uptake from seawater, although their primary mode of nutrient acquisition was likely through filter feeding [214]. The overall dynamics of phosphate uptake in this ancient ecosystem were presumably influenced by the specific composition of the biological community, the prevailing ocean chemistry, and the spatial distribution of phosphate within the reef–lagoon complex. While the fundamental mechanisms of phosphate uptake may have been similar to those observed in modern marine ecosystems, the efficiency and specific pathways might have differed due to the unique evolutionary stage of early Cambrian organisms [215]. Despite limited direct evidence from Cambrian fossils, we can infer from the evolutionary conservation of these traits that early producers likely possessed at least basic versions of these phosphate acquisition strategies, contributing significantly to the phosphorus cycling in this ancient reef–lagoon ecosystem [216].

In the lower Cambrian Las Ermitas reef–lagoon system, iron uptake likely occurred through various mechanisms, driven by the diverse community of primary producers and microorganisms. The dominant photosynthetic organisms, including eukaryotic microalgae, cyanobacteria, Chlorophyta, and Rhodophyta, would have primarily relied on dissolved ferrous iron (Fe^{2+}) for their iron requirements, utilizing specific membrane-bound transport systems [1,2]. However, given the potential for the rapid oxidation of Fe^{2+} to Fe^{3+} in oxic environments, these organisms may have developed strategies to access the less bioavailable ferric iron (Fe^{3+}) [3]. Some producers, particularly cyanobacteria, might have produced siderophores —high-affinity iron-chelating compounds— to scavenge Fe^{3+} from the environment [4]. Microbial mats, significant components of Cambrian reef ecosystems, likely played a crucial role in iron cycling, potentially influencing the local redox conditions and iron speciation [5]. The archaeocyathids, being phylogenetically related to sponges, may have had some capacity for direct iron uptake from seawater, although their primary mode of nutrient acquisition was likely through filter feeding [6]. The overall dynamics of iron uptake in this ancient ecosystem were presumably influenced by the specific

composition of the biological community, the prevailing ocean chemistry, and the spatial distribution of iron within the reef–lagoon complex. While the fundamental mechanisms of iron uptake may have been similar to those observed in modern marine ecosystems, the efficiency and specific pathways might have differed due to the unique evolutionary stage of early Cambrian organisms and the potentially different ocean chemistry [7]. Despite limited direct evidence from Cambrian fossils, we can infer from the evolutionary conservation of iron uptake mechanisms that early producers likely possessed at least basic versions of these iron acquisition strategies, contributing significantly to the iron cycling in this ancient reef–lagoon ecosystem [8].

Table 9. The carbon and phosphorus mass balance analysis in the lower Cambrian Las Ermitas section. The table shows the distribution of carbon and phosphorus (in grams) across different environments and degradation metabolic pathways. Theoretical community values represent the expected C:P ratios, based on the Redfield ratio of 106:16:1, corresponding with 41.11:1 by mass. Carbon and phosphorus mass ratios in the Las Ermitas Cambrian deposits. Community values[1,2] represent theoretical Redfield ratios scaled to total deposit volumes using lagoonal [201] and reefal [200] settings. Ratios for siltstones and limestones[3,4] include total measured concentrations plus estimated organic carbon contributed from metabolic degradation through Fe^{3+} and SO_4^{2-} reduction pathways[5,6]. The preserved organic matter in both siltstones and calcimicrobial limestones is compared with carbon processed through sulfate (SO_4^{2-})[7,8] and ferric iron (Fe^{3+})[9,10] reduction pathways. Deviations from the Redfield ratio are indicated in the "gC/gP ratio-41.11" column, with negative values indicating phosphorus excess and positive values indicating carbon excess.

Area/Lithology	gC	gP	gC/gP Ratio	gC/gP ratio-41.11	C vs. P Balance
Lagoon community[1]	$9.72 \cdot 10^{14}$	$2.36 \cdot 10^{13}$	41.11	-	Balanced
Reef community[2]	$5.20 \cdot 10^{14}$	$1.26 \cdot 10^{13}$	41.11	-	Balanced
C and P in siltstones[3]	$7.88 \cdot 10^{9}$	$9.46 \cdot 10^{8}$	8.33	−32.78	P excess
C and P in calcimicrobial limestones[4]	$2.58 \cdot 10^{9}$	$6.00 \cdot 10^{8}$	4.30	−36.81	P excess
C and P in siltstone total[5]	$6.87 \cdot 10^{10}$	$9.46 \cdot 10^{8}$	72.62	31.51	C excess
C and P in calcimicrobial limestones total[6]	$9.71 \cdot 10^{10}$	$6.00 \cdot 10^{8}$	161.83	120.72	C excess
Corg(SO_4^{2-}) siltstones[7]	$6.03 \cdot 10^{10}$	$9.46 \cdot 10^{8}$	63.74	22.63	C excess
Corg(SO_4^{2-}) calcimicrobial limestones[8]	$9.44 \cdot 10^{10}$	$6.00 \cdot 10^{8}$	157.33	116.22	C excess
Corg(Fe^{3+}) siltstones[9]	$5.22 \cdot 10^{8}$	$9.46 \cdot 10^{8}$	0.55	−40.56	P excess
Corg(Fe^{3+}) calcimicrobial limestones[10]	$7.21 \cdot 10^{7}$	$6.00 \cdot 10^{8}$	0.12	−40.99	P excess

General stoichiometric equations can provide valuable insights into biogeochemical fluxes and biomass production in marine environments, particularly when accounting for nutrient inputs such as the release of phosphate and iron through andesite weathering from continental sources. These equations offer a simplistic framework for understanding the complex relationships between nutrient availability, primary production, and elemental cycling in aquatic ecosystems [217].

The stoichiometry of marine primary producers plays a crucial role in understanding nutrient cycling and ecosystem dynamics in aquatic environments. Two key groups of producers, phytoplankton and multicellular algae, exhibit distinct elemental compositions that reflect their physiological and structural differences.

For phytoplankton, the Redfield ratio, first described by Alfred C. Redfield in 1934 and refined over subsequent years, provides a foundational stoichiometric relationship. This ratio suggests a C:N:P composition of 106:16:1 [206], which can be expressed in the following chemical equation:

$$106 \cdot CO_2 + 16 \cdot NO_3^- + HPO_4^{2-} + 122 \cdot H_2O + 18 \cdot H^+ \rightarrow C_{106}H_{263}O_{110}N_{16}P + 138 \cdot O_2 \quad (4)$$

This ratio has been widely applied in biogeochemistry and marine ecology. However, it is important to note that the Redfield ratio represents an average, and individual species or communities may deviate from this ratio depending on their environmental conditions and physiological states [207].

In contrast, multicellular algae, including macroalgae, often exhibit different elemental compositions. These organisms typically have higher C:N and C:P ratios compared to the Redfield ratio, largely due to their more complex structural components. Atkinson and Smith [188] analyzed a wide range of marine plants and found that their average C:N:P ratio was approximately 550:30:1. Based on this ratio, we can construct a representative equation for macroalgae:

$$550{\cdot}CO_2 + 30{\cdot}NO_3^- + HPO_4^{2-} + 551{\cdot}H_2O + 30{\cdot}H^+ \rightarrow C_{550}H_{1100}O_{550}N_{30}P + 551{\cdot}O_2 \quad (5)$$

However, it is crucial to recognize that macroalgal stoichiometry can vary significantly among species and environments. In this regard, it has been reported C:N:P ratios for marine macroalgae ranging from 119:7:1 to 344:21:1 have been reported [218], illustrating this variability. Comparing these equations reveals that multicellular algae generally incorporate more carbon relative to nitrogen and phosphorus compared to phytoplankton. This difference reflects the distinct physiological and structural characteristics of these organisms, as well as their adaptations to different marine environments. Furthermore, it is important to emphasize that these equations are simplifications of complex biological processes. In reality, the elemental composition of both phytoplankton and macroalgae can vary based on factors such as nutrient availability, light conditions, temperature, and species-specific traits [219].

The geochemical analysis of carbon and phosphorus distributions in the lower Cambrian Las Ermitas section provides significant insights into the biogeochemical cycling patterns of these key nutrients in early Phanerozoic reef–lagoon systems (Table 9). The theoretical nutrient requirements of the ancient communities, based on the Redfield ratio (C:P = 41.11 by mass), indicate balanced nutrient cycling with the lagoon environment requiring $9.72{\cdot}10^{14}$ gC and $2.36{\cdot}10^{13}$ gP, while the reef setting needed $5.20{\cdot}10^{14}$ gC and $1.26{\cdot}10^{13}$ gP. These values represent the idealized nutrient distribution that would have characterized these ecosystems during their active phase, assuming modern-like stoichiometric relationships, an approach that has been successfully applied to other Paleozoic systems [220].

The preserved record reveals substantial deviations from these theoretical ratios. In the raw preserved materials, both environments exhibit a significant phosphorus excess compared to carbon. The siltstones from the lagoon environment show a C/P ratio of 8.33 (32.78 below Redfield), while the calcimicrobial limestones display an even lower C/P ratio of 4.30 (36.81 below Redfield). This marked phosphorus enrichment relative to carbon suggests either the preferential preservation of phosphorus-bearing compounds or extensive carbon loss during early diagenesis, or more likely, a combination of both processes. Similar patterns have been observed in other Cambrian deposits, where phosphorus enrichment has been linked to enhanced phosphogenesis and organic matter preservation conditions [22,221].

The analysis of the organic carbon degradation pathways provides crucial insights into the fate of organic matter. In the sulfate reduction pathway, both environments show a substantial carbon excess relative to phosphorus, with C/P ratios of 63.74 (22.63 above Redfield) in the siltstones and 157.33 (116.22 above Redfield) in the calcimicrobial limestones. Conversely, the ferric iron reduction pathway shows a strong phosphorus excess, with C/P ratios of 0.55 (40.56 below Redfield) in the siltstones and 0.12 (40.99 below Redfield) in the calcimicrobial limestones. These contrasting patterns align with observations from other early Paleozoic black shales [220], suggesting different preservation mechanisms operating under different redox conditions.

When considering the total record, which includes both preserved organic matter and that processed through degradation pathways, the siltstones show a C/P ratio of

72.62 (31.51 above Redfield), while the calcimicrobial limestones exhibit an even more extreme C/P ratio of 161.83 (120.72 above Redfield). This carbon excess in the total record indicates that although most of the carbon was ultimately lost from the system, the amount processed through anaerobic degradation pathways, particularly sulfate reduction, was substantially higher than what would be expected from the Redfield ratio. The observed dominance of sulfate reduction over iron reduction in both the siltstones (6.03×10^{10} gC vs. 5.22×10^{8} gC) and the limestones (9.44×10^{10} gC vs. 7.21×10^{7} gC) suggests that sulfate reduction was a significant metabolic pathway during early diagenesis given the low oxygenation of the seafloor [220]. However, the scarcity of sulfides in the sediments and the prevalence of Fe(II)-bearing phyllosilicates indicate that sulfide production did not dominate the diagenetic mineralization processes. Instead, the high silica concentrations in lower Cambrian seawater [168], driven by elevated weathering rates [3], likely facilitated the sequestration of iron through the formation of iron-silicate phases, such as phyllosilicates. This mechanism reflects the interplay between microbial processes and the geochemical conditions of the Cambrian seas, characterized by high silica availability and limited oxygenation.

These results highlight several key aspects of early Cambrian biogeochemical cycling. First, they demonstrate the differential preservation potential of carbon and phosphorus under varying redox conditions, with distinct patterns emerging between sulfate and iron reduction zones, consistent with observations from other Paleozoic deposits [220]. Second, they reveal the importance of anaerobic degradation pathways in processing organic matter, particularly sulfate reduction, which appears to have been the dominant process in both reef and lagoon environments. Third, they suggest complex early diagenetic processes that led to differential preservation of these key nutrients, with the relative importance of different degradation pathways varying between environments. The stark contrast between the theoretical nutrient requirements of the living communities and the preserved record emphasizes the importance of considering multiple pathways and processes when reconstructing ancient marine ecosystems, particularly in terms of productivity and nutrient cycling, as demonstrated in various studies of early Paleozoic phosphorites and black shales [131,222].

When applying the modified Redfield equation ($C_{550}H_{1100}O_{550}N_{30}P$) to the Las Ermitas materials, which represents a significantly higher C:P ratio of 550:1 (mass ratio of 213.29:1) compared to the traditional Redfield ratio of 106:1 (mass ratio of 41.11:1), the deviations from the stoichiometric balance become even more pronounced. In the preserved organic matter, both of the facies show an extreme phosphorus excess relative to this modified ratio, with the siltstones displaying a C:P mass ratio of 8.33 (−204.96 below the modified ratio) and the calcimicrobial limestones showing an even lower ratio of 4.30 (−208.99 below modified ratio). This pattern continues in the degradation pathways, where the sulfate reduction products show C:P ratios of 63.74 (−149.55 below the modified ratio) in siltstones and 157.33 (−55.96 below the modified ratio) in the calcimicrobial limestones. The iron reduction pathway exhibits the most extreme phosphorus excess, with C:P ratios of 0.55 (−212.74 below the modified ratio) and 0.12 (−213.17 below the modified ratio) in the siltstones and the calcimicrobial limestones respectively.

The total record, including both preserved organic matter and degradation products, maintains this pattern with C:P ratios of 72.62 (−140.67 below the modified ratio) in the siltstones and 161.83 (−51.46 below the modified ratio) in the calcimicrobial limestones. These substantial deviations from the modified Redfield ratio indicate that this higher C:P stoichiometry provides a much poorer fit to the geochemical composition of the Las Ermitas materials compared to the traditional Redfield ratio. This suggests that the biogeochemical cycling in these lower Cambrian environments likely operated closer to the classical Red-

field proportions rather than the modified ratio, providing important constraints on our understanding of early Phanerozoic nutrient cycling.

Las Ermitas data show remarkable variability in C:P ratios, ranging from 0.3 to 417.9 (molar), reflecting diverse depositional environments and metabolic pathways within a single reef complex. Notably, the highest values recorded in the calcimicrobial limestones (417.9 molar) align closely with those documented in the mid-upper Cambrian Alum Shale (403–444 molar), suggesting similar redox conditions and phosphorus cycling mechanisms operated during the early to middle Cambrian.

According to Algeo's work [220], C:P ratios are strongly influenced by benthic redox conditions, with higher ratios indicating poorly ventilated environments and the enhanced preservation of organic carbon coupled with increased diffusive loss of remineralized phosphorus. Las Ermitas data strongly supports this model, with the lowest C:P ratios found in the calcimicrobial settings that likely experienced oxygen-depleted conditions. In contrast, very low ratios (0.3–1.4 molar) characterize Fe^{3+}-dominated environments, indicating well-oxygenated conditions.

The environmental heterogeneity captured in the Las Ermitas system provides unique insights into early Cambrian conditions. The high C:P ratios in certain environments suggest that poorly ventilated conditions, which are identified as typical of the early-middle Paleozoic [22,220], were already established in the early Cambrian. However, the presence of well-oxygenated conditions in Fe^{3+}-rich settings demonstrates that significant redox variability could exist at local scales. This mosaic of redox conditions within a single reef system suggests that nutrient cycling and oxygen availability varied substantially over small spatial scales, potentially creating diverse niches that could have supported early metazoan diversification.

Las Ermitas system appears to capture a critical transition between the generally anoxic conditions of the Precambrian and the gradually increasing oxygenation of the Paleozoic, exhibiting characteristics of both regimes within a single reef complex. This makes it an invaluable record of early Cambrian environmental conditions and their potential influence on early animal evolution.

Furthermore, the marked disparity in the C:P ratios between the sulfate reduction (164.6–406.4 molar) and the iron reduction (0.3–1.4 molar) pathways in the Las Ermitas system reflects both thermodynamic and stoichiometric controls on organic matter degradation. From a thermodynamic perspective, the sequence of electron acceptors follows a well-established redox ladder, where Fe^{3+} reduction occurs at higher redox potentials than sulfate reduction. This explains why iron reduction environments show characteristics more typical of oxidizing conditions, including more efficient phosphorus retention and lower C:P ratios, while sulfate reduction environments display features associated with more reducing conditions, such as enhanced organic carbon preservation and higher C:P ratios.

However, the difference in C:P ratios is further amplified by the distinct stoichiometric requirements of each metabolic pathway. Iron reduction requires a higher number of electron acceptor molecules per unit of organic carbon oxidized, with a typical ratio of one carbon to four Fe^{3+} (1:4). In contrast, sulfate reduction proceeds with a more carbon-favorable stoichiometry, where two carbons are oxidized per sulfate molecule (2:1). This fundamental difference in the carbon consumption efficiency of these pathways contributes to the lower C:P ratios observed in iron-reducing environments compared to sulfate-reducing ones.

The combined effect of redox conditions and stoichiometric requirements creates a powerful mechanism for generating distinct C:P signatures in the rock record. In the Las Ermitas system, this is particularly well demonstrated in both the siltstones and

the calcimicrobial limestones, where the dual influence of the higher redox potential and the lower C:Fe^{3+} ratio in iron-reducing environments results in dramatically lower C:P ratios compared to sulfate-reducing environments. This pattern suggests that the preserved C:P ratios in ancient rocks reflect not just the redox conditions of the depositional environment, but also the specific stoichiometric constraints of the dominant metabolic pathways operating during early diagenesis.

To explore the relative importance of different metabolic pathways in organic matter degradation, we first calculated the theoretical proportions of sulfate versus iron reduction that would yield the original Redfield ratio (106:1) in both environments. For calcimicrobial limestones, where sulfate reduction yielded a C:P ratio of 406.4 and iron reduction yielded a ratio of 0.3, the calculation ($406.4x + 0.3 \cdot (1 - x) = 106$, where·is the proportion of sulfate reduction) indicated that iron reduction would need to be the dominant process (74%) over sulfate reduction (26%). Similarly, for the siltstones ($164.6x + 1.4 \cdot (1 - x) = 106$), the calculation suggested sulfate reduction should account for 64% of organic matter degradation, with iron reduction representing 36%.

However, the examination of the actual amounts of organic carbon consumed through these pathways reveals a markedly different pattern. In the calcimicrobial limestones, sulfate reduction consumed $9.44 \cdot 10^{10}$ g of the carbon (97.2% of total) compared to only $7.21 \cdot 10^{7}$ g (0.07%) through iron reduction. Similarly, in the siltstones, sulfate reduction accounted for $6.03 \cdot 10^{10}$ g (87.8%) versus $5.22 \cdot 10^{8}$ g (0.8%) through iron reduction. This dominance of sulfate reduction, particularly pronounced in the calcimicrobial limestones, suggests that redox conditions, rather than iron availability, controlled the primary pathway of organic matter degradation.

Interestingly, although the lagoon environment where the siltstones formed might have had a higher iron availability from terrestrial inputs, sulfate reduction still dominated the organic matter degradation. This suggests that the more confined nature of the lagoon environment created more reducing conditions that favored sulfate reduction over iron reduction, even in the presence of available iron. This interpretation aligns with observations from modern restricted marine environments, where limited circulation often leads to more reducing conditions and predominant sulfate reduction pathways. The slightly higher proportion of iron reduction in the siltstones (0.8%) compared to the calcimicrobial limestones (0.07%) might reflect this greater iron availability, though its impact on the organic matter degradation remained minimal compared to sulfate reduction.

As discussed above, in addition to carbon, nitrogen, and phosphorus, iron plays a crucial role in marine primary production, particularly in high-nutrient, low-chlorophyll (HNLC) regions where it can be a limiting nutrient. The stoichiometry of iron in relation to other elements in marine primary producers is an important aspect of understanding marine biogeochemical cycles. Given the estimated atmospheric oxygen levels during the early Cambrian, which likely ranged between 10% and 40% of present atmospheric levels (PAL), it is reasonable to infer that the shallow marine environments of that time would have contained a significant presence of Fe^{2+} coexisting alongside Fe^{3+} complexes. Under these conditions, stoichiometric equations should incorporate both ferric complexes and ferrous iron, with their relative proportions contingent upon the prevailing redox conditions.

For phytoplankton, the iron requirement relative to carbon is much lower than that of macronutrients like nitrogen and phosphorus. A generalized stoichiometric equation including iron for phytoplankton might look like the following:

$$106 \cdot CO_2 + 16 \cdot NO_3^- + HPO_4^{2-} + 0.5 \cdot Fe^{2+} + 0.5 \cdot [\text{Fe(III)-complex}] + 122 \cdot H_2O + 18 \cdot H^+ \rightarrow C_{106}H_{263}O_{110}N_{16}PFe + 138 \cdot O_2$$

This equation is based on the work of Ho et al. [208], who found that the Fe:C ratios in marine phytoplankton range from about 5 to 20 μmol/mol. The exact ratio can vary depending on species and environmental conditions.

For multicellular algae, including macroalgae, the iron requirements and stoichiometry can differ from those of phytoplankton. Incorporating iron into our previous macroalgal equation, we might have the following:

$550 \cdot CO_2 + 30 \cdot NO_3^- + HPO_4^{2-} + 0.5 \cdot Fe^{2+} + 0.5 \cdot [Fe(III)\text{-complex}] + 551 \cdot H_2O + 30 \cdot H^+ \rightarrow C_{550}H_{1100}O_{550}N_{30}PFe + 551 \cdot O_2$

This equation is more speculative, as fewer studies have comprehensively examined iron stoichiometry in macroalgae compared to phytoplankton. However, some research suggests that macroalgae may have higher iron requirements relative to carbon than phytoplankton [219,223].

It is important to note that iron availability in marine environments is complex. In oxygenated seawater, iron is primarily present as Fe(III), which is highly insoluble. Much of the bioavailable iron is complexed with organic ligands. The equation we have used simplifies this complexity for the sake of stoichiometric representation.

The C:Fe ratios in Las Ermitas samples show quite variable values that do not align straightforwardly with typical biological iron uptake patterns. When converting these weight-based ratios to molar ratios for comparison with biological requirements, the disparity becomes even more evident. For example, the calcimicrobial limestones show a C:Fe weight ratio of 0.14, which converts to approximately 651 μmol Fe/mol C. The siltstones total C record shows a weight ratio of 2.78, converting to about 12,925 μmol Fe/mol C. These values are orders of magnitude higher than typical phytoplankton Fe:C requirements (5–20 μmol/mol).

Most notably, while the sulfate-related organic carbon shows higher weight ratios (2.44–5.06) than the Fe^{3+}-related fractions (0.02–0.00), all these values when converted to molar ratios are far from the expected biological uptake patterns. This suggests that the C:Fe ratios in Las Ermitas materials likely reflect a complex mixture of preservation effects, diagenetic processes, and depositional conditions rather than providing clear information about the biological iron uptake by the original Cambrian community.

7.5. Linking the Community Diversity, Biomass and Productivity in the Early Cambrian Reef–Lagoon of Las Ermitas

Understanding the relationship between nutrient availability and community diversity in ancient marine ecosystems is crucial for reconstructing early Paleozoic environmental conditions and biological evolution [215]. Modern studies demonstrate that nutrient flux directly influences biomass production, ecosystem complexity, and trophic relationships [224,225], though interpreting these patterns in the fossil record presents significant challenges. However, the reconstruction of paleocommunities faces two major challenges: first, the selective loss of community components that lack a preservation potential, and second, the poor preservation of ecological relationships between producers, consumers, and predators in ancient food webs [226]. This taphonomic bias fundamentally affects our understanding of ancient ecosystem structure and function, as the fossil record typically preserves only a small fraction of the original biological diversity [227]. The preservation potential varies significantly among different organisms and tissues, with biomineralized structures having a much higher likelihood of fossilization compared to soft tissues [128,228].

The lower Cambrian Las Ermitas deposits clearly illustrate these preservation biases. The recovered fossil assemblage is limited to phosphatized skeletal elements and permineralized chitinous walls, while soft-bodied organisms that likely dominated the original community have been lost from the fossil record [32]. This selective preservation

means we primarily see biomineralized organisms like brachiopods and small shelly fossils, while crucial ecosystem components such as soft-bodied algae, early sponges, and various vermiform organisms are underrepresented or absent [229,230]. Such a preservation bias significantly affects our understanding of early Cambrian community structure and diversity [126]. Moreover, the absence of soft-tissue preservation obscures important ecological relationships, including predator-prey interactions and symbiotic associations that would have been vital components of these early complex ecosystems [108,231].

Las Ermitas reef–lagoon paleocommunity exhibits a complex trophic structure, reconstructed from fossil evidence and inferred ecological roles. While ecosystems and biological communities have evolved significantly over Earth's history, particularly with the emergence of novel trophic levels, the core principles of ecosystem dynamics and community structure have remained remarkably consistent since the advent of multicellular life [232]. This suggests that, although increased trophic complexity has enhanced ecological balance and diversity, the fundamental processes governing ecosystem development and structure have been conserved through deep time. In this context, the trophic structure of the Las Ermitas paleocommunity can be reconstructed by examining the autoecological information preserved in the fossil record and comparing it with modern ecosystems that exhibit analogous ecological and functional dynamics (Figure 14) [233].

Following this approach, it can be deduced that the base of the trophic structure of Las Ermitas paleocommunity is composed of primary producers, including cyanobacteria, unicellular algae, and multicellular algae. As discussed above, fossil evidence from microbialites (stromatolites and thrombolites) strongly suggests the dominance of cyanobacteria, which formed extensive microbial mats in both the lagoon and reefal environments, serving as the foundational energy source for the ecosystem [122,234]. While unicellular algae (e.g., green algae) and multicellular algae are not observed in the fossil record at Las Ermitas, their ecological importance is inferred based on their prevalence in modern analogs of shallow marine ecosystems and the nutrient-rich nature of Cambrian lagoons [235]. These producers captured 100% of the ecosystem's energy via photosynthesis [234], which then flowed upward through the trophic levels.

The primary consumers in the Las Ermitas system (Figure 14) include taxa such as Halkieriids, Helcionellids, Chancelloriids, and Orthothecid hyoliths, which represent grazing and suspension-feeding organisms feeding on microbial mats or filtering organic particles from the water column [122,236]. These preserved taxa highlight the diversity of grazers in the system. However, zooplankton, though not preserved, are inferred to have been significant primary consumers, feeding on phytoplankton (unicellular algae) in the lagoonal environment [234]. Primary consumers converted approximately 10%–20% of the available energy from primary producers into their own biomass [235], enabling the flow of energy to secondary consumers. Furthermore, brachiopods as primary consumers in the Las Ermitas paleocommunity align with their ecological role in early Cambrian ecosystems as suspension feeders [237]. Brachiopods likely fed on planktonic or benthic organic material, including unicellular algae and microbial mat detritus. Their absence in the Las Ermitas fossil record is intriguing, as it may result from the acid dissolution of their carbonate shells during phosphatic fossil extraction processes [238]. Unlike phosphatic-shelled organisms (e.g., small shelly fauna), brachiopods with calcareous shells may not have undergone phosphatization, preventing their preservation under such extraction methods [238]. This highlights a preservation bias that can obscure critical trophic components in paleocommunity reconstructions.

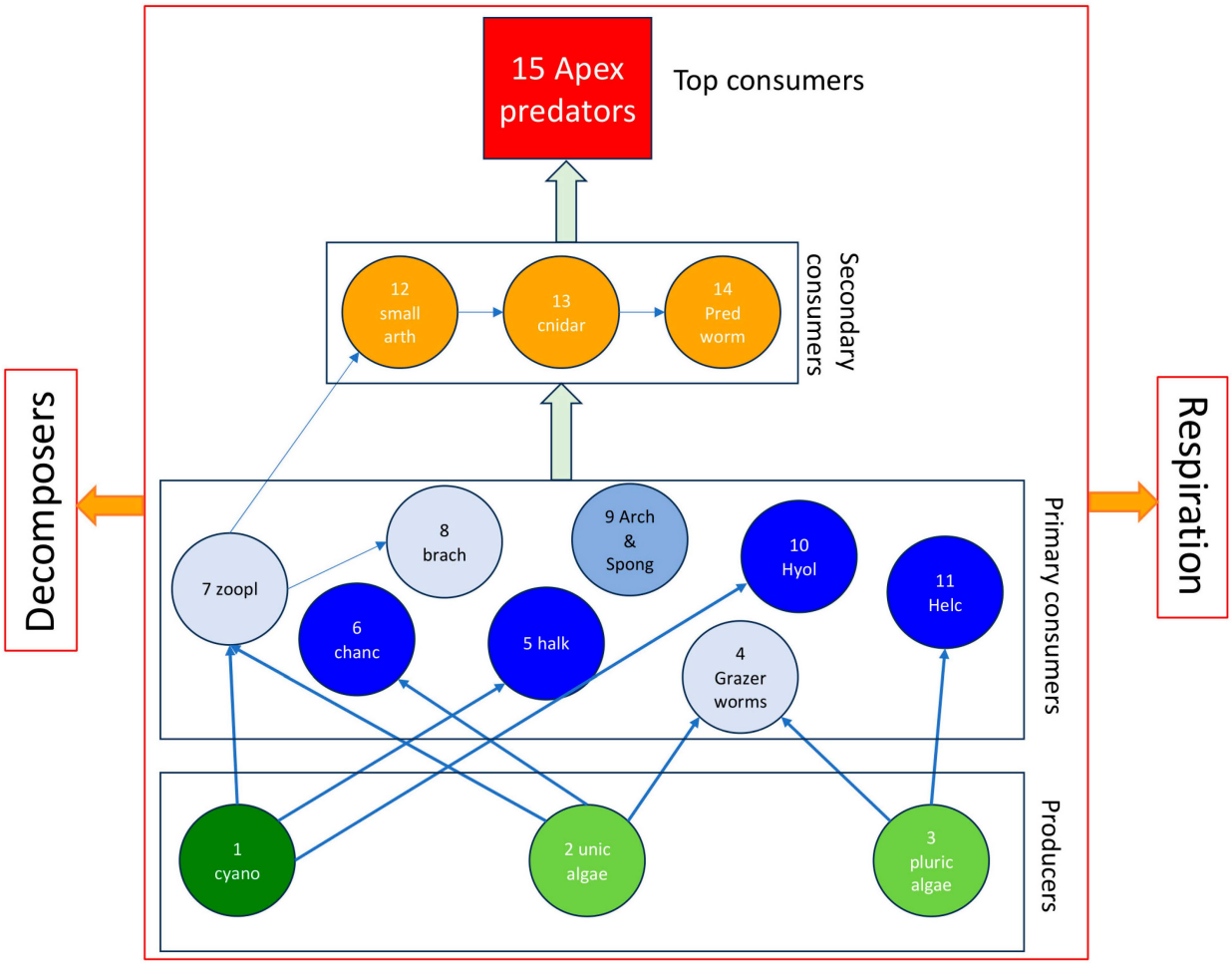

Figure 14. The tentative reconstruction of the community structure and trophic interactions within the Las Ermitas reef–lagoon system. The numbers correspond to specific groups of organisms, grouped by their trophic level: Primary producers include 1—cyanobacteria; 2—unicellular algae; and 3—multicellular algae. Primary consumers include 4—grazing worms; 5—Halkieriids; 6—Chancelloriids; 7—zooplankton; 8—Brachiopods; 9—Archaeocyathids and sponges; 10—Hyoliths; and 11—Helcionellids. Secondary consumers include 12—small arthropods; 13—Cnidarians; and 14—predatory worms. Tertiary consumers consist of 15—apex predators. The arrows indicate the energy flow across the trophic levels, illustrating the structure and dynamics of the paleocommunity. The progressive decrease in biomass from the primary producers to the apex predators reflects the inefficiencies in energy transfer through the trophic web. Additionally, biomass is lost at all the trophic levels through the activity of decomposers and respiration, as indicated by the horizontal arrows.

Sponges and archaeocyathids likely played a significant role in the trophic structure of the Las Ermitas paleocommunity as primary consumers (Figure 14). Both groups were suspension feeders, relying on water filtration to capture organic particles and plankton. Sponges are not preserved in the Las Ermitas materials, but their presence can be inferred based on their ecological importance in similar Cambrian reefal environments, where they contributed to nutrient cycling and benthic community dynamics [11]. In contrast, archaeocyathids are preserved in the form of calcareous skeletons, which in some cases show evidence of silica mineralization. These organisms were among the first reef builders, providing structural complexity to the ecosystem while functioning as efficient suspension feeders [239].

The secondary consumers (Figure 14) are represented by preserved taxa such as small arthropods (e.g., Bradoriida) and Cnidarians (e.g., Byroniida). These organisms

likely preyed on primary consumers such as helcionellids, zooplankton, and other small grazers, fulfilling their roles as predators and scavengers [240,241]. Additionally, soft-bodied predatory worms, including priapulids and possibly nemertean or polychaete-like organisms, are inferred to have been part of this trophic level based on evidence from comparable Cambrian ecosystems such as the Burgess Shale and Chengjiang Lagerstätten. Secondary consumers transferred ~10% of the energy they consumed to tertiary consumers, with significant energy losses due to metabolic processes and inefficiencies [122,235].

The tertiary consumers (Figure 14), or top predators, in the Las Ermitas paleocommunity are represented by large arthropods (e.g., trilobite-like predators) that likely preyed on smaller arthropods, cnidarians, and other secondary consumers. Additionally, inferred predators such as priapulid worms may have also played a significant role in this level, as priapulid fossils from other Cambrian sites suggest their ecological importance as apex predators [240–242]. Tertiary consumers retained only ~5%–10% of the energy from secondary consumers, resulting in a very low biomass at this trophic level, consistent with the energy transfer inefficiencies [122,235].

The energy and biomass within the Las Ermitas system should have followed the same processes of energy and biomass loss through the full trophic web. Primary producers supported 100% of the ecosystem's energy and biomass, with a total biomass production of $1.5{\cdot}10^{9}$ gC·yr^{-1}. Biomass decreased progressively at higher trophic levels due to energy transfer inefficiencies. For example, $1.5{\cdot}10^{9}$ gC·yr^{-1} at the producer level would support approximately $1.5{\cdot}10^{8}$ gC·yr^{-1} at the primary consumer level, $1.5{\cdot}10^{7}$ gC·yr^{-1} at the secondary consumer level, and $1.5{\cdot}10^{6}$ gC·yr^{-1} at the tertiary consumer level (Figure 14). This progressive reduction reflects the inefficiencies in energy transfer, with significant energy lost to respiration, heat, and metabolic processes [122,235]. However, the dominance of microbial mats in the Cambrian environment may have resulted in slightly higher energy retention at lower trophic levels, owing to their rapid turnover rates and efficient detrital recycling [234,236].

A preliminary estimation of community biomass at various trophic levels within the Las Ermitas system was derived by the calculating biovolume based on the preserved fossil record (Figure S7A). By subtracting the organic carbon associated with the preserved organisms from the total estimated organic carbon for a given trophic level, the remaining carbon can be attributed to organisms that are absent from the geological record. For these unrecorded taxa, average biovolumes were inferred using ecological analogs, creating a comparative framework to evaluate the reliability of this approach. Although these calculations rely on assumptions—such as the accuracy of total organic carbon estimates and the representativeness of the fossil record—they offer valuable insights into the approximate biomass and annual productivity of the paleocommunity. While full calculations of biomass for all the trophic elements extend beyond the scope of this paper, the discussion in this section focuses on the relationships between productivity and community diversity, offering key insights into paleocommunity dynamics.

The analysis revealed the relative abundance of well-preserved taxa, such as hyoliths, chancelloriids, and cnidarians, in the Las Ermitas paleocommunity. However, key ecological components, including zooplankton, soft-bodied worms, and algae, are conspicuously absent, likely due to preservation biases [108,240]. These missing taxa were likely critical players in nutrient cycling and energy transfer, underscoring the need to incorporate both preserved and inferred taxa for a more holistic view of the ecosystem's trophic structure. Such an integrative approach bridges the gaps left by preservation biases and helps reconstruct energy dynamics within the paleocommunity.

To quantitatively link the diversity, biomass, and productivity in the Las Ermitas lagoon, a systematic multi-step methodology was employed. First, the biovolume data for

each taxon were converted to the carbon biomass using a standard conversion factor of 0.11 g C per cm^3, a widely used ratio for marine plankton. The total carbon biomass was then calculated by summing these values across all the taxa, providing a basis to explore the relationship between species richness and the total carbon biomass. To estimate the annual productivity, an assumed turnover rate of 10—typical for marine systems—was applied to the total carbon biomass. Furthermore, the phosphorus requirements necessary to sustain this level of productivity were calculated using the Redfield ratio (C:P = 106:1). For example, a hypothetical community comprising 24 species and a total biovolume of 5426.75 cm^3 would yield a carbon biomass of 596.94 g C. Assuming an annual turnover rate of 10, this translates to an annual productivity of 5969.4 g C/year, requiring approximately 56.32 g P/year. By quantifying these parameters, the method not only elucidates the diversity-productivity relationship but also offers insights into nutrient cycling rates. These estimates can be compared against the geological evidence of nutrient availability in the Las Ermitas deposits, yielding a comprehensive picture of the lagoon's biogeochemical dynamics.

Integrating the fossil evidence with the inferred biovolume estimates and the nutrient cycling analyses provides a robust framework for reconstructing the ecological and biogeochemical processes of ancient lagoon systems. This approach underscores the interplay between biodiversity, productivity, and nutrient dynamics, allowing for a deeper understanding of how ancient ecosystems functioned. As a result, these findings contribute significantly to paleobiological studies, emphasizing the importance of connecting preserved records with inferred ecological processes to reconstruct the full complexity of past ecosystems.

8. Conclusions

The analysis of the Las Ermitas reef–lagoon system provides critical insights into the interplay between biogeochemical cycles and early metazoan community development during the early Cambrian. The continental weathering rates were approximately 23 times higher than modern baseline rates, with calcium fluxes of 87.70 $kg \cdot yr^{-1}$ per kilogram of andesite. Annual nutrient fluxes into the lagoon, including 0.286 $g \cdot cm^{-2} \cdot yr^{-1}$ for Fe and 0.0146 $g \cdot cm^{-2} \cdot yr^{-1}$ for PO_4^{3-}, reflect the influence of elevated atmospheric CO_2 and intensified weathering. Lateritic and saprolitic weathering products further support these conclusions.

Nutrient cycling patterns show variable concentrations of Fe (0.14–3.23 wt%), PO_4^{3-} (0.1–20.0 wt%), and Si (0.27–69.0 wt%), linked to the formation of phosphorites and ferrous phyllosilicates under suboxic conditions. Microbial activity played a dominant role, with sulfate-reducing bacteria recycling ~$1.55 \cdot 10^{11}$ g of C compared to $5.94 \cdot 10^8$ g of C via iron reduction, driving nutrient transformation and supporting diverse metabolic strategies. Fossil evidence reveals a diverse community with over 20 taxa, including mollukcs (27.70% biomass) and small shelly fossils, forming a well-organized trophic structure. A log-normal dominance–diversity curve indicates complex ecological organization influenced by nutrient availability.

Spatial gradients show distinct biogeochemical dynamics, with phosphate fluxes ranging from $1.38 \cdot 10^{-7}$ $g \cdot cm^{-2} \cdot yr^{-1}$ in the reef core to $3.08 \cdot 10^{-7}$ $g \cdot cm^{-2} \cdot yr^{-1}$ in the lagoon. Similarly, iron fluxes vary from $1.93 \cdot 10^{-7}$ $g \cdot cm^{-2} \cdot yr^{-1}$ in the reef to $1.51 \cdot 10^{-5}$ $g \cdot cm^{-2} \cdot yr^{-1}$ in the lagoon, demonstrating environmental heterogeneity and the influence of reef structure on nutrient cycling and community distribution.

Phosphate concentrations in steinkerns (20 wt%) and the formation of Fe(II)-bearing phyllosilicates highlight efficient biological nutrient recycling and iron cycling under suboxic conditions. The carbon budget reveals the production of ~$1.49 \cdot 10^{15}$ g of C over the

system's million-year lifespan, with only ~0.01% preserved in the rock record. The C:P ratios (0.12 to 161.83) vary across the facies, reflecting differences in organic matter preservation, particularly in anoxic environments.

This study establishes a framework for exploring early Cambrian biogeochemical systems, with quantified nutrient fluxes providing a basis for comparisons with global reef systems. Future research should refine primary productivity models and explore nutrient ratios' impact on community composition, focusing on microbial roles in nutrient cycling and early metazoan evolution. These findings emphasize the link between biogeochemical conditions and the emergence of complex ecosystems during the Cambrian period.

The integration of geochemical modeling and paleontological analysis highlights the role of diversity, productivity, and nutrient cycling in ecosystem resilience. This methodological framework bridges paleobiology and modern ecological principles, advancing our understanding of ecosystem stability and evolutionary innovation across time.

Supplementary Materials: The following supporting information can be downloaded at: https://www.mdpi.com/xxx/s1. Figure S1. The various stratigraphic sections (Creveling et al. [6]; Fernandez-Remolar et al. [29]; Moreno-Eiris [86]) are systematically organized in a southeast to northwest (SE to NW) direction along the Precambrian paleorelief. These sections represent distinct sedimentary environments and serve as valuable references for this study. Notably, the investigated samples, namely 95E5/2 and 95E5/3, originate from section 95E5. The materials constituting this section are attributed to the deposition within a marginal lagoon environment. Figure S2. A comprehensive reconstruction of stratigraphic section 95E2 uncovers a diverse assemblage of sedimentary materials that evolved along a progressive deepening trend. The section offers an extensive record of shifting depositional environments, mirroring the gradual deepening of the underlying sedimentary basin. The sampling points, indicated by yellow dots, were strategically chosen to collect paleontological information, as depicted in the legend for paleontological content. Figure S3. A comprehensive reconstruction of section 95E5, from which samples 95E5/2 and 95E5/3 were obtained, reveals a remarkable diversity in the paleontological record. The section provides valuable insights into the wide range of fossilized organisms preserved within its layers, offering a comprehensive snapshot of the ancient biological communities that once thrived in the lagoon. Figure S4. (**A**) A silicified stromatolite retrieved from the lower portion of section 95E2 provides evidence of shallow environmental conditions. The scale bar represents a length of 5 cm. (**B**) A bioclastic limestone sample obtained at 95E2/X displays early primary cementation, manifested as layers of isopachous radial fibrous calcite transitioning into micrite. The thin section reveals the complex carbonate fabric characteristic of early Cambrian reef environments. The presence of archaeocyathids with micritized walls indicates a shallow, warm marine setting, typical of early Cambrian reef ecosystems (Wood [82]). The micritization of the archaeocyathid walls suggests early diagenetic processes in a shallow, moderate-energy environment. The subsequent development of the palisade textures coating these micritized structures points to early marine cementation, likely occurring in a well-circulated phreatic zone with high carbonate saturation. This sequence of diagenetic features—micritization followed by palisade cement formation—is indicative of a multi-stage early diagenetic history in a dynamic reef or forereef setting. The reddish coloration of the carbonate matrix, potentially due to the presence of iron-rich minerals such as chlorites with Fe^{3+}, suggests slightly oxidizing conditions. These features collectively imply a slightly alkaline environment, with the pH likely ranging from 8.0 to 8.5, which is consistent with the conditions necessary for carbonate oversaturation and early marine cementation (Riding and Liang [130]). Figure S5. Limestone breccia containing pebbles and displaying a distinct laminar structure, collected from the lowest portion of stratigraphic section 95E2, indicating the prevalence of the sedimentary conditions characteristic of intertidal environments. The scale bar represents a length of 5 cm. Figure S6. **(A)** polished cross-section exhibiting various types of phosphorites, obtained from the northwestern region associated with sedimentary conditions characteristic of a lagoon environment. A) Multiepisodic phosphorite identified in section 95E7. (**B**) Massive phosphorite from stratigraphic section 95E5, transitioning into numerous phosphoritic layers ranging

from centimetric to millimetric in thickness. (**C**) Intervals of phosphorite intercalated with nodulose carbonate-bearing phosphatic fossils from section 95E5. The scale bar represents a length of 5 cm. Figure S7. Photomicrographs of two thin sections prepared from sample 95E5/3 are presented. (**A**) A bioclastic layer sandwiched between two micritic layers reveals sections of hyoliths filled with varying compositions of a phosphatic matrix. (**B**) Bioclastic microfacies containing abundant chancelloriid sclerites, some of which exhibit tiny pyritic crystals (indicated by white arrows). (**C**) A close-up view of a chancelloriid sclerite partially filled with pyrite. Figure S8. An X-ray diffraction (XRD) analysis was conducted on various samples collected from the Las Ermitas site to investigate the mineral composition of the sediments. The results reveal a diverse mineral assemblage, with a significant presence of greenish phyllosilicates and phosphatic minerals. (**A**) The XRD analysis of the insoluble residue from a sample of greenish limestone (95E2/7) treated with acetic acid demonstrates that the dissolution of calcite enhances the intensity of the quartz, chlorite/chamosite, and illite peaks. (**B**) The mineral analysis of sample 95E4/1, obtained from a greenish siltstone containing a carbonate matrix (c), reveals a substantial increase in the 14.2 Å peak of chlorite/chamosite after the matrix was dissolved using acetic acid. (**C**) The XRD analysis of a phosphatic inner mold of an archeocyathid (95E5/2a), where the calcitic matrix was removed, is compared with the rock matrix sample 95E5/2 collected from a phosphatic limestone. (**D**) The XRD analysis of sample 95E5/5, consisting of a carbonate nodule within a greenish siltstone, provides insights into its mineral composition. (**E**) A comparison of minerals found in a calcimicrobial limestone (95E7/0), containing approximately 95% calcite, and a greenish siltstone (95E7/0d), composed of illite and chlorite/chamosite, highlights the contrast in their mineral assemblages. (**F**) The XRD analysis of a reddish siltstone (sample 95E6/1a) after dissolution under acetic acid reveals a higher concentration of detrital components, such as quartz and feldspar, associated with chlorite and illite. Figure S9. **(A**) A bar diagram illustrating the percentage biomass distribution for each taxonomic group, calculated based on the number and the average size of specimens. (**B**–**E**) Several phosphatic complex steinkerns of Hyolitha exhibit preserved phosphatized microbial filaments. The size of these filaments suggests a predominantly fungal origin, highlighting the significant contribution of heterotrophic communities to the recycling of organic matter within the reefal system. (**F**) The dominance–diversity curve for the Las Ermitas system, characterized by a steep initial decline, reflects the presence of a small number of taxa that dominate the community biomass, consistent with the "trophic nucleus" concept. In this case, mollusks and small shelly fossils are the dominant taxa, contrasting with the arthropod-dominated Burgess Shale fauna. The observed long tail of the curve suggests a stable and mature ecosystem with high diversity among less abundant taxa. However, the absence of soft-bodied organisms due to a taphonomic bias, along with the lack of distinct breaks in the curve, highlights the limitations of the preserved biomass data in reconstructing the full community structure.

Author Contributions: Conceptualization, methodology, formal analysis, investigation, resources, writing—original draft preparation, writing—review and editing, visualization, supervision, and funding acquisition, D.C.F.-R. and T.H. All authors have read and agreed to the published version of the manuscript.

Funding: The project was supported by the National Key Research and Development Program of China (2021YFA0716100 (D.C.F.-R.); 2022YFF0504000 (T.H.)) and the Science and Technology Development Fund (FDCT) (0005/2020/A1 (D.C.F.-R. and T.H.))

Data Availability Statement: The data are contained within the article and the Supplementary Materials.

Acknowledgments: The authors are deeply grateful to Zong Qiugang, Director of the SKL Lunar and Planetary Sciences, for his generous support and dedication to fostering research within the laboratory, which has greatly contributed to the completion of this work. Furthermore, we extend our gratitude to Yihao Xie for conducting the LA-ICP/MS analysis, which was essential for determining the nutrient reservoir content presented in this study.

Conflicts of Interest: The authors declare no conflicts of interest.

References

1. Gasquet, D.; Levresse, G.; Cheilletz, A.; Azizi-Samir, M.R.; Mouttaqi, A. Contribution to a geodynamic reconstruction of the Anti-Atlas (Morocco) during Pan-African times with the emphasis on inversion tectonics and metallogenic activity at the Precambrian–Cambrian transition. *Precambrian Res.* **2005**, *140*, 157–182. [CrossRef]
2. Yajioui, Z.; Karaoui, B.; Chew, D.; Breitkreuz, C.; Mahmoudi, A. U–Pb zircon geochronology of the Ediacaran volcano-sedimentary succession of the NE Saghro inlier (Anti-Atlas, Morocco): Chronostratigraphic correlation on the northwestern margin of Gondwana. *Gondwana Res.* **2020**, *87*, 263–277. [CrossRef]
3. Hearing, T.W.; Harvey, T.H.P.; Williams, M.; Leng, M.J.; Lamb, A.L.; Wilby, P.R.; Gabbott, S.E.; Pohl, A.; Donnadieu, Y. An early Cambrian greenhouse climate. *Sci. Adv.* **2018**, *4*, eaar5690. [CrossRef] [PubMed]
4. Álvaro, J.J.; Bellido, F.; Gasquet, D.; Pereira, M.F.; Quesada, C.; Sánchez-García, T. Diachronism in the late Neoproterozoic–Cambrian arc-rift transition of North Gondwana: A comparison of Morocco and the Iberian Ossa-Morena Zone. *J. Afr. Earth Sci.* **2014**, *98*, 113–132. [CrossRef]
5. Quesada, C. Precambrian successions in SW Iberia: Their relationship to 'Cadomian' orogenic events. *Geol. Soc. Lond. Spec. Publ.* **1990**, *51*, 353–362. [CrossRef]
6. Creveling, J.R.; Fernández-Remolar, D.; Rodríguez-Martínez, M.; Menéndez, S.; Bergmann, K.D.; Gill, B.C.; Abelson, J.; Amils, R.; Ehlmann, B.L.; García-Bellido, D.C.; et al. Geobiology of a lower Cambrian carbonate platform, Pedroche Formation, Ossa Morena Zone, Spain. *Palaeogeogr. Palaeoclimatol. Palaeoecol.* **2013**, *386*, 459–478. [CrossRef]
7. Álvaro, J.J.; Clausen, S. Botoman (Lower Cambrian) turbid- and clear-water reefs and associated environments from the High Atlas, Morocco. *Geol. Soc. Lond. Spec. Publ.* **2007**, *275*, 51–70. [CrossRef]
8. Álvaro, J.J.; Debrenne, F. The Great Atlasian Reef Complex: An early Cambrian subtropical fringing belt that bordered West Gondwana. *Palaeogeogr. Palaeoclimatol. Palaeoecol.* **2010**, *294*, 120–132. [CrossRef]
9. Hicks, M.; Rowland, S.M. Early Cambrian microbial reefs, archaeocyathan inter-reef communities, and associated facies of the Yangtze Platform. *Palaeogeogr. Palaeoclimatol. Palaeoecol.* **2009**, *281*, 137–153. [CrossRef]
10. Zhao, Y.; Yan, H.; Tucker, M.E.; Han, M.; Zhao, H.; Mao, G.; Peng, C.; Han, Z. Calcimicrobes in Cambrian microbialites (Shandong, North China) and comparison with experimentally produced biomineralization precipitates. *Carbonates Evaporites* **2020**, *35*, 119. [CrossRef]
11. Zhuravlev, A.Y. Paleoecology of Cambrian Reef Ecosystems. In *The History and Sedimentology of Ancient Reef Systems*; Stanley, G.D., Ed.; Springer: Boston, MA, USA, 2001; pp. 121–157.
12. Na, L.; Kiessling, W. Diversity partitioning during the Cambrian radiation. *Proc. Nat. Acad. Sci. USA* **2015**, *112*, 4702–4706. [CrossRef] [PubMed]
13. Servais, T.; Cascales-Miñana, B.; Harper, D.A.T.; Lefebvre, B.; Van Bocxlaer, B.; Wang, W. Cambrian explosion and Ordovician biodiversification or Cambrian biodiversification and Ordovician explosion? *Evol. Earth* **2023**, *1*, 100018. [CrossRef]
14. Marshall, C.R. Explaining the Cambrian"explosion" of animals. *Annu. Rev. Earth Planet. Sci.* **2006**, *34*, 355–384. [CrossRef]
15. Knoll, A.H. Biological and Biogeochemical Preludes to the Ediacaran Radiation. In *Origin and Early Evolution of the Metazoa*; Lipps, J.H., Signor, P.W., Eds.; Springer: Boston, MA, USA, 1992; pp. 53–84.
16. Erwin, D.H.; Laflamme, M.; Tweedt, S.M.; Sperling, E.A.; Pisani, D.; Peterson, K.J. The Cambrian Conundrum: Early Divergence and Later Ecological Success in the Early History of Animals. *Science* **2011**, *334*, 1091–1097. [CrossRef] [PubMed]
17. Reinhard, C.T.; Planavsky, N.J.; Gill, B.C.; Ozaki, K.; Robbins, L.J.; Lyons, T.W.; Fischer, W.W.; Wang, C.; Cole, D.B.; Konhauser, K.O. Evolution of the global phosphorus cycle. *Nature* **2017**, *541*, 386–389. [CrossRef]
18. Brasier, M.D. Paleoceanography and Changes in the Biological Cycling of Phosphorus across the Precambrian-Cambrian Boundary. In *Origin and Early Evolution of the Metazoa*; Lipps, J.H., Signor, P.W., Eds.; Topics in Geobiology; Springer: Boston, MA, USA, 1992; pp. 483–523.
19. Li, W.-P.; Zhao, Y.-Y.; Zhao, M.-Y.; Zha, X.-P.; Zheng, Y.-F. Enhanced weathering as a trigger for the rise of atmospheric O2 level from the late Ediacaran to the early Cambrian. *Sci. Rep.* **2019**, *9*, 10630. [CrossRef]
20. Horton, F. Did phosphorus derived from the weathering of large igneous provinces fertilize the Neoproterozoic ocean? *Geochem. Geophys. Geosyst.* **2015**, *16*, 1723–1738. [CrossRef]
21. Wang, R.; Lang, X.; Ding, W.; Liu, Y.; Huang, T.; Tang, W.; Shen, B. The coupling of Phanerozoic continental weathering and marine phosphorus cycle. *Sci. Rep.* **2020**, *10*, 5794. [CrossRef]
22. Creveling, J.R.; Johnston, D.T.; Poulton, S.W.; Kotrc, B.; März, C.; Schrag, D.P.; Knoll, A.H. Phosphorus sources for phosphatic Cambrian carbonates. *GSA Bull.* **2014**, *126*, 145–163. [CrossRef]
23. Libes, S. *Introduction to Marine Biogeochemistry*; Elsevier: Amsterdam, The Netherlands, 2009.
24. Kroeck, D.M.; Mullins, G.; Zacaï, A.; Monnet, C.; Servais, T. A review of Paleozoic phytoplankton biodiversity: Driver for major evolutionary events? *Earth-Sci. Rev.* **2022**, *232*, 104113. [CrossRef]
25. Boyd, P.W.; Ellwood, M.J. The biogeochemical cycle of iron in the ocean. *Nat. Geosci.* **2010**, *3*, 675–682. [CrossRef]
26. Butterfield, N.J. Macroevolution and macroecology through deep time. *Palaeontology* **2007**, *50*, 41–55. [CrossRef]

27. Gougeon, R.C.; Mángano, M.G.; Buatois, L.A.; Narbonne, G.M.; Laing, B.A. Early Cambrian origin of the shelf sediment mixed layer. *Nat. Commun.* **2018**, *9*, 1909. [CrossRef] [PubMed]
28. Zhuravlev, A.Y.; Mitchell, E.G.; Bowyer, F.; Wood, R.; Penny, A. Increases in reef size, habitat and metacommunity complexity associated with Cambrian radiation oxygenation pulses. *Nat. Commun.* **2022**, *13*, 7523. [CrossRef]
29. Fernández-Remolar, D.C. The phosphoritic limestones of the Lower Ovetian from the Sierra de Córdoba, Spain. *Bol. Real Soc. Española Hist. Natural. Secc. Geológica* **1999**, *95*, 15–45.
30. Brasier, M.D. The Lower Cambrian transgression and glauconite-phosphate facies in western Europe. *J. Geol. Soc.* **1980**, *137*, 695. [CrossRef]
31. Rowland, S.M.; Shapiro, R.S. Reef Patterns and Environmental Influences in the Cambrian and Earliest Ordovician. *Phaneroz. Reef Patterns* **2002**, *72*, 95–128. [CrossRef]
32. Fernandez-Remolar, D.C. Latest Neoproterozoic to Middle Cambrian body fossil record in Spain (exclusive of trilobites and archaeocyaths) and their stratigraphic significance. *Gff* **2001**, *123*, 73–80. [CrossRef]
33. LoDuca, S.T.; Bykova, N.; Wu, M.; Xiao, S.; Zhao, Y. Seaweed morphology and ecology during the great animal diversification events of the early Paleozoic: A tale of two floras. *Geobiology* **2017**, *15*, 588–616. [CrossRef]
34. Bykova, N.; LoDuca, S.T.; Ye, Q.; Marusin, V.; Grazhdankin, D.; Xiao, S. Seaweeds through time: Morphological and ecological analysis of Proterozoic and early Paleozoic benthic macroalgae. *Precambrian Res.* **2020**, *350*, 105875. [CrossRef]
35. Tréguer, P.J.; De La Rocha, C.L. The World Ocean Silica Cycle. *Annu. Rev. Mar. Sci.* **2013**, *5*, 477–501. [CrossRef]
36. Dutkiewicz, S.; Follows, M.J.; Parekh, P. Interactions of the iron and phosphorus cycles: A three-dimensional model study. *Glob. Biogeochem. Cycles* **2005**, *19*, 1–22. [CrossRef]
37. Föllmi, K.B. The phosphorus cycle, phosphogenesis and marine phosphate-rich deposits. *Earth-Sci. Rev.* **1996**, *40*, 55–124. [CrossRef]
38. Raiswell, R.; Canfield, D. The Iron Biogeochemical Cycle Past and Present. *Geochem. Perspect. Lett.* **2012**, *1*, 1–220.
39. Menéndez, S.; Perejón, A.; Moreno-Eiris, E.; Rodríguez-Martínez, M. Arqueociatos del Cámbrico inferior de la Sierra de Córdoba (Sierra Morena, España): Nuevo registro. *Bol. Real Soc. Española Hist. Natural. Secc. Geológica* **2016**, *110*, 89–101.
40. Perejón, A.; Moreno-Eiris, E. Biostratigraphy and paleobiogeography of the archaeocyaths on the southwestern margin of Gondwana. *Z. Dtsch. Ges. Für Geowiss.* **2006**, *157*, 611–627.
41. Moreno-Eiris, E. Los montículos arrecifales de Algas y Arqueociatos del Cámbrico Inferior de Sierra Morena. IV: Bioestratigrafía y Sistemática de los Arqueociatos. *Boletín Geológico y Minero de España* **1987**, *XCVIII*, 729–779.
42. Sutak, R.; Camadro, J.-M.; Lesuisse, E. Iron Uptake Mechanisms in Marine Phytoplankton. *Front. Microbiol.* **2020**, *11*, 566691. [CrossRef]
43. Raven, J.A.; Evans, M.C.W.; Korb, R.E. The role of trace metals in photosynthetic electron transport in O_2-evolving organisms. *Photosynth. Res.* **1999**, *60*, 111–150. [CrossRef]
44. Hedrich, S.; Schlömann, M.; Johnson, D.B. The iron-oxidizing proteobacteria. *Microbiology* **2011**, *157*, 1551–1564. [CrossRef]
45. Madigan, M.; Sattley, W.; Aiyer, J.; Stahl, D.; Buckley, D. *Brock Biology of Microorganisms*, 16th ed.; Pearson: Hudson Street, NY USA, 2021.
46. Martin, J.H.; Gordon, M.; Fitzwater, S.E. The case for iron. *Limnol. Oceanogr.* **1991**, *36*, 1793–1802. [CrossRef]
47. Zehr, J.P.; Kudela, R.M. Nitrogen Cycle of the Open Ocean: From Genes to Ecosystems. *Annu. Rev. Mar. Sci.* **2011**, *3*, 197–225. [CrossRef] [PubMed]
48. Martinez, S.; Grover, R.; Baker David, M.; Ferrier-Pagès, C. Symbiodiniaceae Are the First Site of Heterotrophic Nitrogen Assimilation in Reef-Building Corals. *mBio* **2022**, *13*, e01601–e01622. [CrossRef]
49. Moore, C.M.; Mills, M.M.; Arrigo, K.R.; Berman-Frank, I.; Bopp, L.; Boyd, P.W.; Galbraith, E.D.; Geider, R.J.; Guieu, C.; Jaccard, S.L.; et al. Processes and patterns of oceanic nutrient limitation. *Nat. Geosci.* **2013**, *6*, 701–710. [CrossRef]
50. Tice, M.M.; Lowe, D.R. Photosynthetic microbial mats in the 3416-Myr-old ocean. *Nature* **2004**, *431*, 549–552. [CrossRef]
51. Tortell, P.D.; Maldonado, M.T.; Price, N.M. The role of heterotrophic bacteria in iron-limited ocean ecosystems. *Nature* **1996**, *383*, 330–332. [CrossRef]
52. Moore, J.K.; Doney, S.C.; Glover, D.M.; Fung, I.Y. Iron cycling and nutrient-limitation patterns in surface waters of the World Ocean. *Deep Sea Res. Part II Top. Stud. Oceanogr.* **2001**, *49*, 463–507. [CrossRef]
53. Liu, X.; Millero, F.J. The solubility of iron in seawater. *Mar. Chem.* **2002**, *77*, 43–54. [CrossRef]
54. Suzuki, Y.; Kuma, K.; Kudo, I.; Matsunaga, K. Iron requirement of the brown macroalgae Laminaria japonica, Undaria pinnatifida (Phaeophyta) and the crustose coralline alga Lithophyllum yessoense (Rhodophyta), and their competition in the northern Japan Sea. *Phycologia* **1995**, *34*, 201–205. [CrossRef]
55. Falkowski, P.G.; Barber, R.T.; Smetacek, V. Biogeochemical controls and feedbacks on ocean primary production. *Science* **1998**, *281*, 200–206. [CrossRef]
56. Croot, P.L.; Heller, M.I. The Importance of Kinetics and Redox in the Biogeochemical Cycling of Iron in the Surface Ocean. *Front. Microbiol.* **2012**, *3*, 219. [CrossRef] [PubMed]

57. Gledhill, M.; Buck, K.N. The Organic Complexation of Iron in the Marine Environment: A Review. *Front. Microbiol.* **2012**, *3*, 1–17. [CrossRef] [PubMed]
58. Morrissey, J.; Bowler, C. Iron Utilization in Marine Cyanobacteria and Eukaryotic Algae. *Front. Microbiol.* **2012**, *3*, 43. [CrossRef] [PubMed]
59. Shaked, Y.; Kustka, A.B.; Morel, F.M.M. A general kinetic model for iron acquisition by eukaryotic phytoplankton. *Limnol. Oceanogr.* **2005**, *50*, 872–882. [CrossRef]
60. Berman-Frank, I.; Cullen, J.T.; Shaked, Y.; Sherrell, R.M.; Falkowski, P.G. Iron availability, cellular iron quotas, and nitrogen fixation in Trichodesmium. *Limnol. Oceanogr.* **2001**, *46*, 1249–1260. [CrossRef]
61. Urry, L.A.; Cain, M.L.; Wasserman, S.A.; Minorsky, P.V.; Orr, R. *Campbell Biology*; Pearson: Hudson Street, NY, USA, 2021; p. 1488.
62. Vance, C.P.; Uhde-Stone, C.; Allan, D.L. Phosphorus acquisition and use: Critical adaptations by plants for securing a nonrenewable resource. *New Phytol.* **2003**, *157*, 423–447. [CrossRef]
63. Gérard, F. Clay minerals, iron/aluminum oxides, and their contribution to phosphate sorption in soils—A myth revisited. *Geoderma* **2016**, *262*, 213–226. [CrossRef]
64. Bustin, R.M.; Wüst, R.A.J. Maturation, organic. In *Encyclopedia of Sediments and Sedimentary Rocks*; Middleton, G.V., Church, M.J., Coniglio, M., Hardie, L.A., Longstaffe, F.J., Eds.; Springer: Dordrecht, The Netherlands, 2003; pp. 425–429.
65. Froelich, P.N. Kinetic control of dissolved phosphate in natural rivers and estuaries: A primer on the phosphate buffer mechanism1. *Limnol. Oceanogr.* **1988**, *33*, 649–668. [CrossRef]
66. Paytan, A.; McLaughlin, K. The Oceanic Phosphorus Cycle. *Chem. Rev.* **2007**, *107*, 563–576. [CrossRef]
67. Conley, D.J.; Carey, J.C. Silica cycling over geologic time. *Nat. Geosci.* **2015**, *8*, 431–432. [CrossRef]
68. De Wever, P.; Dumitrica-Jud, R.; Caulet, J.P.; Nigrini, C.; Caridroit, M. *Radiolarians in the Sedimentary Record*; CRC Press: London, UK, 2001.
69. Raven, J.A.; Waite, A.M. The evolution of silicification in diatoms: Inescapable sinking and sinking as escape? *New Phytol.* **2004**, *162*, 45–61. [CrossRef]
70. Maldonado, M.; Carmona, M.C.; Velásquez, Z.; Puig, A.; Cruzado, A.; López, A.; Young, C.M. Siliceous sponges as a silicon sink: An overlooked aspect of benthopelagic coupling in the marine silicon cycle. *Limnol. Oceanogr.* **2005**, *50*, 799–809. [CrossRef]
71. Uriz, M.-J. Mineral skeletogenesis in sponges. *Can. J. Zool.* **2006**, *84*, 322–356. [CrossRef]
72. Müller, W.E.G.; Wang, X.; Cui, F.-Z.; Jochum, K.P.; Tremel, W.; Bill, J.; Schröder, H.C.; Natalio, F.; Schloßmacher, U.; Wiens, M. Sponge spicules as blueprints for the biofabrication of inorganic–organic composites and biomaterials. *Appl. Microbiol. Biotechnol.* **2009**, *83*, 397–413. [CrossRef]
73. Reincke, T.; Barthel, D. Silica uptake kinetics of Halichondria panicea in Kiel Bight. *Mar. Biol.* **1997**, *129*, 591–593. [CrossRef]
74. Maldonado, M.; Navarro, L.; Grasa, A.; Gonzalez, A.; Vaquerizo, I. Silicon uptake by sponges: A twist to understanding nutrient cycling on continental margins. *Sci. Rep.* **2011**, *1*, 30. [CrossRef]
75. Conley, D.J. Terrestrial ecosystems and the global biogeochemical silica cycle. *Glob. Biogeochem. Cycles* **2002**, *16*, 68-61–68-68. [CrossRef]
76. Berner, R.A. Weathering, plants, and the long-term carbon cycle. *Geochim. Cosmochim. Acta* **1992**, *56*, 3225–3231. [CrossRef]
77. Ragueneau, O.; Tréguer, P.; Leynaert, A.; Anderson, R.F.; Brzezinski, M.A.; DeMaster, D.J.; Dugdale, R.C.; Dymond, J.; Fischer, G.; François, R.; et al. A review of the Si cycle in the modern ocean: Recent progress and missing gaps in the application of biogenic opal as a paleoproductivity proxy. *Glob. Planet. Change* **2000**, *26*, 317–365. [CrossRef]
78. DeMaster, D.J. The accumulation and cycling of biogenic silica in the Southern Ocean: Revisiting the marine silica budget. *Deep Sea Res. Part II Top. Stud. Oceanogr.* **2002**, *49*, 3155–3167. [CrossRef]
79. Maliva, R.G.; Knoll, A.H.; Siever, R. Secular change in chert distribution; a reflection of evolving biological participation in the silica cycle. *PALAIOS* **1989**, *4*, 519–532. [CrossRef] [PubMed]
80. Liu, Y.; Dai, M.; Chen, W.; Cao, Z. Distribution of biogenic silica in the upwlling zones in the South China Sea. *Adv. Geosci.* **2012**, *28*, 55–65.
81. Filippelli, G.M. The global phosphorus cycle: Past, present, and future. *Elements* **2008**, *4*, 89–95.
82. Wood, R. The ecological evolution of reefs. *Annu. Rev. Ecol. Evol. Syst.* **1998**, *29*, 179–206. [CrossRef]
83. Wood, R.A. Paleoecology of the earliest skeletal metazoan communities: Implications for early biomineralization. *Earth-Sci. Rev.* **2011**, *106*, 184–190.
84. Wood, A.R. *Reef Evolution*; Oxford University Press: New York, NY, USA, 1999; p. 414.
85. Montañez, I.P. Biological skeletal carbonate records changes in major-ion chemistry of paleo-oceans. *Proc. Nat. Acad. Sci. USA* **2002**, *99*, 15852–15854. [CrossRef]
86. Moreno-Eiris, E. Los montículos arrecifales de Algas y Arqueociatos del Cámbrico Inferior de Sierra Morena. I: Estratigrafía y Facies. *Boletín Geológico Min.* **1987**, *XCVIII*, 295–317.
87. Vennin, E.; Álvaro, J.J.; Moreno-Eiris, E.; Perejón, A. Early Cambrian coelobiontic communities in tectonically unstable crevices developed in Neoproterozoic andesites, Ossa-Morena, southern Spain. *Lethaia* **2003**, *36*, 53–65. [CrossRef]

88. Fernández-Remolar, D.C. Estudio Paleontológico de Taxones Problemáticos del Cámbrico de Sierra Morena. Ph.D. Thesis, Universidad Complutense de Madrid, Madrid, Spain, 1999.
89. Pruss, S.B.; Dwyer, C.H.; Smith, E.F.; Macdonald, F.A.; Tosca, N.J. Phosphatized early Cambrian archaeocyaths and small shelly fossils (SSFs) of southwestern Mongolia. *Palaeogeogr. Palaeoclimatol. Palaeoecol.* **2019**, *513*, 166–177. [CrossRef]
90. Das, B. Theoretical Study of Small Iron–Oxyhydroxide Clusters and Formation of Ferrihydrite. *J. Phys. Chem. A* **2018**, *122*, 652–661. [CrossRef]
91. Fernandez-Remolar, D. Chancelloridae del Ovetiense Inferior de la Sierra de Córdoba. *Rev. Española De Paleontol.* **2001**, *16*, 39–61. [CrossRef]
92. Zhang, F.; Blasiak Leah, C.; Karolin Jan, O.; Powell Ryan, J.; Geddes Chris, D.; Hill Russell, T. Phosphorus sequestration in the form of polyphosphate by microbial symbionts in marine sponges. *Proc. Natl. Acad. Sci. USA* **2015**, *112*, 4381–4386. [CrossRef] [PubMed]
93. Anthony, J.W.; Bideaux, R.A.; Bladh, K.W.; Nichols, M.C. *Handbook of Mineralogy: Arsenates, Phosphates, Vanadates. Vol. 4*; Mineral Data Publishing: Tucson, AZ, USA, 2000.
94. Burton, J.H.; Krinsley, D.H.; Pye, K. Authigenesis of Kaolinite and Chlorite in Texas Gulf Coast Sediments. *Clays Clay Miner.* **1987**, *35*, 291–296. [CrossRef]
95. Velde, B. 9.12—Green Clay Minerals. In *Treatise on Geochemistry*, 2nd ed.; Holland, H.D., Turekian, K.K., Eds.; Elsevier: Oxford, UK, 2014; pp. 351–364.
96. Fernández-Remolar, D.C. first record of Tannuolina Fonin & Smirnova, 1967 (Tommotiida) from the Lower Cambrian Pedroche Formation, Southern Spain. *Rev. Española De Micropaleontol.* **2002**, *34*, 39–51.
97. Bischoff, G.C.O. Byroniida, new order, from early Palaeozoic strata of eastern Australia (Cnidaria, thecate scyphopolyps). *Senckenberg. Lethaea* **1989**, *69*, 467–521.
98. Mergl, M.; Kraft, P. Byronids and similar tubular fossils from the Devonian of the Barrandian area (Czech Republic). *Earth Environ. Sci. Trans. R. Soc. Edinb.* **2022**, *113*, 373–390. [CrossRef]
99. Creveling, J.R.; Knoll, A.H.; Johnston, D.T. Taphonomy of Cambrian phosphatic small shelly fossils. *PALAIOS* **2014**, *29*, 295–308. [CrossRef]
100. Liu, F.; Skovsted, C.B.; Topper, T.P.; Zhang, Z. Soft part preservation in hyolithids from the lower Cambrian (Stage 4) Guanshan Biota of South China and its implications. *Palaeogeogr. Palaeoclimatol. Palaeoecol.* **2021**, *562*, 110079. [CrossRef]
101. Marek, L.; Yochelson, E.L. Aspects of the biology of Hyolitha (Mollusca). *Lethaia* **1976**, *9*, 65–82. [CrossRef]
102. Allmon, W.; Bottjer, D. *Evolutionary Paleoecology*; Columbia University Press: New York, NY, USA, 2001.
103. Bengtson, S.; Hou, X. The integument of Cambrian chancelloriids. *Acta Palaeontol. Pol.* **2001**, *46*, 1–22.
104. Dunne, J.A.; Williams, R.J.; Martinez, N.D.; Wood, R.A.; Erwin, D.H. Compilation and Network Analyses of Cambrian Food Webs. *PLOS Biol.* **2008**, *6*, e102. [CrossRef] [PubMed]
105. Pratt, B.; Spincer, B.R.; Wood, R.; Zhuravlev, A. Ecology and evolution of Cambrian reefs. In *Ecology of the Cambrian Radiation*; Zhuravlev, A., Riding, R., Eds.; Columbia University Press: New York, NY, USA, 2001; pp. 254–274.
106. Whalen, M.A.; Stachowicz, J.J. Suspension feeder diversity enhances community filtration rates in different flow environments. *Mar. Ecol. Prog. Ser.* **2017**, *570*, 1–13. [CrossRef]
107. Muscente, A.D.; Schiffbauer, J.D.; Broce, J.; Laflamme, M.; O'Donnell, K.; Boag, T.H.; Meyer, M.; Hawkins, A.D.; Huntley, J.W.; McNamara, M.; et al. Exceptionally preserved fossil assemblages through geologic time and space. *Gondwana Res.* **2017**, *48*, 164–188. [CrossRef]
108. Conway Morris, S. The community structure of the Middle Cambrian Phyllopod Bed (Burgess Shale). *Palaeontology* **1986**, *29*, 423–467.
109. Magurran, A.E. *Ecological Diversity and Its Measurement*; Princeton University Press: Princeton, NJ, USA, 1988.
110. Moreno-Eiris, E. Los montículos arrecifales de Algas y Arqueociatos delCámbrico lnferior de Sierra Morena II: Las algas calcáreas. *Boletín Geológico Min.* **1987**, *XCVIII*, 449–459.
111. Pratt, B.R. Epiphyton and Renalcis; diagenetic microfossils from calcification of coccoid blue-green algae. *J. Sediment. Res.* **1984**, *54*, 948–971. [CrossRef]
112. Altermann, W.; Kazmierczak, J.; Oren, A.; Wright, D.T. Cyanobacterial calcification and its rock-building potential during 3.5 billion years of Earth history. *Geobiology* **2006**, *4*, 147–166. [CrossRef]
113. Spring, S.; Sorokin, D.Y.; Verbarg, S.; Rohde, M.; Woyke, T.; Kyrpides, N.C. Sulfate-Reducing Bacteria That Produce Exopolymers Thrive in the Calcifying Zone of a Hypersaline Cyanobacterial Mat. *Front. Microbiol.* **2019**, *10*, 862. [CrossRef]
114. Perejón, A. Biostratigrafia de los arqueociatos en España. *Cuad. De Geol. Ibérica* **1984**, *9*, 213–265.
115. Gandin, A.; Debrenne, F. Distribution of the archaeocyath-calcimicrobial bioconstructions on the Early Cambrian shelves. *Palaeoworld* **2010**, *19*, 222–241. [CrossRef]
116. Hatcher, B.G. Coral reef primary productivity. A hierarchy of pattern and process. *Trends Ecol. Evol.* **1990**, *5*, 149–155. [CrossRef] [PubMed]

117. Odum, H.T.; Odum, E.P. Trophic Structure and Productivity of a Windward Coral Reef Community on Eniwetok Atoll. *Ecol. Monogr.* **1955**, *25*, 291–320. [CrossRef]
118. Riding, R. Microbial carbonates: The geological record of calcified bacterial–algal mats and biofilms. *Sedimentology* **2000**, *47*, 179–214. [CrossRef]
119. Moorhead, D.; Schmeling, J.; Hawes, I.A.N. Modelling the contribution of benthic microbial mats to net primary production in Lake Hoare, McMurdo Dry Valleys. *Antarct. Sci.* **2005**, *17*, 33–45. [CrossRef]
120. Wilkinson, C.R. Net Primary Productivity in Coral Reef Sponges. *Science* **1983**, *219*, 410–412. [CrossRef]
121. Binkley, K.L.; Wilkinson, B.H.; Owen, R.M. Vadose beachrock cementation along a Southwestern Michigan marl lake. *J. Sediment. Resesarch* **1980**, *50*, 953–962.
122. Lindeman, R.L. The Trophic-Dynamic Aspect of Ecology. *Ecology* **1942**, *23*, 399–417. [CrossRef]
123. Arias-González, J.E.; Delesalle, B.; Salvat, B.; Galzin, R. Trophic functioning of the Tiahura reef sector, Moorea Island, French Polynesia. *Coral Reefs* **1997**, *16*, 231–246. [CrossRef]
124. Fernández López, S. Sitemas tafonómicos: Función y evolución. *Rev. Española De Paleontol.* **1991**, *6*, 21–34.
125. Jørgensen, B.B.; Findlay, A.J.; Pellerin, A. The Biogeochemical Sulfur Cycle of Marine Sediments. *Front. Microbiol.* **2019**, *10*, 849.
126. Butterfield, N.J. Exceptional Fossil Preservation and the Cambrian Explosion. *Integr. Comp. Biol.* **2003**, *43*, 166–177. [CrossRef] [PubMed]
127. Briggs Derek, E.G.; Wilby Philip, R. The role of the calcium carbonate-calcium phosphate switch in the mineralization of soft-bodied fossils. *J. Geol. Soc.* **1996**, *153*, 665–668. [CrossRef]
128. Briggs, D.E.G.; Kear, A.J.; Martill, D.M.; Wilby, P.R. Phosphatization of soft-tissue in experiments and fossils. *J. Geol. Soc.* **1993**, *150*, 1035–1038. [CrossRef]
129. Sagemann, J.; Bale, S.J.; Briggs, D.E.G.; Parkes, R.J. Controls on the formation of authigenic minerals in association with decaying organic matter: An experimental approach. *Geochim. Cosmochim. Acta* **1999**, *63*, 1083–1095. [CrossRef]
130. Riding, R.; Liang, L. Geobiology of microbial carbonates: Metazoan and seawater saturation state influences on secular trends during the Phanerozoic. *Palaeogeogr. Palaeoclimatol. Palaeoecol.* **2005**, *219*, 101–115. [CrossRef]
131. Porter, S.M. Halkieriids in Middle Cambrian phosphatic limestones from Australia. *J. Paleontol.* **2004**, *78*, 574–590. [CrossRef]
132. Xiao, S.; Schiffbauer, J.D. Microfossil Phosphatization and Its Astrobiological Implications. In *From Fossils to Astrobiology: Records of Life on Earth and Search for Extraterrestrial Biosignatures*; Seckbach, J., Walsh, M., Eds.; Springer: Dordrecht, The Netherlands, 2008; pp. 89–117.
133. Rodríguez, H.; Fraga, R. Phosphate solubilizing bacteria and their role in plant growth promotion. *Biotechnol. Adv.* **1999**, *17*, 319–339. [CrossRef]
134. Burdige, D.J. The biogeochemistry of manganese and iron reduction in marine sediments. *Earth-Sci. Rev.* **1993**, *35*, 249–284. [CrossRef]
135. Knauth, L.P.; Kennedy, M.J. The late Precambrian greening of the Earth. *Nature* **2009**, *460*, 728–732. [CrossRef]
136. Bethke, C.M. *Geochemical and Biogeochemical Reaction Modeling*; Cambridge University Press: Cambridge, UK, 2008.
137. Accotto, C.; Azor, A.; Martínez Poyatos, D.; Pedrera, A.; González Lodeiro, F. Reorganization of Northern Peri-Gondwanan Terranes at Cambrian–Ordovician Times: Insights from the Detrital Zircon Record of the Ossa-Morena Zone (SW Iberian Massif). *Lithosphere* **2022**, *2022*, 6187518. [CrossRef]
138. Liñan, E. Bioestratigrafia de la Sierra de Córdoba. Ph.D. Thesis, Universidad de Granada, Granada, Spain, 1978.
139. Liñan, E.; Palacios, T. Aportaciones micropaleontológicas para el conocimiento del límite Precámbrico-Cámbrico en la sierra de Córdoba, España. *Comun. Dos Serviços Geológicos De Port.* **1983**, *69*, 227–234.
140. Delgado-Quesada, M.; Liñan, E.; Pascual Martínez, E.; Pérez Lorente, F. Criterios para la diferenciación de dominios en Sierra Morena Central. *Stud. Geol.* **1977**, *12*, 75–90.
141. Sarrionandia, F.; Carracedo Sánchez, M.; Eguiluz, L.; Ábalos, B.; Rodríguez, J.; Pin, C.; Gil Ibarguchi, J.I. Cambrian rift-related magmatism in the Ossa-Morena Zone (Iberian Massif): Geochemical and geophysical evidence of Gondwana break-up. *Tectonophysics* **2012**, *570–571*, 135–150. [CrossRef]
142. Dessert, C.; Dupré, B.; Gaillardet, J.; François, L.M.; Allègre, C.J. Basalt weathering laws and the impact of basalt weathering on the global carbon cycle. *Chem. Geol.* **2003**, *202*, 257–273. [CrossRef]
143. Stumm, W.; Morgan, J.J. *Aquatic Chemistry*; John Wiley & Sons: New York, NY, USA, 1996.
144. Poulton, S.W.; Raiswell, R. The low-temperature geochemical cycle of iron: From continental fluxes to marine sediment deposition. *Am. J. Sci.* **2002**, *302*, 774–805. [CrossRef]
145. Poulton, S.W.; Canfield, D.E. Ferruginous Conditions: A Dominant Feature of the Ocean through Earth's History. *Elements* **2011**, *7*, 107–112. [CrossRef]
146. Singer, P.C.; Stumm, W. Acidic Mine Drainage: The Rate-Determining Step. *Science* **1970**, *167*, 1121–1123. [CrossRef]
147. Lenton, T.M.; Daines, S.J.; Mills, B.J.W. COPSE reloaded: An improved model of biogeochemical cycling over Phanerozoic time. *Earth-Sci. Rev.* **2018**, *178*, 1–28. [CrossRef]

148. Krause, A.J.; Mills, B.J.W.; Zhang, S.; Planavsky, N.J.; Lenton, T.M.; Poulton, S.W. Stepwise oxygenation of the Paleozoic atmosphere. *Nat. Commun.* **2018**, *9*, 4081. [CrossRef]
149. He, T.; Zhu, M.; Mills, B.J.W.; Wynn, P.M.; Zhuravlev, A.Y.; Tostevin, R.; Pogge von Strandmann, P.A.E.; Yang, A.; Poulton, S.W.; Shields, G.A. Possible links between extreme oxygen perturbations and the Cambrian radiation of animals. *Nat. Geosci.* **2019**, *12*, 468–474. [CrossRef]
150. Schlesinger, W.H.; Bernhard, J.M. *Biogeochemistry. An Analysis of Global Change*, 4th ed.; Academic Press: London, UK, 2020.
151. Schön, J.r. *Physical Properties of Rocks: Fundamentals and Principles of Petrophysics*, 2nd ed.; Elsevier: Amsterdam, The Netherlands, 2015; Volume 65, p. 497.
152. Welch, S.A.; Vandevivere, P. Effect of microbial and other naturally occurring polymers on mineral dissolution. *Geomicrobiol. J.* **1994**, *12*, 227–238. [CrossRef]
153. Vandevivere, P.; Welch, S.A.; Ullman, W.J.; Kirchman, D.L. Enhanced dissolution of silicate minerals by bacteria at near-neutral pH. *Microb. Ecol.* **1994**, *27*, 241–251. [CrossRef] [PubMed]
154. Kraemer, S.M. Iron oxide dissolution and solubility in the presence of siderophores. *Aquat. Sci.* **2004**, *66*, 3–18. [CrossRef]
155. Kraemer, S.M.; Butler, A.; Borer, P.; Cervini-Silva, J. Siderophores and the Dissolution of Iron-Bearing Minerals in Marine Systems. *Rev. Mineral. Geochem.* **2005**, *59*, 53–84. [CrossRef]
156. Fernández-Remolar, D.C.; Morris, R.V.; Gruener, J.E.; Amils, R.; Knoll, A.H. The Rio Tinto Basin, Spain: Mineralogy, sedimentary geobiology, and implications for interpretation of outcrop rocks at Meridiani Planum, Mars. *Earth Planet. Sci. Lett.* **2005**, *240*, 149–167.
157. Gutzmer, J.; Bueukes, N.J. Earliest laterites and possible evidence for terrestrial vegetation in the Early Proterozoic. *Geology* **1998**, *26*, 263–266.
158. Cornell, R.M.; Schwertmann, U. *The Iron Oxides*, 2nd ed.; Wiley-VCH: Weinheim, Germany, 2003; p. 664.
159. Och, L.M.; Shields-Zhou, G.A. The Neoproterozoic oxygenation event: Environmental perturbations and biogeochemical cycling. *Earth-Sci. Rev.* **2012**, *110*, 26–57. [CrossRef]
160. Bjerrum, C.J.; Canfield, D.E. Ocean productivity before about 1.9 Gyr ago limited by phosphorus adsorption onto iron oxides. *Nature* **2002**, *417*, 159–162. [CrossRef]
161. Lijklema, L. Interaction of orthophosphate with iron(III) and aluminum hydroxides. *Environ. Sci. Technol.* **1980**, *14*, 537–541. [CrossRef]
162. Doucet, F.J.; Schneider, C.; Bones, S.J.; Kretchmer, A.; Moss, I.; Tekely, P.; Exley, C. The formation of hydroxyaluminosilicates of geochemical and biological significance. *Geochim. Cosmochim. Acta* **2001**, *65*, 2461–2467. [CrossRef]
163. Oelkers, E.H.; Gislason, S.R. The mechanism, rates and consequences of basaltic glass dissolution: I. An experimental study of the dissolution rates of basaltic glass as a function of aqueous Al, Si and oxalic acid concentration at 25 °C and pH = 3 and 11. *Geochim. Cosmochim. Acta* **2001**, *65*, 3671–3681. [CrossRef]
164. Tosca, N.J.; Guggenheim, S.; Pufahl, P.K. An authigenic origin for Precambrian greenalite: Implications for iron formation and the chemistry of ancient seawater. *GSA Bull.* **2016**, *128*, 511–530. [CrossRef]
165. Berner, R.A.; Rao, J.-L. Phosphorus in sediments of the Amazon River and estuary: Implications for the global flux of phosphorus to the sea. *Geochim. Cosmochim. Acta* **1994**, *58*, 2333–2339. [CrossRef]
166. Planavsky, N.J.; Rouxel, O.J.; Bekker, A.; Lalonde, S.V.; Konhauser, K.O.; Reinhard, C.T.; Lyons, T.W. The evolution of the marine phosphate reservoir. *Nature* **2010**, *467*, 1088–1090. [CrossRef] [PubMed]
167. Treguer, P.; Nelson, D.M.; Van Bennekom, A.J.; DeMaster, D.J.; Leynaert, A.; Quéguiner, B. The Silica Balance in the World Ocean: A Reestimate. *Science* **1995**, *268*, 375.
168. Siever, R. The silica cycle in the Precambrian. *Geochim. Cosmochim. Acta* **1992**, *56*, 3265–3272. [CrossRef]
169. Mackin, J.E.; Aller, R.C. Dissolved Al in sediments and waters of the East China Sea: Implications for authigenic mineral formation. *Geochim. Cosmochim. Acta* **1984**, *48*, 281–297. [CrossRef]
170. Mackenzie, F.T.; Kump, L.R. Reverse Weathering, Clay Mineral Formation, and Oceanic Element Cycles. *Science* **1995**, *270*, 586. [CrossRef]
171. Dalrymple, R.W.; Narbonne, G.M.; Smith, L. Eolian action and the distribution of Cambrian shales in North America. *Geology* **1985**, *13*, 607–610. [CrossRef]
172. Beerling, D.J.; Chaloner, W.G.; Woodward, F.I.; Algeo, T.J.; Scheckler, S.E. Terrestrial-marine teleconnections in the Devonian: Links between the evolution of land plants, weathering processes, and marine anoxic events. *Philos. Trans. R. Soc. London Ser. B Biol. Sci.* **1998**, *353*, 113–130. [CrossRef]
173. Anbar, A.D.; Knoll, A.H. Proterozoic ocean chemistry and evolution: A bioorganic bridge? *Science* **2002**, *297*, 1137–1142. [CrossRef] [PubMed]
174. Expósito, I.; Jiménez-Bonilla, A.; Delchiaro, M.; Yanes, J.L.; Balanyá, J.C.; Moral-Martos, F.; Della Seta, M. Geomorphic signature of segmented relief rejuvenation in the Sierra Morena, Betic forebulge, Spain. *Earth Surf. Dynam.* **2022**, *10*, 1017–1039. [CrossRef]

175. Deer, W.A.F.; Howie, R.A.; Zussman, J. *An Introduction to the Rock-Forming Minerals*; The Mineral Society: London, UK, 2013. [CrossRef]
176. McClellan, G.H. Mineralogy of carbonate fluorapatites. *J. Geol. Soc.* **1980**, *137*, 675–681. [CrossRef]
177. Fernández-Remolar, D.C.; Preston, L.J.; Sánchez-Román, M.; Izawa, M.R.M.; Huang, L.; Southam, G.; Banerjee, N.R.; Osinski, G.R.; Flemming, R.; Gómez-Ortíz, D.; et al. Carbonate precipitation under bulk acidic conditions as a potential biosignature for searching life on Mars. *Earth Planet. Sci. Lett.* **2012**, *351*, 13–26. [CrossRef]
178. Avigad, D.; Sandler, A.; Kolodner, K.; Stern, R.J.; McWilliams, M.; Miller, N.; Beyth, M. Mass-production of Cambro–Ordovician quartz-rich sandstone as a consequence of chemical weathering of Pan-African terranes: Environmental implications. *Earth Planet. Sci. Lett.* **2005**, *240*, 818–826. [CrossRef]
179. Liivamägi, S.; Somelar, P.; Mahaney, W.C.; Kirs, J.; Vircava, I.; Kirsimäe, K. Late Neoproterozoic Baltic paleosol: Intense weathering at high latitude? *Geology* **2014**, *42*, 323–326. [CrossRef]
180. Mayoral, E.; Dies Álvarez, M.E.; Gámez Vintaned, J.A.; Gozalo, R.; Liñán, E.; Molina, J.M. Cerro del Hierro, Spain: The largest exposed early Cambrian palaeokarst. *Geol. Mag.* **2021**, *158*, 811–824. [CrossRef]
181. Tiessen, H.; Lo Monaco, S.; Ramirez, A.; Santos, M.C.D.; Shang, C. Phosphate minerals in a lateritic crust from Venezuela. *Biogeochemistry* **1996**, *34*, 1–17. [CrossRef]
182. Charpy, L. Phosphorus supply for atoll biological productivity. *Coral Reefs* **2001**, *20*, 357–360. [CrossRef]
183. Ruttenberg, K.C. 10.13—The Global Phosphorus Cycle. In *Treatise on Geochemistry*, 2nd ed.; Holland, H.D., Turekian, K.K., Eds.; Elsevier: Oxford, UK, 2014; pp. 499–558.
184. Dale, A.W.; Nickelsen, L.; Scholz, F.; Hensen, C.; Oschlies, A.; Wallmann, K. A revised global estimate of dissolved iron fluxes from marine sediments. *Glob. Biogeochem. Cycles* **2015**, *29*, 691–707. [CrossRef]
185. Xin, H.; Jiang, S.; Yang, J.; Wu, H.; Pi, D. Rare earth element geochemistry of phosphatic rocks in Neoproterozoic Ediacaran Doushantuo Formation in Hushan Section from the Yangtze Gorges Area, South China. *J. Earth Sci.* **2016**, *27*, 204–210. [CrossRef]
186. Naipauer, M.; Cingolani, C.A.; Vujovich, G.I.; Chemale, F. Geochemistry of Neoproterozoic-Cambrian metasedimentary rocks of the Caucete Group, Sierra de Pie de Palo, Argentina: Implications for their provenance. *J. South Am. Earth Sci.* **2010**, *30*, 84–96. [CrossRef]
187. Ruttenberg, K.C. 8.13—The Global Phosphorus Cycle. In *Treatise on Geochemistry*; Holland, H.D., Turekian, K.K., Eds.; Pergamon: Oxford, UK, 2003; pp. 585–643.
188. Atkinson, M.J.; Smith, S.V. C:N:P ratios of benthic marine plants. *Limnol. Oceanogr.* **1983**, *28*, 568–574. [CrossRef]
189. Dufour, P.; Andréfouët, S.; Charpy, L.; Garcia, N. Atoll morphometry controls lagoon nutrient regime. *Limnol. Oceanogr.* **2001**, *46*, 456–461. [CrossRef]
190. Rasheed, M.; Badran, M.I.; Richter, C.; Huettel, M. Effect of reef framework and bottom sediment on nutrient enrichment in a coral reef of the Gulf of Aqaba, Red Sea. *Mar. Ecol. Prog. Ser.* **2002**, *239*, 277–285. [CrossRef]
191. Atkinson, M.J. Biogeochemistry of Nutrients. In *Coral Reefs: An Ecosystem in Transition*; Dubinsky, Z., Stambler, N., Eds.; Springer: Dordrecht, The Netherlands, 2011; pp. 199–206.
192. Tribovillard, N.; Algeo, T.J.; Lyons, T.; Riboulleau, A. Trace metals as paleoredox and paleoproductivity proxies: An update. *Chem. Geol.* **2006**, *232*, 12–32. [CrossRef]
193. Odin, G.S. *Green Marine Clays*; Elsevier: Amsterdam, The Netherlands, 1988; Volume 45, p. 445.
194. Worden, R.H.; Morad, S. Clay Minerals in Sandstones: Controls on Formation, Distribution and Evolution. *Int. Assoc. Sedimentol. Spec. Pub.* **1999**, *34*, 1–41.
195. Worden, R.H.; Griffiths, J.; Wooldridge, L.J.; Utley, J.E.P.; Lawan, A.Y.; Muhammed, D.D.; Simon, N.; Armitage, P.J. Chlorite in sandstones. *Earth-Sci. Rev.* **2020**, *204*, 103105. [CrossRef]
196. Fernández-Remolar, D.C.; Harir, M.; Carrizo, D.; Schmitt-Kopplin, P.; Amils, R. Productivity Contribution of Paleozoic Woodlands to the Formation of Shale-Hosted Massive Sulfide Deposits in the Iberian Pyrite Belt (Tharsis, Spain). *J. Geophys. Res. Biogeosci.* **2018**, *123*, 1017–1040. [CrossRef]
197. Rickard, D.; Luther, G.W. Chemistry of Iron Sulfides. *Chem. Rev.* **2007**, *107*, 514–562. [CrossRef]
198. Thiel, J.; Byrne, J.M.; Kappler, A.; Schink, B.; Pester, M. Pyrite formation from FeS and H_2S is mediated through microbial redox activity. *Proc. Natl. Acad. Sci. USA* **2019**, *116*, 6897–6902. [CrossRef] [PubMed]
199. Canfield, R.E.; Liu, A.K. The Disulfide Bonds of Egg White Lysozyme (Muramidase). *J. Biol. Chem.* **1965**, *240*, 1997. [CrossRef]
200. Canfield, D.E.; Des Marais, D.J. Biogeochemical cycles of carbon, sulfur, and free oxygen in a microbial mat. *Geochim. Cosmochim. Acta* **1993**, *57*, 3971–3984. [CrossRef] [PubMed]
201. Atkinson, M.J.; Grigg, R.W. Model of a coral reef ecosystem. *Coral Reefs* **1984**, *3*, 13–22. [CrossRef]
202. Hedges, J.I.; Keil, R.G. Sedimentary organic matter preservation: An assessment and speculative synthesis. *Mar. Chem.* **1995**, *49*, 81–115. [CrossRef]
203. Berner, R.A. The long-term carbon cycle, fossil fuels and atmospheric composition. *Nature* **2003**, *426*, 323–326. [CrossRef]

204. Lee, C.; Fike, D.A. Organic carbon burial efficiency in the early Cambrian Yangtze Platform, South China. *Geochim. Cosmochim. Acta* **2021**, *307*, 1–20.
205. Canfield, D.E. Factors influencing organic carbon preservation in marine sediments. *Chem. Geol.* **1994**, *114*, 315–329. [CrossRef]
206. Redfield, A.C. The biological control of chemical factors in the environment. *Am. Sci.* **1958**, *46*, 230A.
207. Geider, R.; La Roche, J. Redfield revisited: Variability of C:N:P in marine microalgae and its biochemical basis. *Eur. J. Phycol.* **2002**, *37*, 1–17. [CrossRef]
208. Ho, T.-Y.; Quigg, A.; Finkel, Z.V.; Milligan, A.J.; Wyman, K.; Falkowski, P.G.; Morel, F.M.M. The elemental composition of som marine phytoplankton. *J. Phycol.* **2003**, *39*, 1145–1159. [CrossRef]
209. Planavsky, N.J. The elements of marine life. *Nat. Geosci.* **2014**, *7*, 855–856. [CrossRef]
210. Björnsäter, B.R.; Wheeler, P.A. Effect of nitrogen and phosphorus supply on growth and tissue composition of ulva fenestrata and enteromorpha intestinalis (ulvales, chlorophyta). *J. Phycol.* **1990**, *26*, 603–611. [CrossRef]
211. Britta, S. Short-term nutrient pulses as tools to assess responses of coral reef macroalgae to enhanced nutrient availability. *Mar. Ecol. Prog. Ser.* **1999**, *182*, 305–310.
212. Walther, K.; Fries, L. Extracellular Alkaline Phosphatase in Multicellular Marine Algae and Their Utilization of Glycerophosphate. *Physiol. Plant.* **1976**, *36*, 118–122. [CrossRef]
213. Riding, R. The Nature of Stromatolites: 3500 Million Years of History and a Century of Research. In *Advances in Stromatolite Geobiology*; Reitner, J., Quéric, N.-V., Arp, G., Eds.; Springer: Berlin/Heidelberg, Germany, 2011; pp. 29–74.
214. Antcliffe, J.B.; Callow, R.H.T.; Brasier, M.D. Giving the early fossil record of sponges a squeeze. *Biol. Rev.* **2014**, *89*, 972–1004. [CrossRef]
215. Lenton, T.M.; Boyle, R.A.; Poulton, S.W.; Shields-Zhou, G.A.; Butterfield, N.J. Co-evolution of eukaryotes and ocean oxygenation in the Neoproterozoic era. *Nat. Geosci.* **2014**, *7*, 257–265. [CrossRef]
216. Falkowski, P.G.; Katz, M.E.; Knoll, A.H.; Quigg, A.; Raven, J.A.; Schofield, O.; Taylor, F.J.R. The Evolution of modern eukaryotic phytoplankton. *Science* **2004**, *305*, 354–360. [CrossRef]
217. Follows, M.J.; Dutkiewicz, S. Modeling Diverse Communities of Marine Microbes. *Annu. Rev. Mar. Sci.* **2011**, *3*, 427–451. [CrossRef]
218. Duarte, C.M. Nutrient concentration of aquatic plants: Patterns across species. *Limnol. Oceanogr.* **1992**, *37*, 882–889. [CrossRef]
219. Sterner, R.W.; Elser, J.J. *Ecological Stoichiometry: The Biology of Elements from Molecules to the Biosphere*; Princeton University Press: Princeton, NJ, USA, 2002.
220. Algeo, T.J.; Ingall, E. Sedimentary Corg:P ratios, paleocean ventilation, and Phanerozoic atmospheric pO2. *Palaeogeogr. Palaeoclimatol. Palaeoecol.* **2007**, *256*, 130–155. [CrossRef]
221. Brasier, M.D.; Callow, R.H.T. Changes in the Patterns of Phosphatic Preservation across the Proterozoic-Cambrian Transition. *Mem. Assoc. Australas. Palaeontol.* **2007**, 377–389.
222. Canfield, D.E.; Poulton, S.W.; Narbonne, G.M. Late-Neoproterozoic Deep-Ocean Oxygenation and the Rise of Animal Life. *Science* **2007**, *315*, 92–95. [CrossRef]
223. Sterner, R.W.; Andersen, T.; Elser, J.J.; Hessen, D.O.; Hood, J.M.; McCauley, E.; Urabe, J. Scale-dependent carbon:nitrogen:phosphorus seston stoichiometry in marine and freshwaters. *Limnol. Oceanogr.* **2008**, *53*, 1169–1180. [CrossRef]
224. Crowe, T.P. Impacts of changing biodiversity on marine ecosystem functioning. In *Marine Ecosystems: Human Impacts on Biodiversity, Functioning and Services*; Crowe, T.P., Frid, C.L.J., Eds.; Ecology, Biodiversity and Conservation; Cambridge University Press: Cambridge, UK, 2015; pp. 111–134.
225. Benkwitt, C.E.; Wilson, S.K.; Graham, N.A.J. Biodiversity increases ecosystem functions despite multiple stressors on coral reefs. *Nat. Ecol. Evol.* **2020**, *4*, 919–926. [CrossRef]
226. Briggs, D.E.G. The role of decay and mineralization in the preservation of soft-bodied fossils. *Annu. Rev. Earth Planet. Sci.* **2003**, *31*, 275–301. [CrossRef]
227. Kidwell, S.M.; Flessa, K.W. The Quality of the Fossil Record: Populations, Species, and Communities. *Annu. Rev. Ecol. Syst.* **1995**, *26*, 269–299.
228. Allison, P.A.; Briggs, D.E.G. Exceptional fossil record: Distribution of soft-tissue preservation through the Phanerozoic. *Geology* **1993**, *21*, 527–530. [CrossRef]
229. Steiner, M.; Li, G.; Qian, Y.; Zhu, M.; Erdtmann, B.-D. Neoproterozoic to Early Cambrian small shelly fossil assemblages and a revised biostratigraphic correlation of the Yangtze Platform (China). *Palaeogeogr. Palaeoclimatol. Palaeoecol.* **2007**, *254*, 67–99. [CrossRef]
230. Porter, S.M. Closing the Phosphatization Window: Testing for the Influence of Taphonomic Megabias on the Pattern of Small Shelly Fossil Decline. *PALAIOS* **2004**, *19*, 178–183. [CrossRef]
231. Conway Morris, S. The Cambrian "explosion": Slow-fuse or megatonnage? *Proc. Nat. Acad. Sci. USA* **2000**, *97*, 4426–4429. [CrossRef] [PubMed]

232. Vannier, J. Early Cambrian origin of complex marine ecosystems. In *Deep-Time Perspectives on Climate Change: Marrying the Signal from Computer Models and Biological Proxies*; Princeton University Press: Princeton, NJ, USA, 2007. [CrossRef]
233. Bambach, R.K. Seafood through time: Changes in biomass, energetics, and productivity in the marine ecosystem. *Paleobiology* **1993**, *19*, 372–397. [CrossRef]
234. Butterfield, N.J. Plankton ecology and the Proterozoic-Phanerozoic transition. *Paleobiology* **1997**, *23*, 247–262. [CrossRef]
235. Odum, E.P. Energy Flow in Ecosystems: A Historical Review. *Am. Zool.* **1968**, *8*, 11–18.
236. Bengtson, S. Early skeletal fossils. *Paleontol. Soc. Pap.* **2004**, *10*, 67–78. [CrossRef]
237. Ager, D.V. Brachiopod palaeoecology. *Earth-Sci. Rev.* **1967**, *3*, 157–179. [CrossRef]
238. Jeppsson, L.; Anehus, R. A buffered formic acid technique for conodont extraction. *J. Paleontol.* **1995**, *69*, 790–794. [CrossRef]
239. Zhuravlev, A.Y.; Wood, R.A. Anoxia as the cause of the mid-Early Cambrian (Botomian) extinction event. *Geology* **1996**, *24*, 311–314. [CrossRef]
240. Conway Morris, S. Fossil priapulid worms. *Spec. Pap. Palaeontol.* **1977**, *20*, 1–155.
241. Yang, X.-y.; Vannier, J.; Yang, J.; Wang, D.; Zhang, X.-g. Priapulid worms from the Cambrian of China shed light on reproduction in early animals. *Geosci. Front.* **2021**, *12*, 101234. [CrossRef]
242. Vinther, J.; Eibye-Jacobsen, D.; Harper, D.A.T. An Early Cambrian stem polychaete with pygidial cirri. *Biol. Lett.* **2011**, *7*, 929–932. [CrossRef] [PubMed]